HIGHWAY RESEARCH BOARD

Bulletin 339

Bridge Deck Design and Loading Studies

1962

National Academy of Sciences—
National Research Council

publication 1021

HIGHWAY RESEARCH BOARD

Officers and Members of the Executive Committee

1962

OFFICERS

R. R. BARTELSMEYER, *Chairman* C. D. CURTISS, *First Vice Chairman*

WILBUR S. SMITH, *Second Vice Chairman*

FRED BURGGRAF, *Director* WILLIAM N. CAREY, JR., *Assistant Director*

Executive Committee

REX M. WHITTON, *Federal Highway Administrator, Bureau of Public Roads* (ex officio)

A. E. JOHNSON, *Executive Secretary, American Association of State Highway Officials* (ex officio)

LOUIS JORDAN, *Executive Secretary, Division of Engineering and Industrial Research, National Research Council* (ex officio)

PYKE JOHNSON, *Retired* (ex officio, Past Chairman 1960)

W. A. BUGGE, *Director of Highways, Washington Department of Highways* (ex officio, Past Chairman 1961)

R. R. BARTELSMEYER, *Chief Highway Engineer, Illinois Division of Highways*

E. W. BAUMAN, *Director, National Slag Association, Washington, D. C.*

DONALD S. BERRY, *Professor of Civil Engineering, Northwestern University*

MASON A. BUTCHER, *County Manager, Montgomery County, Md.*

J. DOUGLAS CARROLL, JR., *Director, Chicago Area Transportation Study*

C. D. CURTISS, *Special Assistant to the Executive Vice President, American Road Builders' Association*

HARMER E. DAVIS, *Director, Institute of Transportation and Traffic Engineering, University of California*

DUKE W. DUNBAR, *Attorney General of Colorado*

MICHAEL FERENCE, JR., *Executive Director, Scientific Laboratory, Ford Motor Company*

D. C. GREER, *State Highway Engineer, Texas State Highway Department*

JOHN T. HOWARD, *Head, Department of City and Regional Planning, Massachusetts Institute of Technology*

BURTON W. MARSH, *Director, Traffic Engineering and Safety Department, American Automobile Association*

OSCAR T. MARZKE, *Vice President, Fundamental Research, U. S. Steel Corporation*

J. B. MCMORRAN, *Superintendent of Public Works, New York State Department of Public Works*

CLIFFORD F. RASSWEILER, *Vice President for Research and Development, Johns-Manville Corporation*

GLENN C. RICHARDS, *Commissioner, Detroit Department of Public Works*

C. H. SCHOLER, *Applied Mechanics Department, Kansas State University*

WILBUR S. SMITH, *Wilbur Smith and Associates, New Haven, Conn.*

K. B. WOODS, *Head, School of Civil Engineering, and Director, Joint Highway Research Project, Purdue University*

Editorial Staff

FRED BURGGRAF
2101 Constitution Avenue

HERBERT P. ORLAND
Washington 25, D. C.

HIGHWAY RESEARCH BOARD

Bulletin 339

Bridge Deck Design and Loading Studies

1962

Presented at the
41st ANNUAL MEETING
January 8-12, 1962

$2.00

National Academy of Sciences—
National Research Council
Washington, D.C.
1962

Department of Design

T. E. Shelburne, Chairman
Director of Research
Virginia Department of Highways
Charlottesville

COMMITTEE ON BRIDGES

J. N. Clary, Chairman
Bridge Engineer
Virginia Department of Highways
Richmond

W. C. Anderson, Chief, Research and Development Engineer, The Union Metal Manufacturing Company, Canton, Ohio
Raymond Archibald, Kalispell, Montana
W. E. Baumann, Engineer of Bridge and Traffic Structures, Illinois Division of Highways, Springfield
J. M. Biggs, Associate Professor of Structural Engineering, Massachusetts Institute of Technology, Cambridge
Vernon J. Burns, Assistant Deputy Chief Engineer (Bridge), New York State Department of Public Works, Albany
E. M. Cummings, Manager of Sales, Bethlehem Steel Company, Bethlehem, Pennsylvania
Frederick H. Dill, Assistant to Vice President - Engineering, American Bridge Division, United States Steel Corporation, Pittsburgh, Pennsylvania
Arthur L. Elliott, Bridge Engineer - Planning, California Division of Highways, Sacramento
Eric L. Erickson, Chief, Bridge Division, Office of Engineering, Bureau of Public Roads, U. S. Department of Commerce, Washington, D. C.
R. S. Fountain, Bridge Engineer, Portland Cement Association, Chicago, Illinois
F. M. Fuller, Assistant Vice President, Raymond International, Inc., New York, N. Y.
H. deR. Gibbons, The Union Metal Manufacturing Company, Canton, Ohio
T. R. Higgins, Director of Engineering and Research, American Institute of Steel Construction, New York, N. Y.
John J. Hogan, Consulting Structural Engineer, Portland Cement Association, New York, N. Y.
C. L. Hulsbos, Department of Civil Engineering, Lehigh University, Bethlehem, Pennsylvania
J. J., Kozak, Supervising Bridge Engineer Special Studies, California Division of Highways, Sacramento
W. T. Lankford, Applied Research Laboratory, United States Steel Corporation, Monroeville, Pennsylvania
C. A. Marmelstein, Bridge Engineer, Georgia State Highway Department, Atlanta
William H. Munse, Jr., Department of Civil Engineering, University of Illinois, Urbana
LeRoy T. Oehler, Physical Research Engineer, Research Laboratory Division, Michigan State Highway Department, Lansing
D. H. Overman, Columbus, Ohio
Adrian Pauw, Professor of Civil Engineering, University of Missouri, Columbia
M. N. Quade, Consulting Engineer, Parsons, Brinckerhoff, Quade and Douglas, New York, N. Y.
William H. Rabe, Columbus, Ohio

C. P. Siess, Department of Civil Engineering, University of Illinois, Urbana
Charles B. Trueblood, Armco Drainage and Metal Products, Inc., Middletown, Ohio
Ivan M. Viest, Structural Engineer, Sales Engineering Division, Bethlehem Steel Corporation, Bethlehem, Pennsylvania
George S. Vincent, Bureau of Public Roads, U. S. Department of Commerce, Washington, D. C.

Contents

Forced Vibration of Continuous Highway Bridges

D. A. LINGER and C. L. HULSBOS, Respectively, Associate Professor of Civil Engineering, New Mexico State University; and Research Professor of Civil Engineering, Chairman, Structural Concrete Division, Lehigh University

This paper presents a correlation of forced vibration theory with dynamic impact tests for three continuous highway bridges and a simple span highway bridge. The experimental impact was determined at the centerline of the single span highway bridge and in the outer and inner spans and at the interior supports for the three types of continuous four-span highway bridges. The effect of the vehicle is assumed to be an oscillating forcing function whose frequency is the frequency of axle repetition and whose force is the oscillating load effect of a constant force traversing a beam. The correlation of the theoretical and experimental impact indicates that the simplifications made in the effect of the vehicles are justified for the bridges tested and the experimental vehicle velocities used. These results show qualitatively that the amount of impact is a function of the ratio of the frequency of axle repetition to the loaded natural frequency of the structure.

•IN THE DESIGN of highway bridges, the static live load is multiplied by a factor to compensate for the dynamic effect of moving vehicles. This factor, commonly referred to as an impact factor, is intended to provide for the dynamic response of the bridge to moving loads and suddenly applied forces. Many investigators have published research that contradicts the current impact formula (1, 4, 18). Some investigators feel not only that the problem of impact deals with the increase in over-all static live load but also that it is an integral part of a dynamic load distribution problem (25).

The current expanded highway program with the large number of required bridge structures emphasizes the need for investigating some of the dynamic behavior problems that have been generally ignored by highway engineers. These problems generally result from the inability of a designer to predict the dynamic response of a bridge structure. Many different investigations have been made of particular portions of the over-all dynamic problem. The results of these varied investigations are inevitably followed by a number of unanswered questions. Ironically, many of the unanswered questions are those of immediate concern in the design of highway bridges, and this emphasizes the need for additional research on the problem of impact.

Nature of the Investigation

This investigation is a study of the dynamic magnification of static load, commonly referred to as impact, resulting from the vibrations produced by a vehicle traversing the length of the bridge. More specifically, the purpose of this investigation is to correlate the response of actual continuous highway bridges under the effects of moving vehicles with vibration theory. The problem is then to determine by means of experimental data, the important parameters affecting bridge vibration and to develop thereby a theoretical correlation of these parameters.

The experimental investigation was designed to determine if the simplifications made in the theoretical impact analysis are justified in the application of this theory to actual structures. In this experimental work the impact was determined at midspan of a single span highway bridge and in the outer and inner spans and at the interior supports for

three types of continuous four-span highway bridges. The bridge structures investigated are as follows:

1. A simple span bridge with six post-tensioned prestressed concrete beams 100 ft long constructed to act compositely with a reinforced concrete roadway. The roadway is 30 ft wide with a 3-ft safety curb on both sides.
2. A fully continuous structure, 220 ft long with four aluminum stringers constructed to act compositely with a reinforced concrete roadway. The roadway is 30 ft wide with a 3-ft safety curb on both sides.
3. A fully continuous composite structure 240 ft long and similar to the previous bridge but with four steel wide flange stringers. The reinforced concrete roadway is 28 ft wide with a 3-ft safety curb on both sides.
4. A continuous reinforced concrete roadway 24 ft wide with a 2-ft safety curb on both sides supported by six pretensioned prestressed concrete beams in each of the four spans.

The ends of the simple span beams were encased by a cast-in-place diaphragm at the piers. The continuous roadway slab, constructed to act compositely with the stringers, and the pier diaphragm result in a relatively continuous 198.75-ft bridge.

The types of bridges chosen give a wide range of the various parameters involved in vibration. The aluminum stringer bridge is outstanding in that it allows a comparison of the effect of a lighter material with a smaller elastic modulus in a structure similar in its other aspects to the steel stringer bridge. The continuous pretensioned prestressed concrete bridge resembles the other continuous bridges except that it is only partially continuous in its action.

The mass per unit length is nearly equal for the three continuous bridges. To investigate the effect of a variation in the mass per unit length, the much heavier post-tensioned prestressed concrete bridge was studied. Also these bridges provide a number of variables in their structural qualities which may affect structural damping. The characteristic of damping is theoretically important because it provides an upper limit for the amplitude of forced vibration and might determine the maximum amount of impact for that structure.

Definitions

Impact Factor.—The impact factor used herein, is the ratio of the difference between the dynamic and static effect of a vehicle to the static effect. It is therefore the fractional increase in the static live load; in this case, the vehicle, which is required for the static live load to produce an effect equivalent to that of the dynamically applied live load.

Natural Frequency.—The frequency of a free vibration is called the natural frequency of the elastic system. The elastic system used herein is the bridge structure itself.

Resonance.—When an elastic system is acted on by an external periodic forcing function having the same frequence as a natural frequency of the system, it is in a state of resonance.

Notations

E = modulus of elasticity;
f = natural frequency in cycles per unit of time;
f_L = loaded natural frequency in cycles per unit of time;
$f(x, t)$ = a function of position and time;
g = acceleration due to gravity;
I = moment of inertia;
L = length of span;
M = mass of the load;
m = mass per unit length of span;
N = number of cycles;

n_b = damping coefficient;
s = spacing of the vehicle axles;
t = time;
T = a function of time;
v = velocity;
W = weight of the load;
w = frequency of the forcing function;
x = horizontal coordinates a distance measured in the direction of the length of the span;
X = a function of the horizontal coordinate;
y = vertical ordinates deflected displacement due to the static live load;
Y_d = vertical ordinates deflected displacement due to the dynamic live load.

THEORETICAL INVESTIGATION

Forced Vibration

The analytical work of Inglis (10), although not touching on this problem, does offer a great deal of insight into an analysis of the effect of multiple axle vehicles traversing a flexural system.

Inglis incorporates the use of a Fourier sine series for the representation of the various bridge loadings. A concentrated load W at section x = a is expressed by a Fourier series in the form

$$\text{Loading} = \frac{2W}{L} \sum_{i=1}^{i=\infty} \sin \frac{i\pi a}{L} \sin \frac{i\pi x}{L} \tag{1}$$

in which L is the span length. The deflection resulting from this load function provides a basis for some simplifications of the load function. The deflection curve must satisfy the relationship

$$EI \frac{d^4y}{dx^4} = \text{Loading}$$

or

$$EI \frac{d^4y}{dx^4} = \frac{2W}{L} \sum_{i=1}^{i=\infty} \sin \frac{i\pi a}{L} \sin \frac{i\pi x}{L} \tag{2}$$

When the load is near the center of a simple span, the static centerline deflection is obtained approximately by using only the first harmonic component of the load series. The resulting static deflection is

$$y = \frac{2WL^3}{\pi^4 EI} = \frac{WL^3}{48.7EI} \tag{3}$$

in which EI is the elastic constant of the beam. Therefore, by using only the first harmonic component of the load, a very close approximation to the exact value of $WL^3/48EI$ is obtained. Thus, only the first harmonic component was used by Inglis for most of his solutions.

The preceding calculation for deflection was made with the assumption that the elastic curve of the beam is free to rotate at the support, which is the elastic curve of a simply supported beam. The exactness of this solution for deflection is a result of the small difference between the simple beam deflection curve for a concentrated load and the

deflection resulting from the first component of the harmonic representation of load, a sine curve. Therefore, the type of solution that results in a sine deflection curve is applicable to a simply supported beam, but it requires some justification before it can be applied to a continuous beam. However, to do this it is only necessary to consider the computations for natural frequency by the energy method. It has been shown by Linger and Hulsbos (13) that the assumed sine deflection curve gives a very good approximation in determining the first mode natural frequency. This indicates the closeness of the sine curve to the exact theoretical first mode vibration curve of a continuous beam.

To represent a moving load, the distance that the load travels is taken as vt, where v is the velocity of the load and t is the time required for the load to traverse the distance a. The series representing the moving load of constant magnitude then takes the form

$$\frac{2W}{L} \sum_{i=1}^{i=\infty} \sin \frac{i\pi vt}{L} \sin \frac{i\pi x}{L} \tag{4}$$

Moving Loads of Constant Magnitude.—The oscillations produced in a beam by a single moving load of constant magnitude are found by solving the differential equation of motion (Eq. 5) with the load function given in Eq. 4. The differential equation of motion is

$$EI \frac{d^4y}{dx^4} + m \frac{d^2y}{dt^2} = f(x, t) \tag{5}$$

in which m is the mass per unit length of span, and f(x, t) is load function. The solution of this problem by Inglis (10, p. 27) is shown, using only the primary component of the load function, in Eq. 6. The dynamic deflection due to a single concentrated force is

$$y_d = \frac{2WL^3}{\pi^4 EI} \left[\frac{\sin \frac{\pi x}{L}}{1 - \left(\frac{v}{2Lf}\right)^2} \left(\sin 2\pi\left(\frac{v}{2L}\right) t - \left(\frac{v}{2Lf}\right) \sin 2\pi ft \right) \right] \tag{6}$$

Due to the practical limitations of speed, the term $\left(\frac{v}{2Lf}\right)^2$ in the denominator is negligible in comparison with unity and can be ignored. Similarly it can be shown that a simplification of this equation for the maximum dynamic deflection at midspan (i.e., vt = L/2 and x = L/2) becomes

$$y_d = y_{st} \left[1 - \left(\frac{v}{2Lf}\right) \sin 2\pi ft \right] \tag{7}$$

in which y_{st} is the static deflection for the given load function. It is apparent that the right-hand term in the parenthesis is an amplification factor representing the vibratory oscillations resulting from a single force traversing the beam, or that the increased dynamic effect can be represented by a static oscillating load factor of

$$W \left(\frac{v}{2Lf}\right) \sin 2\pi ft$$

Therefore, the effect of a series of forces can be represented by a load function whose frequency of application is determined by the repetition of axles and whose magnitude of oscillation is W (v/2Lf).

Repetition of Axles.—The frequency of the impulses representing the passage of axles is given by

$$w = \frac{v}{s} \tag{8}$$

in which s is the spacing of the axles and v is the velocity of the vehicle. The harmonic oscillation which is assumed to represent the dynamic effect of the repetition of axles is then taken as

$$W \left(\frac{v}{2Lf}\right) \sin 2\pi wt \tag{9}$$

The differential equation of motion used in the forced vibration analysis will include the effect of damping:

$$EI \frac{d^4y}{dx^4} + 4\pi n_b m \frac{dy}{dt} + m \frac{d^2y}{dt^2} = f(x, t) \tag{10}$$

in which $4\pi n_b m$ is the damping constant. The harmonic forcing function $f(x, t)$ which represents the dynamic effect of the axle impulses is represented by the first harmonic component of the load series and includes the effect of the mass of the load. The loading function, or forcing function, is

$$f(x, t) = \left(\frac{2}{L}\right) \left[W \frac{v}{2Lf} \sin 2\pi wt - M \frac{d^2\bar{y}}{dt^2} \right] \sin \frac{\pi x}{L} \tag{11}$$

in which $\bar{y}$ is the vertical deflection of the mass. The form of the solution of this partial differential equation may be taken, as shown by Inglis (10), as

$$y = T(t) \sin \frac{\pi x}{L} \tag{12}$$

The solution of Eq. 10 using the forcing function in Eq. 11 is given by

$$y_d = \frac{2WL^3}{\pi^4 EI} \left(\frac{v}{2Lf}\right) \left[\frac{\sin(2\pi wt - \alpha) - e^{-q}\left(\frac{w}{f_L}\right) \sin 2\pi f_L t}{\sqrt{\left(1 - \frac{w^2}{f_L^2}\right)^2 + \left(\frac{2n_b w}{f^2}\right)^2}} \right] \sin \frac{\pi x}{L} \tag{13}$$

in which

$q = 2\pi n_b \left(\frac{f_L}{f}\right)^2$;

f = the natural frequency of the bridge; and

f_L = the natural frequency of the bridge with the load on it.

The right-hand term in the numerator of the brackets varies as a function of the damping. Consequently, it dies out as the load passes along the bridge. Therefore, the maximum amplitude of this vibration occurs when the term $\left[\sin(2\pi wt - \alpha) \sin \frac{\pi x}{L} \right]$ is a maximum, and is given by

$$\frac{2WL^3}{\pi^4 EI} \frac{\frac{v}{2Lf}}{\sqrt{\left(1 - \frac{w^2}{f_L^2}\right)^2 + \left(\frac{2n_b w}{f^2}\right)^2}} \tag{14}$$

Because this deflection occurs as a result of the oscillating load factor w(v/2Lf), it is in effect the dynamic variation of the elastic curve about the static deflection position of this curve. Therefore, the impact factor as previously defined, for the maximum amplitude of vibration is the ratio of this amplitude to the static deflection. This impact factor can be written

$$\frac{\frac{v}{2Lf}}{\sqrt{\left(1 - \frac{w^2}{f_L^2}\right)^2 + \left(\frac{2n_b w}{f^2}\right)^2}} \tag{15}$$

This impact factor closely resembles the amplification factor normally associated with forced vibrations. The ratio (v/2Lf) in the numerator represents the amount of the load effective in the forcing function as the driving force, and is evaluated from the oscillations produced in a beam by a single moving load of constant magnitude. These oscillations, although they result from a single load of constant magnitude, are similar to those of an oscillating driving force. The effect of these oscillations will be increased if a repetition of axles occurs with the moving load of constant magnitude and if these axles are in phase with the oscillating load. The phase difference between these two effects is not considered here since it is possible for the oscillating load effect and the repetitive axle effect to occur together at many different positions in a continuous structure. Instead, these two effects are considered to be in phase, thus giving an upper boundary impact factor for the forced vibration of bridges by the optimum combination of the repetition of axles with the oscillating effect of a smoothly rolling load.

EXPERIMENTAL INVESTIGATION

Test Structures

The bridges tested in this research are part of the Interstate highway system around Des Moines, Iowa. They have all been built within the last seven years and are similar to the type of bridge being built in Iowa's primary and Interstate road system. The approaches to these structures are paved and there is a smooth transition to the bridge roadway. One factor used in selecting the bridges was the uniformity of their actual roadway profile. All of the bridges tested are constructed of longitudinal stringers designed to act integrally with a reinforced concrete roadway slab. However, a variety in this general type of structure was desirable to determine the limitations of the theoretical forced vibration approach presented herein. The variety was obtained by selecting three continuous bridges in which different materials were used to fabricate the longitudinal stringers. The mass per unit length is approximately the same in these bridges. A simple span bridge with a mass per unit length approximately double that of the other structures was also tested.

Simple Span Prestressed Concrete Bridge.—The simple span bridge investigated has six post-tensioned prestressed concrete beams and a span of 100 ft. The stringers are designed and constructed to act compositely with the reinforced concrete roadway slab. The roadway is 30 ft wide with a 3-ft safety curb on both sides (Fig. 1). This structure is one span of a seven-span bridge carrying westbound traffic on Interstate 35 over the Des Moines River north of Des Moines, Iowa. Each span of this bridge is isolated from adjacent spans by a 1-in. expansion joint.

Continuous Aluminum Stringer Bridge.—This structure is a 220-ft continuous four-span bridge with four aluminum stringers which act compositely with a reinforced concrete roadway. This bridge has a 30-ft roadway with a 3-ft safety curb on both sides

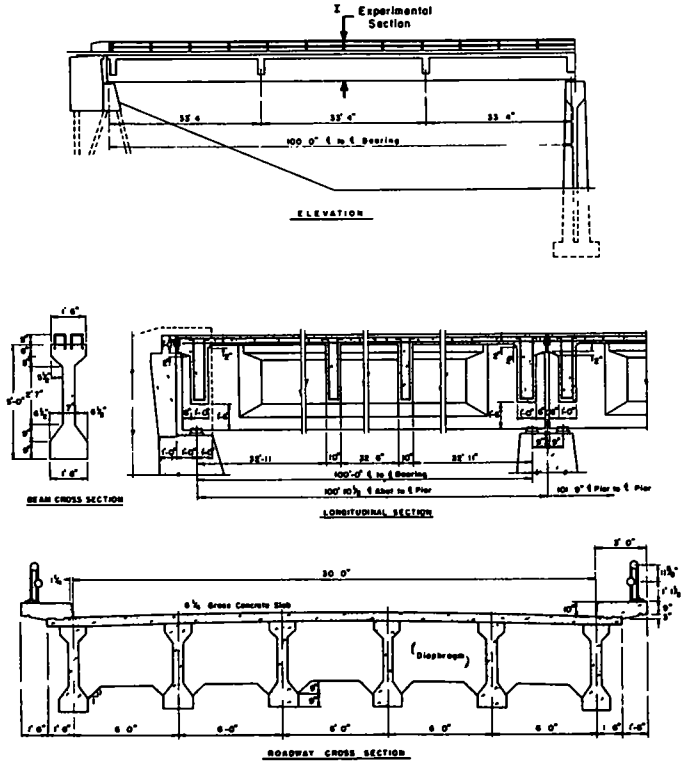

Figure 1. Details of simple span prestressed concrete bridge.

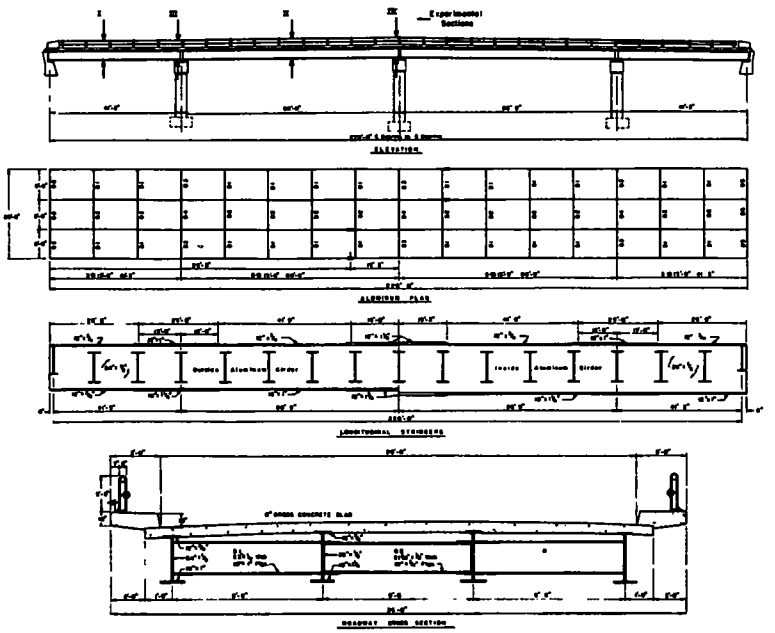

Figure 2. Details of continuous aluminum stringer bridge.

(Fig. 2). It carries traffic on Clive Road over Interstate 35 northwest of Des Moines, Iowa.

Continuous Steel Stringer Bridge.—This 240-ft continuous four-span structure is similar to the previous bridge except for the longitudinal stringers. The four steel stringers act compositely with a reinforced concrete roadway that is 28 ft wide with a 3-ft safety curb on both sides (Fig. 3). This structure carries the traffic on Ashworth Road over Interstate 35 west of Des Moines, Iowa.

Partially Continuous Prestressed Bridge.—This four-span bridge is 198.75 ft long with a 24-ft roadway. The reinforced concrete roadway slab is continuous over the interior supports and has a 2-ft safety curb on both sides. In each of the four spans there are six pretensioned prestressed concrete beams. The ends of the simple span beams are encased by a cast-in-place diaphragm at the piers. These pier diaphragms plus the continuous roadway slab, which acts compositely with the stringers, result in a relatively continuous bridge structure (Fig. 4). This structure carries traffic over Interstate 35 at the Cumming Interchange southwest of Des Moines, Iowa.

Test Vehicles

The vehicle effect has been simplified as much as possible in the theoretical analysis. The only parameters considered to be affected by the vehicles are the forcing function and the loaded frequency of the bridge. The forcing function is a function of the axle spacing and the velocity of the vehicle, and the loaded frequency of the bridge is a function of the ratio of the mass of the vehicle to the mass of the bridge span. The other variables of the loading vehicles, and there are many, were disregarded.

Vehicle A is an International L-190 van-type truck (Fig. 5). This truck, used to check the Iowa State Highway Commission scales, has a wheelbase of 14 ft 8 in. and a

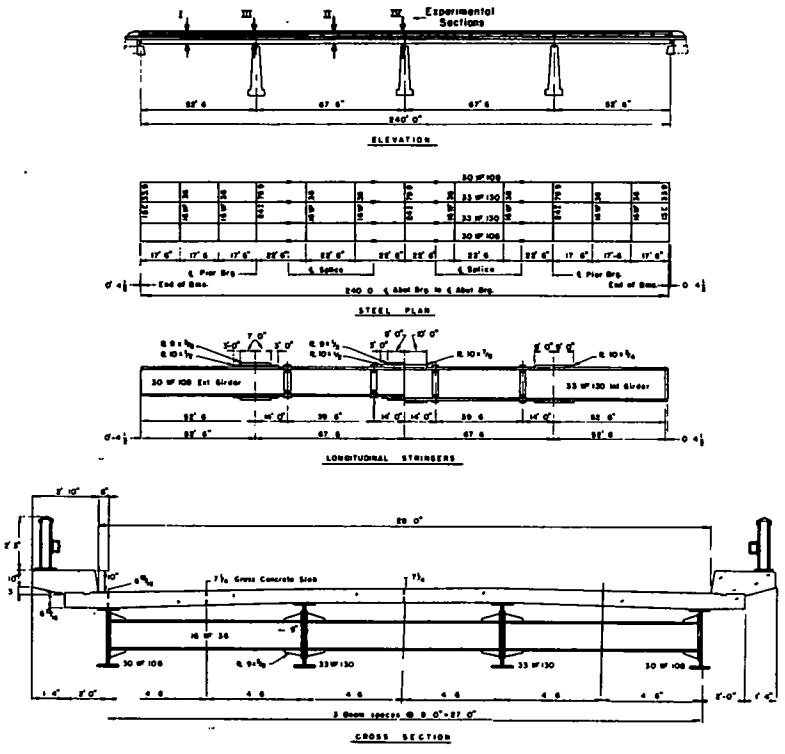

Figure 3. Details of continuous steel WF stringer bridge.

tread of 6 ft. It weighs 40,650 lb with 31,860 lb on the rear tandem axle. The forced vibration resulting from this vehicle at any velocity has two possible frequencies; that is, this vehicle could have the forced vibration frequency determined by the passage of

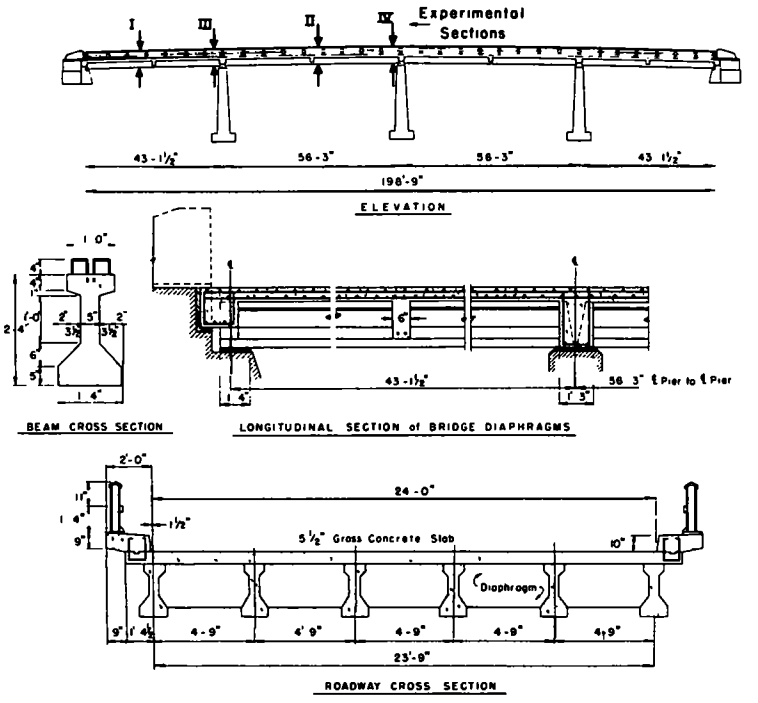

Figure 4. Details of partially continuous prestressed concrete bridge.

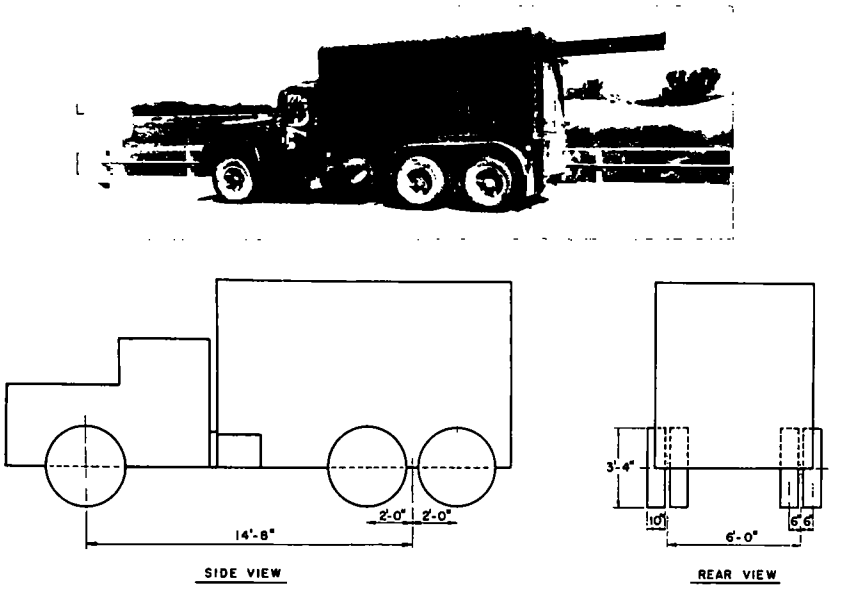

Figure 5. Vehicle A.

the individual axles in the tandem rear axle, in which the forcing frequency is v/4, or it could have a frequency determined by the passage of the front and rear axles, in which the forcing frequency is v/14.67. In the latter the axle spacing has been taken as the distance to the center of the rear tandems.

Vehicle B is a tandem axle, International VF-190 truck tractor pulling a 36-ft Monnon flat bed trailer (Fig. 6). The tractor has a wheelbase of 13 ft 1 in. and a tread of 6 ft. The trailer wheelbase is 23 ft, and the tread of the trailer wheels is 6 ft. The total weight of this vehicle is 73,500 lb, with 32,900 lb on the trailer tandem axle and 31,700 lb on the tractor tandem rear axle. This vehicle has three effective axle spacings, and therefore the forced vibration resulting from this vehicle for any given velocity has three possible frequencies. These three frequencies are v/4 resulting from the individual axle spacings of the tractor and trailer tandem axles, v/13.08 resulting from the tractor wheelbase axle spacing, and v/23 resulting from the trailer wheelbase axle spacing. For the tractor and trailer wheelbase, the axle spacing has been taken as the distance to the center of the tandems.

Instrumentation

To determine the dynamic effect of the vehicles, the static and dynamic bridge moments were computed from the strain measured at the extreme bottom fiber of each stringer. To measure the strains, standard SR-4 strain gages were used. The types of SR-4 gages used were A-1, A-5, and A-9. The resistance to the ground of the SR-4 gages used on the steel and aluminum girders was as follows: the A-1 gages, 1,000,000 to 1,000,000 ohms; the A-5 gages, 500,000 to 1,000,000 ohms. The A-9 gages have approximately a 6-in. gage length and were used to record the strains in the concrete girders.

The strain readings were recorded by a Brush universal amplifier (BL-520) and a Brush direct-writing recorder (BL-274). This equipment produces a continuous record of strain for which the time base can be varied by the speed of the recording paper. The speeds available vary from 1 to to 250 mm per sec. For a check of the time base as determined by the speed of the paper, a 1-sec timer was used to actuate an event marker on the edge of the record. The Brush Universal amplifiers have a number of attenuator settings which vary from 1 μ in. per in. of strain per Attenuator-Line to 1,000 μ in. per in. of strain per Attenuator-Line, and therefore allow a wide choice of amplification of the strain. The power for this Brush recording equipment was obtained from a 10 KW Onan motor generator.

The strains were measured in all the stringers at the centerline of the single span bridge and in the outer and inner spans and at the interior supports for the continuous bridges. This allowed the impact to be evaluated at all the sections of maximum bending

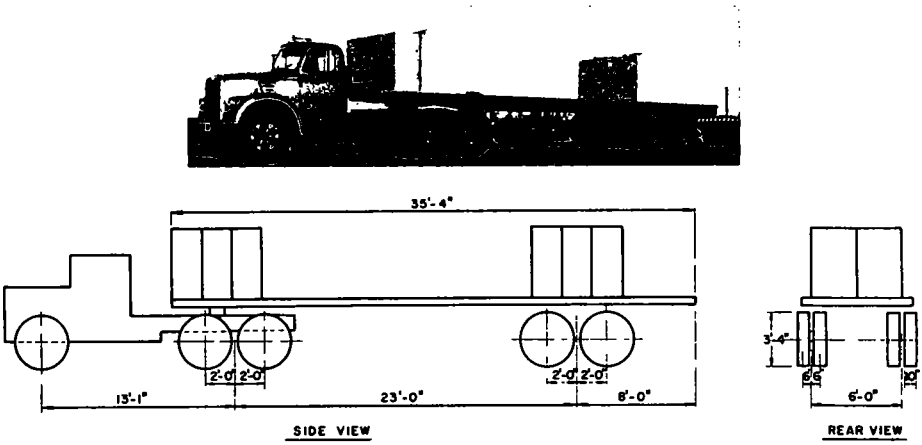

Figure 6. Vehicle B.

moment for the entire length of the bridge structures. Because the continuous bridges are symmetrical about their center interior support it was necessary to instrument only one-half of these bridges with strain gages.

Experimental Sections.—The experimental sections instrumented for the evaluation of the bridge moments are described and shown on the elevation view of each respective bridge plan.

1. Section I is located at a point four-tenths of the outer span from the end support for all the four-span continuous bridges. Section I for the simple span prestressed concrete bridge is at the middle of the span.
2. Section II is located at the middle of the interior span for the continuous steel stringer and aluminum stringer bridges. In the partially continuous four-span prestressed concrete structure, Section II was offset 1 ft 6 in. toward the center interior support to eliminate the effect of a transverse diaphragm at the middle of the interior span.
3. Section III is located at the first interior support of the continuous bridges. To eliminate or reduce any effect the reaction diaphragms might have, Section III was offset from the centerline of the reaction toward the exterior span 1 ft 6 in. and 1 ft 8 in. for the aluminum stringer, the steel stringer, and the prestressed concrete stringer bridges, respectively.
4. Section IV is located at the center interior support of the continuous bridges. This section is offset from the centerline of the reaction a distance equal to the offset of Section III for each respective continuous structure.

All of the bridges were instrumented at each of these section with an SR-4 strain gage at the center of the bottom flange, or the extreme lower fiber of each stringer.

Experimental Neutral Axes.—To obtain the moments required to evaluate the impact, the section moduli or relative section moduli of the stringers were required at the sections where the strains were measured. The effective section of the steel and the aluminum stringers vary considerably depending on their cross-section, due to cover plates or variable flanges, and the proximity of the curbing to the outer stringers. These changes in cross-section result in large changes in the moments of inertia and section moduli from one section to another. The actual section moduli and moments of inertia of the longitudinal stringers were determined experimentally by obtaining the position of the neutral axis of the longitudinal stringers. Because the bridges are symmetrical about their lateral and longitudinal centerlines it was necessary to instrument only one quadrant of each bridge for the determination of the position of the neutral axes of all the experimental sections used to evaluate impact. To obtain the neutral axis five SR-4 strain gages were positioned on each stringer. One gage was located at the center of gravity of the longitudinal stringer, and the other four gages at the extreme fibers and the quarter points of the stringer. The locations of the neutral axes were then used to determine the amount of concrete slab that acts compositely with the stringers. The entire roadway slab thickness was used in these calculations. The moment of inertia was then determined using the necessary amount of slab. A modular ratio of 10 was used for the steel stringer bridge and a ratio of 3.33 was used for the aluminum stringer bridge in these calculations. However, once the position of the neutral axis is known the moment of inertia is independent of the modular ratio used.

In both of the prestressed concrete stringer bridges, the lateral spacing of the stringers is much smaller and the cross-sections of the stringers do not vary along the beams. Moreover, the magnitude of the strains in the web and upper flanges of the prestressed concrete stringers was so small that it made the determination of a neutral axis very uncertain. Therefore, the section moduli of the longitudinal prestressed concrete stringers were assumed to be equal at each section investigated. It was found that in the steel and aluminum stringers in which the experimental neutral axes were determined the actual variation in the section moduli made very little difference in the impact because the impact is a difference in moments or a relative difference in the recorded strains. Thus the assumption made in the prestress concrete bridges will not appreciably affect the results regardless of the exact section moduli.

Experimental Procedure

The impact resulting from the action of the loading vehicles has been derived analytically. To determine experimentally the dynamic effect (the impact), static tests were first performed by the loading vehicle creeping across the bridge with the motor idling. The maximum moment in the bridge cross-section and the longitudinal position of the vehicle were computed. This was used as a base for the evaluation of the results of the dynamic tests. The dynamic tests were then conducted at vehicle speeds beginning at approximately 10 mph and increasing by increments up to the maximum attainable speed. The maximum dynamic moment was obtained in the cross-section for the vehicle in approximately the same longitudinal position as the maximum static moment. The dynamic and static tests were performed along four different lanes on the bridge roadway, two lanes for each direction of travel with one lane corresponding to the highway lane and the other lane at the longitudinal centerline of the bridge. For each assigned lane, the left front tire on the vehicle was guided along a painted stripe indicating the lane on the bridge roadway. During the runs a variation to one side or the other of the painted stripe was never more than 1½ in.

Pneumatic tubes were placed across the bridge roadway at the centerline of one exterior support and at the centerline of the center interior support for the continuous bridges and at the centerline of both exterior supports for the simple span bridge. The signal produced when the vehicle tire passed over this tube activated an event marker on the strain record. Knowing the chart speed and the distance between tubes, the average vehicle velocity was computed. These event markers on the strain record also enabled the longitudinal position of the vehicle to be determined at any time.

The testing of the continuous aluminum and steel stringer bridges was divided into two series for both test vehicles due to the limitation of the number of channels of Brush recording equipment. Section I and III were tested in one series and Sections II and IV in the second series. Both vehicles A and B were used in the dynamic testing of these bridges. The increased number of stringers in both the prestressed concrete bridges necessitated one series of tests for the test vehicle for each experimental section. Only Vehicle A was used in the dynamic testing of these bridges. At each test section the strain was measured at the extreme lower fiber of the stringers. In each series of tests the vehicle made four static runs, one in each lane, and sixteen or twenty dynamic runs, four or five in each lane, depending on the maximum speed obtainable for the particular structure. A continuous strain time record was obtained for each run. Each strain record, therefore, contains a continuous recording of the outer fiber strains for the stringers at the test section, an event marker trace for the longitudinal location of the vehicle and vehicle speed, and a time base with a 1-sec interval.

The test record shown in Figure 7 is a typical dynamic strain record showing the variation of the outer fiber strain as a vehicle moves across the bridge. The static strain time curve has been superimposed on the dynamic strain time curve and is indicated by a dotted line. This record was obtained from a stringer at Section I of the simple span prestressed concrete stringer bridge with Vehicle A traversing the bridge at 38.4 ft per sec.

The maximum static bridge moment is obtained by summing the moments in all the stringers computed from the maximum static strains. Similarly, the total maximum dynamic bridge moment is determined by summing the dynamic moments in all the stringers computed from the maximum dynamic strains. The dynamic effect, or the impact, of the vehicle was then evaluated from the moments as the ratio of the difference of the total dynamic and static bridge moments to the total static bridge moment.

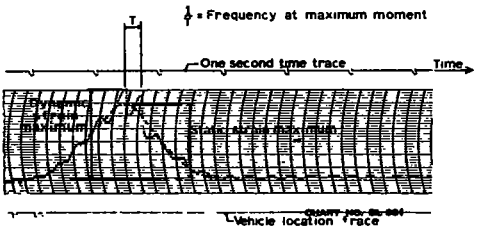

Figure 7. Typical strain record.

The passage of the front axle and each individual axle of the tandems over the pneumatic tubes is clearly shown by the vehicle location trace. In effect, the ve-

hicle is moving from left to right, and this trace indicates the time each individual axle crosses over the centerline of the exterior supports.

The upper event marker, used as the time base, indicates time in 1-sec intervals. This time base was used for determining the vehicle speed and the frequency of bridge vibration. The frequency of vibration of the bridge at maximum moment was determined by using the maximum peak-to-peak period of vibration indicated by the T in Figure 7.

The amplitude of the residual vibration that continues after the vehicle has gone off the bridge was very small in this run. This was the usual case for the concrete stringer bridges; however, the amplitude of residual vibration for the steel and aluminum stringer bridges was usually much larger. The unloaded natural frequency of the bridge and the bridge damping was evaluated from this residual vibration.

RESULTS

Natural Frequencies

The theoretical methods that may be employed to determine the natural frequency of bridges and the effect of live load on the natural frequencies of bridges can be found in many references on vibrations and are discussed by the authors (13).

First Mode of Vibration.—The theoretically computed natural frequencies determined by the authors (5, 13) are compared in Table 1 with the experimentally obtained natural frequencies. The moment of inertia used in the theoretical computations is the moment of inertia of the entire cross-section and includes the sidewalk curb. A modular ratio, the modulus of elasticity of the stringer over the modulus of elasticity of the reinforced

TABLE 1

NATURAL FREQUENCIES

Frequency[1]	Bridge			
	Aluminum Stringer	Steel Stringer	Continuous Concrete Stringer	Simple Span Concrete Stringer
L_2(ft)	68.75	67.50	56.25	100.0
$\frac{L_1}{L_2}$	0.600	0.777	0.766	-
E_2I_2(psi)	185.1×10^{10}	213.4×10^{10}	197.8×10^{10}	$1,609 \times 10^{10}$
$\frac{E_1I_1}{E_2I_2}$	0.615	1.0	1.0	-
$m_2 \frac{(lb/sec^2)}{(in.^2)}$	0.924	0.889	0.889	1.721
$\frac{m_1}{m_2}$	0.989	1.0	1.0	-
KL_2(rad)	3.400	3.399	3.408	3.1416
$f_{theo.}$ (cps)	3.825	4.34	6.06	3.34
$f_{exper.}$ (cps)	3.97	4.57	7.80	4.26
$\frac{f_{theo.}}{f_{exper.}}$	0.964	0.951	0.780	0.784

[1]Subscripts 1 and 2 indicate exterior and interior spans, respectively.

concrete roadway slab, of 3.44, 10, and 1.25 was used in the aluminum, steel, and both concrete bridges, respectively. Thus the modulus of elasticity of the reinforced concrete roadway slab and the prestressed concrete stringers were taken as the value used in design for each case; this probably accounts for most of the error in the theoretical frequency determination of the prestressed concrete stringer bridges. It was observed during the experimental testing that the natural frequency of the bridges reduced more than theory indicates it should, when a vehicle first enters the bridge span. However, once the vehicle is on the bridge the reduction in natural frequency, as the vehicle position changes, is similar to the theoretically calculated value; but it is extremely difficult to measure accurately.

Higher Modes of Vibration.—The first mode of vibration was usually found to be prevalent in controlling the response of the bridges to the forcing function of the axles. This was true in most cases and at Sections III and IV where the first mode, or higher odd modes, have the least effect. However, an outstanding exception occurred in the case of the aluminum stringer bridge. In this structure the experimental impact at Section IV, the section at the center interior support, was found to be a function of a higher mode of vibration. The resonance condition in this case is a function of the second mode. This is the first root of the even-mode frequency equation for a four-span symmetrical bridge, and corresponds approximately to the vibration of the beam with both ends fixed. Therefore, it is reasonable to assume that this vibration, when it occurs, will result in the largest dynamic increase in moment at the supports. The second mode frequency computed theoretically agrees closely with the measured frequencies occurring while the vehicle was on the inner spans vibrating the bridge at its second mode. However, this frequency could not be compared with an experimental unloaded natural frequency because this mode of vibration occurred only when the vehicle was on the inner span.

Effect of Vehicle.—The loaded natural frequency is the natural frequency of the bridge which occurs when the vehicle is on the span. This value of loaded natural frequency will control the resonance conditions of the frequency of the vehicle forcing function with the natural frequency of the bridge. This resonance condition has the greatest effect on the amount of impact when the vehicle is near the position of maximum moment.

The reduction in natural frequency due to the mass of the vehicle has been theoretically determined and although it could not be correlated with the experimental reduction, due to the difficulty of measuring it, it is desirable that the effect of the vehicle mass be taken into account.

The different lengths of the spans in the continuous bridges result in a different loaded natural frequency for the load in each span. Therefore, in the correlation of the experimental and theoretical impact, an impact curve is obtained for the loaded frequency as each span is loaded. Moreover, inasmuch as the truck tractor and trailer of Vehicle B were used as separate masses, the reduction in frequency is different for each part of the vehicle. All of the various values of loaded frequency will have an individual impact curve determined by Eq. 15. To reduce the number of these closely spaced curves and to simplify the presentation of the impact data, only two curves are shown for the reduction in natural frequency. These curves are for Vehicle A and the truck tractor of Vehicle B in the outer and inner spans. These two loads have the same effect on the reduction in frequency because their masses are within 0.1 percent of each other. The various theoretical loaded natural frequencies obtained for the vehicles in the outer and inner spans are 98 and 94.9 percent, 97.1 and 95.2 percent and 96.6 and 94.6 percent of the unloaded natural frequencies of the continuous aluminum, steel and concrete stringer bridges, respectively. The loaded natural frequency of the simple span bridge is 95.3 percent of the unloaded natural frequency for Vehicle A at the center of the span.

Forced Vibration

In the determination of impact, the frequency of the forcing function of the vehicle has been taken as the cyclical repetition of the axles. This cyclical repetition is determined by the frequency of passage of the axles across the bridge. To determine

the applicability of this concept, it must be shown that the forcing frequency of the axles is predominant in the forced vibration of the bridge, or that the response of the bridge is similar to that of a steady state forced vibration. The frequency of vibration of the structure was determined at the time the vehicle was producing the maximum moment. This value of frequency was obtained by using the one or two cycles of vibration at the maximum amplitudes of vibration. It was found in this experimental work that the natural frequency of the structure was prevalent as the vehicle entered the bridge, and further, that this natural frequency more nearly corresponds to the computed value than to the experimental value of natural frequency obtained after the vehicle had left the bridge. As the vehicle approached the position of maximum moment the frequency became approximately equal to the frequency of the forcing function (Figs. 8 to 12). Because there are two different forcing frequencies available for Vehicle A and three for Vehicle B, there were a number of different frequencies that could be used as the frequency of the forcing function. However, only one axle spacing was predominant in determining the frequency of the forcing function. This is readily shown in Figures 8 to 12 in which the frequency of the bridge vibration caused by the vehicle at the maximum moment point ($w = v/s$) is shown as a function of the velocity of the vehicle. Variations in this result from the tendency of the bridge vibration to remain near the resonant frequency of the structure at higher speeds where the forcing frequency is impressed by the axle spacing of the vehicle wheelbase.

An exception to the well-defined forcing frequency of the velocity divided by the axle spacing occurred in the continuous prestressed concrete bridge (Fig. 13). This structure was constructed by placing a continuous reinforced concrete roadway over four

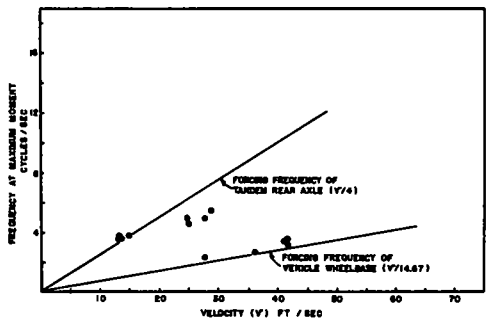

Figure 8. Frequency of forced vibration of simple span concrete bridge for Vehicle A.

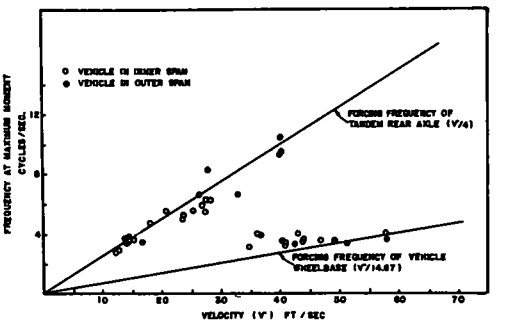

Figure 9. Frequency of forced vibration of aluminum stringer bridge for Vehicle A.

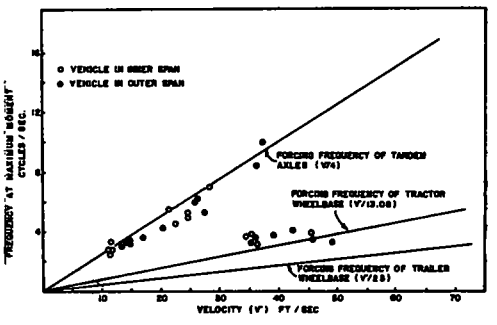

Figure 10. Frequency of forced vibration of aluminum stringer bridge for Vehicle B.

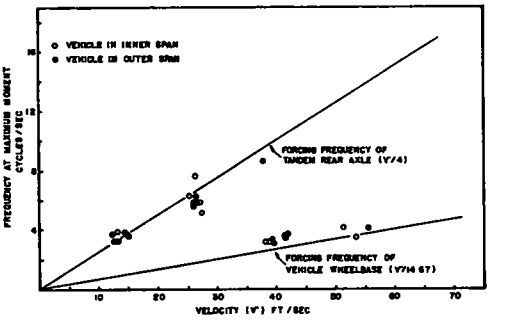

Figure 11. Frequency of forced vibration of steel stringer bridge for Vehicle A.

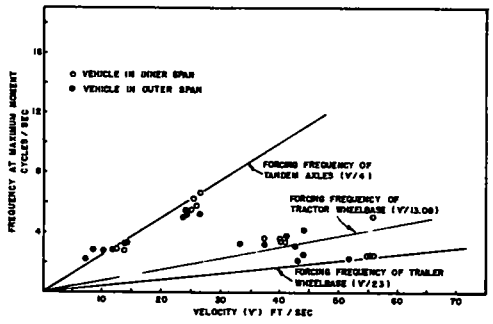

Figure 12. Frequency of forced vibration of steel stringer bridge for Vehicle B.

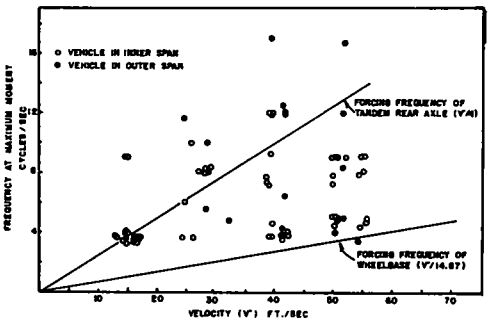

Figure 13. Frequency of forced vibration of continuous concrete stringer bridge for Vehicle A.

spans of simply supported prestressed concrete beams. Unlike the other bridges tested, this bridge does not have a point bearing to allow free rotation at the supports and it is not fully continuous. The interior supports have a 15-in. reinforced concrete diaphragm resting on an 11/32-in. preformed fabric bearing pad. These diaphragms encase the ends of the beams at each interior support and combine with the roadway slab to make the structure partially continuous. The exterior supports have approximately 16 in. of the end of the beam resting on similar 11/32-in. bearing pads. The effect of the large, flat bearing surfaces at the supports heavily damps the vibration of the continuous bridge. These bearings also cause a certain amount of fixity at each support, thus further complicating the vibratory system. Moreover, the pier diaphragms acting with the continuous reinforced concrete roadway slab allow only the negative moments to be transmitted across the piers or interior supports. Positive bending at the piers is eliminated due to the tension in the bottom fibers of the pier diaphragms. These diaphragms are not reinforced to resist tension in that direction. Therefore, it is very difficult to establish a well-defined vibratory system in such an incongruous structure. This is shown in Figure 14 by the random vibration of the structure at the maximum moment which results from the passage of Vehicle A. For this reason, the application of the forced vibration theory presented herein for the determination of the response of this structure to the forcing function of the repetition of axles has little significance.

The impact as determined herein is a function of the amplitude of forced vibration. The derivation of the theoretical impact was made by assuming that the forcing frequency of the axles was predominant in producing the impact. The denominator of the theoretical impact factor is a function of the ratio of the forcing freqency to the loaded natural frequency of the structure and the ratio of the damping factor to the unloaded natural frequency of the structure. The numerator of this impact factor is a function of the ratio velocity to the length of the span. Therefore, because the forcing frequency is the ratio of the velocity of the vehicle to the axle spacing, the magnitude of the theoretical impact will depend on the velocity, axle spacing, length of span, loaded natural frequency, unloaded natural frequency, and the damping factor.

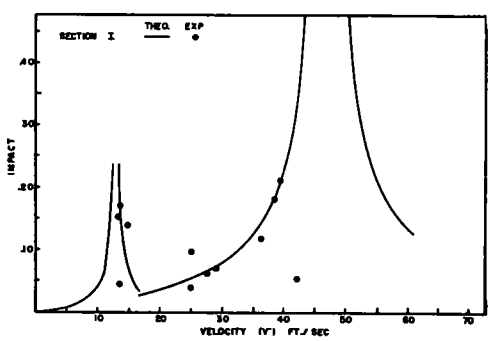

Figure 14. Impact for simple span concrete stringer bridge at Section I for Vehicle A.

The damping factor was obtained experimentally from the decreasing amplitude of the residual vibrations. To determine this experimentally, the amplitude of displacement Y of the strain time curve is measured at time t_o and at a later time t_N which

is N cycles later. The ratio of these amplitudes (Y_o/Y_N) is a constant, for viscous damping, and 1/N times the natural logarithm of this ratio is called the average logarithmic decrement.. This quantity therefore does not depend on the way the damping was defined in the original equation of motion and thus is often used as the measure of the damping capacity of a structure. The average logarithmic decrement is then given as

$$\frac{1}{N} \log_e \frac{Y_o}{Y_N}$$

The damping capacity of each bridge is given in terms of the average logarithmic decrement.

Simple Span Prestressed Concrete Bridge.—The correlation of the experimental and theoretical impact for the post-tensioned prestressed concrete bridge is shown in Figure 14. The experimental impact values determined at the centerline of the simple span (Section 1) are shown with the theoretical impact curves obtained by Eq. 15. A loaded natural frequency which is 95.3 percent of the theoretical natural frequency of 3.34 cycles per sec was used in determining the theoretical impact curves. The average logarithmic decrement for this bridge is 0.0916. The resulting amount of damping did not affect the theoretical curves except at resonance. Therefore, for the portion of the impact curves shown in this figure, the effect of the damping is insignificant. Resonance occurs when the ratio of the forcing frequency or the frequency of the repetition of the axles to the loaded natural frequency of the structure is one. This condition occurs two times for Vehicle A. The individual axles of the tandem rear axle unit acting individually cause a resonance at the smaller velocities, and the front axle combined with the tandem rear axle acting as one unit cause resonance at the larger velocities. The impact increases as the ratio of the forcing function to the loaded natural frequency approaches one. The experimental impact values agree with the theoretical impact curves, which, as previously discussed yield an upper limit of impact for the assumptions made in the derivation. The maximum vehicle velocity limited a complete investigation of the wheelbase resonance condition.

Continuous Aluminum Stringer Bridge.—The experimental and theoretical impact for this structure is shown in Figures 15 to 18. The theoretical curves show a good agreement with the experimental impact values. As previously discussed an additional resonance occurred in this structure when the bridge was excited at its second mode of vibration by the individual axles of the tandem rear axle unit. This condition is most prominent at the center interior support. A correlation of the theory presented herein for the upper limit of the wheelbase resonance condition was not obtained due to the limited velocity of the vehicles. Similarly, the resonance condition of the trailer wheelbase could not be investigated. A loaded natural frequency of 98.0 percent and

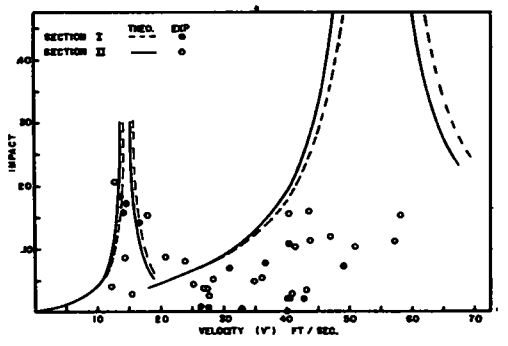

Figure 15. Impact for aluminum stringer bridge at Sections I & II for Vehicle A.

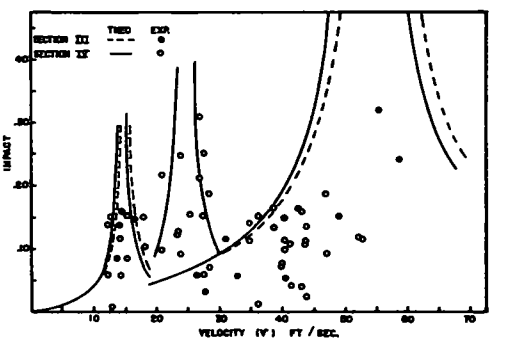

Figure 16. Impact for aluminum stringer bridge at Sections III & IV for Vehicle A.

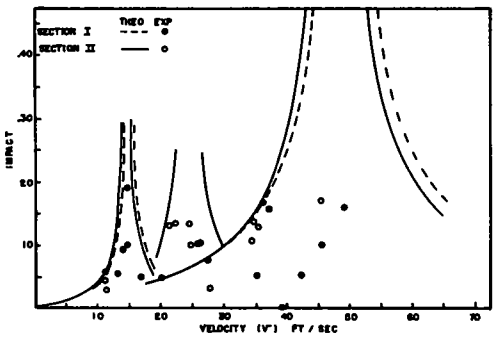

Figure 17. Impact for aluminum stringer bridge at Sections I & II for Vehicle B.

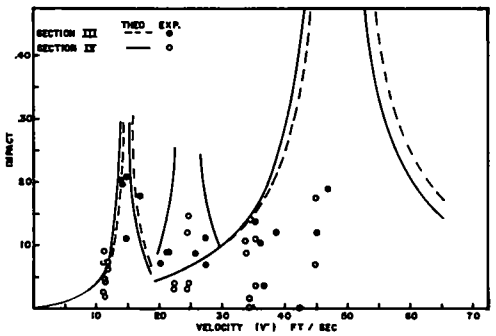

Figure 18. Impact for aluminum stringer bridge at Sections III & IV for Vehicle B.

94.9 percent of the theoretical natural frequency of 3.825 cycles per sec was used for the outer and inner span resonance curves, respectively. The average logarithmic decrement for this bridge is 0.050. The resulting amount of damping did not affect the theoretical curves except at resonance. The maximum values of impact written as a percentage vary from 20.6 to 31.9 percent and 19.1 to 20.8 percent for Vehicles A and B at the positive and negative sections, respectively. Moreover, the resonance condition of the individual axles of the tandem rear axle unit causes an experimental impact almost as large as the resonance condition of the vehicle wheelbase at higher velocities. Therefore, the resonance effect of the repetition of axles is important at the slower speeds.

Continuous Steel Stringer Bridge.—The correlation of the experimental and theoretical impact for this bridge is shown in Figures 19 to 22. More experimental impact values lie outside the theoretical impact envelope in this bridge than in the previous bridges. The greatest discrepancy occurs as the resonance condition is approached from the left side of the figure. That is, the large number of experimental points outside the theoretical envelope at velocities lower than the resonance velocities might result from the loaded natural frequency of the bridge being smaller than the value used to obtain the impact curves. A smaller loaded natural frequency would move the theoretical curves to the left in these figures. However, the theoretical curves shown still qualitatively describe the variations in the experimental impact. There is no indication in this structure of any higher modes of vibration. Moreover, not enough experimental data were obtained for a good evaluation of the resonance condition of the individual axles of the tandem axle unit with the first mode of vibration. Therefore, the experimental impact values for the tandem axles were smaller than those obtained by the resonance condition for the vehicle wheelbase. Also, a large enough velocity was not obtained for the trailer wheelbase to cause a resonance condition. The maximum values of impact, written as a percentage, vary from 44.1 to 26.5 percent and 22.8 to 39.2 percent for Vehicles A and B at the positive and negative sections, respectively. A loaded natural frequency of 97.1 and 95.2 percent of the theoretical unloaded natural frequency of 4.34 cycles per sec was used for the outer and inner span impact curves, respectively. The average logarithmic decrement of this bridge is 0.062. This amount of damping did not affect the theoretical curves except at resonance.

Partially Continuous Concrete Stringer Bridge.—The correlation of the experimental and theoretical impact for this bridge is shown in Figures 23 and 24. A loaded natural frequency of 94.6 percent of the theoretical unloaded natural frequency of 6.06 cycles per sec was used to obtain this curve. The curve for the vehicle on the outer span is not shown inasmuch as it is just to the right of this curve similar to those in the previous figures. This curve includes the effect of damping, which was considerably larger for this structure than for the previous structures. The average logarithmic decrement

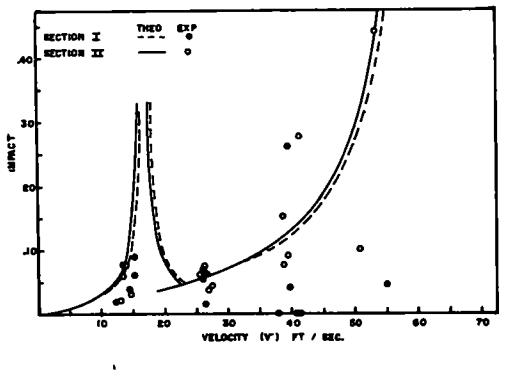

Figure 19. Impact for steel stringer bridge at Sections I & II for Vehicle A.

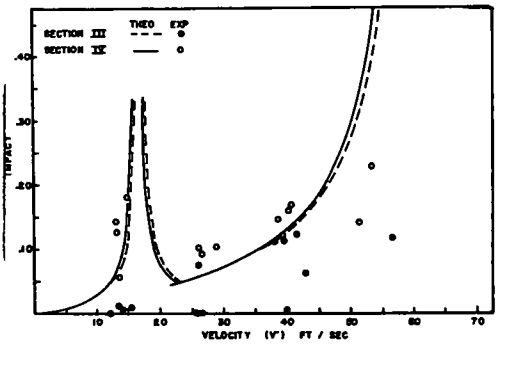

Figure 20. Impact for steel stringer bridge at Sections III & IV for Vehicle A.

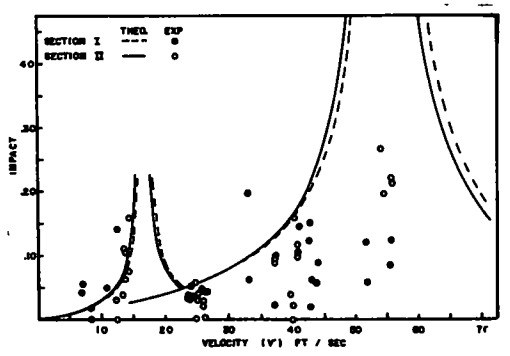

Figure 21. Impact for steel stringer bridge at Sections I & II for Vehicle B.

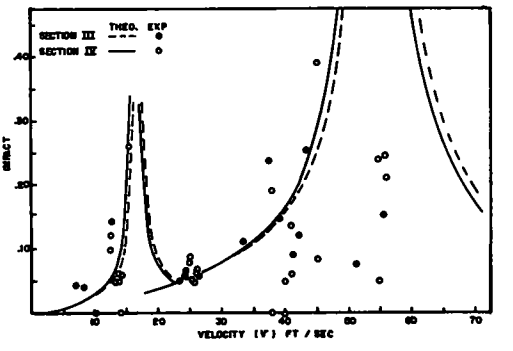

Figure 22. Impact for steel stringer bridge at Sections III & IV for Vehicle B.

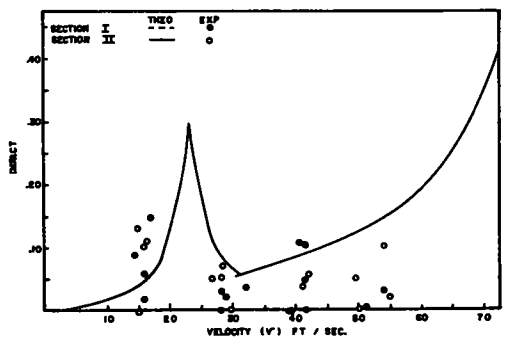

Figure 23. Impact for continuous concrete stringer bridge at Sections I & II for Vehicle A.

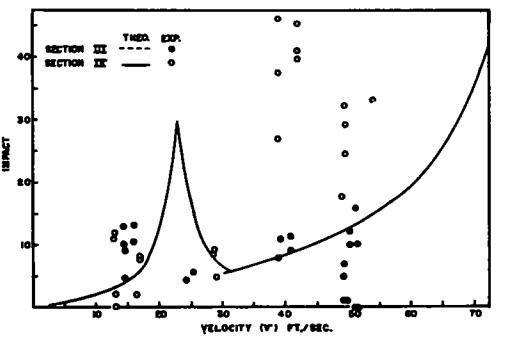

Figure 24. Impact for continuous concrete stringer bridge at Sections III & IV for Vehicle A.

of the residual vibration of this structure is 0.406. This amount of damping results in a reasonable upper limit for the impact curves of 0.298 for the resonance condition caused by the individual axles of the tandem axle unit. Because there are not enough experimental impact data at the velocity corresponding to this resonance condition, this upper limit could not be verified. The experimental impact values show some agreement with the theory at the positive moment sections. However, at the negative moment sections some of the impact values are large at the higher velocities. But, because the total moment in the section is small, the large impact value does not result in an overstress. The large impact results because a very small static live load strain at the center interior support was obtained as the vehicle moved across the bridge with the motor idling. Then, when the load was applied dynamically at larger velocities, the strains became significantly larger. Therefore, the values of impact at Section IV become quite large due to a relatively large increase in small value. This action is the result of the different dynamic and static responses of a bridge that acts as a continuous beam for negative moments at the interior supports and as a simply supported beam for positive moments at these supports. This inconsistent response is, therefore, due to the nonhomogeneous or incongruous structural system. It was shown previously that the experimental unloaded natural frequency of this structure corresponds to the theoretical unloaded natural frequency determined on the basis of a continuous structure. However, the forced vibration frequency of this structure did not correspond at all to the frequency of the forcing function at maximum moment. These inconsistencies in the response of the bridge will not allow the dynamic response of this structure to be analyzed by the forced vibration analysis as presented herein.

CONCLUSIONS

Natural Frequency

The theoretical unloaded natural frequencies of the bridge structures, neglecting damping, agree very well with the experimentally determined unloaded natural frequencies for the aluminum and steel stringer bridges and rather well for the concrete stringer bridges. When the theoretical loaded natural frequency reduction is applied to both frequencies to obtain the theoretical and experimental loaded natural frequencies, it is found that the theoretical loaded natural frequency compares better with the forced vibration resonances than the experimental loaded natural frequency, which was quite difficult to determine accurately.

The reduction in natural frequency due to the addition of the vehicle mass to the vibratory system was analyzed by the authors using an energy method (13). The use of an assumed sinusoidal curve enabled the effect of the mass of the vehicle on the unloaded natural frequency to be taken into account. The accuracy of the sinusoidal curve in determining the unloaded natural frequency also led to the assumption that the deflection curve in the forced vibration analysis of continuous bridges is a sine curve.

Forcing Function

The effect of the vehicle is assumed to be an oscillating forcing function whose frequency is the frequency of axle repetition and whose oscillating force is the oscillating load effect of a constant force. Thus the effect of the vehicle has been simplified as much as possible. The correlation of the theoretical and experimental impact indicates that the simplifications made in the effect of the vehicle are justified for the bridges tested and the experimental velocities used.

Forced Vibration

Impact, as presented herein, is determined by the application of forced vibration theory to the dynamic problem of multiple axle vehicles traversing continuous highway bridges. The results of this study show a good qualitative correlation between the amount of impact and the proximity of the frequency of axle repetition to the loaded natural frequency of the structure, or the resonance condition. The correlation is good for bridge structures that have a well-defined vibratory system. That is, if the

structure responds to a forced vibration without changing its natural modes of vibration, as obtained for the free vibrations of the structure, the response of the structure is similar to that of a steady state forced vibration.

RECOMMENDATIONS

The research contained in this study has taken into account, theoretically, the factors in a bridge structure that will affect its response to a forced vibration. The correlation of this theory is obtained by field testing of existing bridge structures. The field testing, as a means of evaluating impact indicates that forced vibration theory is applicable to the problem of bridge impact. However, the factors affecting the response of the bridge structure need to be investigated further. An example of this is the variation in the amount of composite action exhibited between the reinforced concrete slab and the longitudinal stringers along the length of the bridge. This aspect of the bridge structure is not entirely known for continuous bridges, and is basic to the response of the bridge to live loads. Another problem in the response of the bridge is the effect of the live load mass. A theoretical analysis was used in this research, but the irregularities exhibited by the concrete bridges indicate that the effect of the load may be more complicated than the simple effect of the mass of the vehicle. An experimental investigation of this phenomenon could include an additional objective which might be more important than the analysis of the effect of the live load mass. The other problem that could be investigated in a similar manner is the very important problem of an upper limit for the amplitude of forced vibration at resonance. At the onset of this research it was felt that the damping would limit the maximum impact for the resonance condition. It has been shown that this is not true for most of the bridges tested. This problem of the maximum amplitude of forced vibration (or maximum impact) and the lesser problem of the effect of the vehicle mass on the natural frequency of the structure could be investigated by a study of the forced vibration of a structure with a large variable speed oscillator. This oscillator, used in conjunction with a stationary vehicle on the bridge, would provide some answers to the problem of the natural frequency of the bridge and vehicle. In addition, the use of this oscillator with varying amounts of the oscillatory force could be used to investigate the problem of an upper limit for the impact curves. It is felt by the authors that a form of damping, which is evidently not viscous, limits the amplitude of the vibratory motion of the structure, notwithstanding the effect of the springing of the vehicle which has been disregarded. It is possible that this damping becomes a function of amplitude after the amplitude of vibratory motion exceeds a certain value.

The research indicated is based on the theory that before the effect of the various parameters of the vehicle and the roadway surface is integrated into the problem of impact, a thorough knowledge of the vibratory action and response of the structure is desirable.

ACKNOWLEDGMENTS

Acknowledgment is due to the Iowa Highway Research Board who sponsored this project. Also, the cooperation and assistance of Mark Morris, former Director of Highway Research; Neil Welden, Bridge Engineer; and Carl Schach, Engineer of Planning, all of the Iowa Highway Commission are especially appreciated.

Thanks are also due to J. N. Dunn, District Manager of the International Harvester Company, and C. A. Suss, Assistant Manager, for the truck tractor used as a loading vehicle.

REFERENCES

1. Biggs, J. M., and Suer, H. S., "Vibration Measurements of Simple-Span Bridges." HRB Bull. 124, 1-15 (1955).
2. Darnley, E. R., "The Traverse Vibrations of Beams and the Whirling of Shafts Supported at Intermediate Points." Lond. Edin. and Dublin Phil. Mag., Ser. 6, 41:81-96 (1921).
3. Duncan, W. J., "Free and Forced Oscillations of Continuous Beams: Treatment by the Admittance Method." Lond. Edin. and Dublin Phil. Mag., Ser. 7, 34:49-63 (1943).

4. Edgerton, R. C., and Beecroft, G. W., "Dynamic Studies of Two Continuous Plate-Girder Bridges." HRB Bull. 124, 33-46 (1955).
5. Ford, G. "Transverse Vibration of a Two-Span Beam Under Action of a Moving Constant Force." Unpublished Ph.D thesis, Stanford Univ. (1950).
6. Foster, G. M., and Oehler, L. T., "Vibration and Deflection of Rolled-Beam and Plate Girder Bridges." HRB Bull. 124, 79-110 (1955).
7. Goodman, L. E., "How We Get Our Present Impact Specification." Illinois Structural Engineering Conf., Urbana, Nov. 12-14, 1952, Proc., 2:96-107 (1952).
8. Hayes, J. M., and Sbarounis, J. A., "Vibration Study of Three-Span Continuous I-Beam Bridge." HRB Bull. 124, 47-78 (1955).
9. Hillerborg, A., "A Study of Dynamic Influences of Moving Loads on Girders." Internat. Assoc. for Bridge and Structural Engineering Congress, 3:661-667 (1948).
10. Inglis, C. E., "A Mathematical Treatise on Vibration in Railway Bridges." Cambridge Univ. Press, London (1934).
11. Jeffcott, H. H., "On the Vibration of Beams Under the Action of Moving Loads." Lond. Edin. and Dublin Phil. Mag., Ser. 7, 8:66-97 (1929).
12. Kryloff, A. N., "Ueber der Erzwungen Schwingungen von Gleichförmigen Elastischen Staben." Mathematische Annalen, 61:211-230 (1905).
13. Linger, D. A., and Hulsbos, C. L., "Dynamics of Highway Bridges." Iowa Engineering Exp. Station Bull. 188 (Nov. 1960).
14. Looney, T. G., "High-Speed Computer Applied to Bridge Impact." Jour. Structural Division, ASCE Vol. 84:Paper 1759 (Sept. 1958).
15. Pöschl, T., "Ueber die Angenäherte Berechnung der Schwingzahlen von Rahmenträgern." Ingenieur-Archiv, 1:469-480 (1929).
16. Prentzas, E. G., "Dynamic Behavior of Two Continuous I-Beam Bridges." Iowa HRB Bull. 14 (Aug. 1958).
17. Schallenkamp, A., "Schwingungen von Tragern bei Bewegten Lasten." Ingenieur-Archiv, 8:182-198 (1937).
18. Scheffey, C. F., "Dynamic Load Analysis and Design of Highway Bridges." HRB Bull. 124, 16-32 (1955).
19. Steuding, H., "Die Schwingung von Trägern bei Bewegten Lasten." Ingenieur-Archiv, 5:275-305 (1934).
20. Stokes, G. G., "Discussion of a Differential Equation Relating to the Breaking of Railway Bridges." In Stokes, G. G., "Mathematical and physical papers." 2:179-220. Cambridge Univ. Press, Cambridge (1883).
21. Suer, H. S., "Dynamic Response of Simple Span Highway Bridges to Moving Vehicle Loads." Unpublished Ph.D. thesis, Mass. Inst. of Technol. (1955).
22. Timoshenko, S. P., "Vibration Problems in Engineering." 3rd ed. Van Nostrand (1955).
23. Tung, T. P., Goodman, L. E., Chen, T. Y., and Newmark, N. M., "Highway-Bridge Impact Problems." HRB Bull. 124, 111-134 (1955).
24. Willis, R., "Extracts from the Appendix of the Report of the Commissioners Appointed to Inquire into the Application of Iron to Railway Structures." In Barlow, P. A., "Treatise on the Strength of Materials." 6th ed., pp. 326-386, Lockwood and Co., London (1867).
25. Wise, J. A., "Dynamics of Highway Bridges." HRB Proc., 32:180-187 (1953).

Research on Hybrid Plate Girders

A. A. TOPRAC, Associate Professor of Civil Engineering, University of Texas

This report presents the results of a series of tests on welded plate girders with 100,000-psi yield point constructional alloy steel flanges and ASTM A36 carbon steel web. Five tests were made on two specimens by subjecting them to moment and shear loading. The report discusses the deflection, buckling, and yielding characteristics of the specimens.

Results indicate that hybrid girders of the type tested can function satisfactorily under static load when properly designed. These girders are best suited for long spans in which the ratio of live load to total load is small. When this ratio is large, live load deflections may become excessive.

Strain gage data taken show that plane sections before bending remain plane even after the web has yielded considerably. These results and the load-deflection characteristics show that ordinary bending theory can be used in the design and analysis of hybrid beams and girders.

•IN CONTINUING efforts to build more economical bridge and building structures, engineers are exploring the use of new high-strength steels developed by the steel industry. Whereas some of these steels were developed the last 10 years, others have been in existence for 30 years. Many designers, however, have been relatively reluctant to use the high-strength steels. Undoubtedly, one of the reasons for this reluctance may be the lack of experimental information on the behavior of structural members built with such steel.

To meet this need a series of tests was performed in the Civil Engineering Laboratories of the University of Texas in which plate girders with 100,000-psi minimum yield strength constructional alloy steel flanges and carbon steel webs were used. The high-strength steel used for the flanges was Sheffield Super-Strength 100 and the carbon steel was ASTM A36 60 T. Such plate girders are referred to in this paper as hybrid with cross-sections made of two or more steels. This will distinguish them from the composite girders in which the variation in steel is along the length of the girder while throughout each cross-section the same steel is used.

Use of New Steels

Efforts by the steel industry to increase and improve the properties of steels used in construction have resulted in several grades of structural steels. In general, these steels can be separated into three major groups: (a) the carbon steels consisting of A7, A373, and A36; (b) the high-strength low-alloy steels consisting of A440, A441 and A242; and (c) the superstrength heat-treated steels.

In the carbon group, ASTM A36 steel has a minimum yield point of 36,000 psi and thus possesses a 9.1 percent higher yield point than ASTM A7 steel, long considered the common denominator of structural design. The yield point of the second group varies from 42,000 psi for thicknesses above 1½ in. to 50,000 for thicknesses of ¾ in. or less. Finally, the yield point of the quenched and tempered steels, that of the third group, is 100,000 psi. Included in the last group are such steels with proprietary names as USS T-1, USS Type T1-A, Jalloy S-100, N-A-XTRA 100, and SSS-100.

This report is focused on the third group of steels. In addition to their high yield strength and good ductility these new steels have excellent welding qualities which make

them particularly suitable for long-span plate girder construction. The erected cost of plate girders fabricated using these new steels is only 1½ to 2 times as high as the cost of girders with carbon steels. Because the web of a plate girder accounts for a large portion of its weight but contributes only a small part of its moment-carrying capacity, the use of cheaper low-strength steel for the web becomes intuitively apparent. This has been done by the California Division of Highways in some of its recent heavy bridges (1).

Another reason that makes it desirable to use carbon steel for the web of plate girders is that current design specifications permit the use of thinner webs for carbon steel girders than for higher strength steel girders when the minimum depth-to-thickness ratio governs in the design.

Objectives and Methods

The purpose of this investigation was to determine what effect yielding of the web would have on the ultimate static carrying capacity of the hybrid girder. Fatigue loading was not investigated.

In these tests two girders were fabricated with 100,000-psi yield strength constructional alloy steel flanges and A 36-60 T steel webs. Each specimen was first subjected to a static load test with load located at the third points, and then each specimen was modified and tested again with the loads applied at different points. Because of a failure in the lateral support system the second test was repeated for one specimen.

In this report the specimens are referred to as S1 and S2 indicating specimens 1 and 2. A further designation indicates the test number; thus, S1-T1 indicates test 1 on specimen 1.

Girder S1 had a 24- by ¼-in. web with no intermediate stiffeners. For test S1-T2 transverse stiffeners were added in one end panel and bearing stiffeners added at the new load points. Girder S2 had a 24- by 3/16-in. web with pairs of transverse stiffeners at 12 ¾-in. centers in each end panel. For the second test on S2, additional bearing stiffeners were added at the new load points which were nearer the center of the span.

In tests S1-T1 and S2-T1 the load was applied at the third points. These tests were terminated before the girders were severely damaged so that the specimens could be modified for tests S1-T2 and S2-T2. In tests S1-T2 and S2-T3 the loads were located as shown in Figure 1.

Resumé of Experimental Results

Except for test S2-T2, the results of the tests were as anticipated. S1-T1 was terminated at a load level of 203 kips. At this load it had deflected 2.833 in. The top flange had deflected about ⅝ in. laterally and a slight buckle was evident in the web in one end panel. Test S1-T2 was ended when the web of the specimen buckled in the unstiffened end panel under a load of 260 kips. In test S2-T1, the web was almost completely yielded in the end panels, when the test was ended with a load of 190 kips. Test S2-T2 ended unexpectedly when the top flange buckled laterally because of failure in one lateral support. Failure occurred with the load between 150 and 160 kips. Because it was impossible to know what effect the support failure had on the failure of the girder, this test was repeated as S2-T3 after repairs were made on the specimen. This time the support did not fail; however, the girder failed in the same manner and at the same load as in the first test.

TEST PROGRAM INSTRUMENTATION AND PROCEDURE

Two specimens were ordered for this investigation, shown in Figure 1. All girders were tested over a span length of 25 ft 6 in.

Girder S1 was fabricated without stiffeners except for bearing stiffeners at the load points (third points). After the first test was completed, the girder was modified by adding bearing stiffeners at points 2 ft nearer the ends. Intermediate stiffeners were also added in one end panel as shown.

Girder S2 was fabricated with bearing stiffeners at the third points and 2- by 3/16-in.

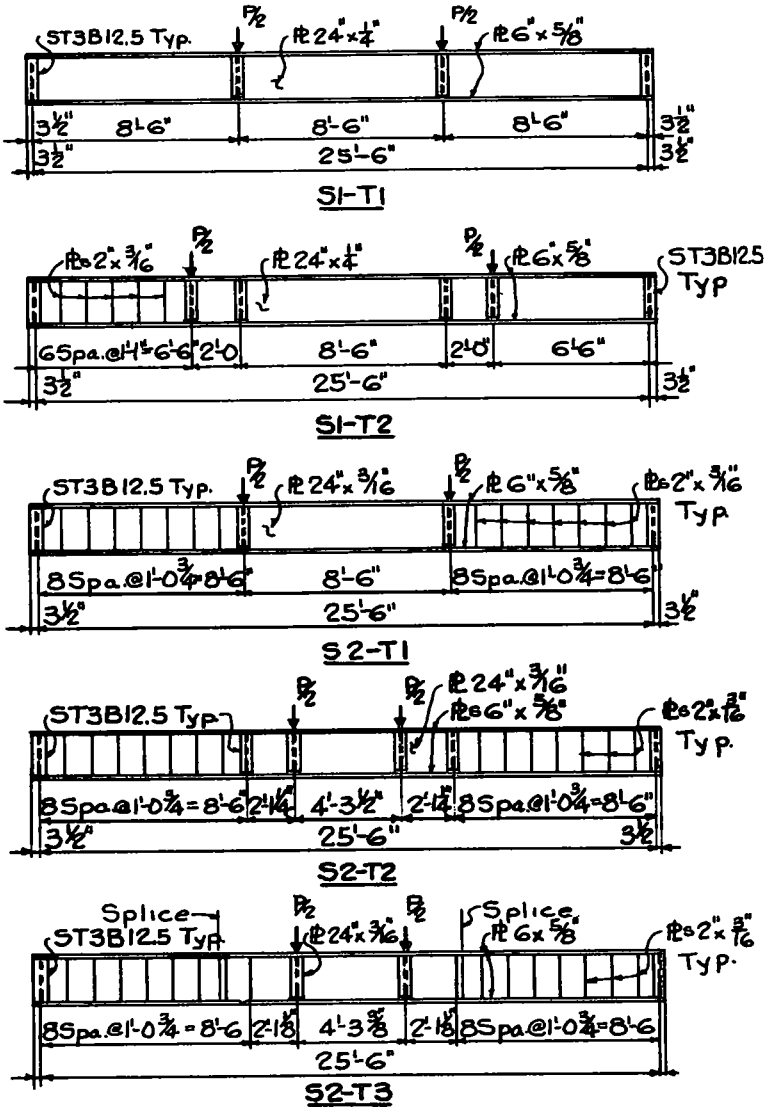

Figure 1. Test specimens.

intermediate stiffeners in the end panels. On completion of this test, new bearing stiffeners were added at points 10 ft 7 ¼ in. from the end bearings. When this specimen failed due to the failure of one of the lateral supports, it was repaired by cutting out a section 10 ft 2 in. long from the center portion and replacing it with a new piece.

The basic test setup is shown in Figure 2. Lateral support for the specimens was supplied as shown in this figure.

Three sets of data were obtained from the specimen. Strains were measured with SR-4 gages. Vertical deflections were measured with Ames dials located under the specimen. Local buckling in the web was measured with Ames dials. All specimens were whitewashed to make the observation of yield line development easier.

The steel used in the flanges of both girders was "SSS-100" produced by the Sheffield Division of Armco Steel Corporation. Tensile coupons for determining the yield point were prepared from plate samples furnished by the fabricator. Results of tests on the

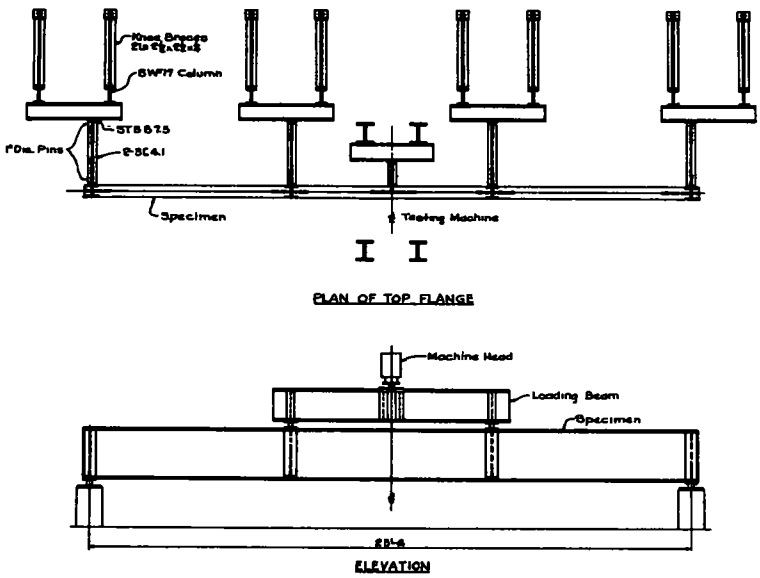

Figure 2. Test setup.

flange coupons revealed an average static yield point strength of 109,800 psi with 28 to 32 percent elongation over a 2-in. gage length. Tests of coupons cut from the A 36 steel web samples showed a static yield strength of 43,300 psi for the ¼-in. web and 36,950 psi for the $^{3}/_{16}$-in. web. Results of all coupon tests are given in Table 1. Mill test data for the SSS-100 is also included in this table.

Reference loads and moments were calculated in accordance with the plastic design theory and the plate girder design method presented by Basler (2). Table 2 gives the reference moments, loads, and deflections.

TEST RESULTS AND OBSERVATIONS

Test results are discussed separately for each specimen and test. Results of strain gage measurements are presented at the end of this section.

Test S1-T1

In reference to the load deflection curve for this test (Fig. 3), the deflection varies only slightly from a straight line throughout the load range. No deviation is noticeable until the stress in the extreme fiber of the web, σ_{yw}, as calculated by the $\frac{Mc}{I}$ formula, is well above the yield point of the web material.

According to the theory presented by Basler (2), the web of this specimen could be expected to buckle at an ultimate shear, Vu, of 105 kips. This shear corresponds to a moment of 895 ft-kips. The plastic moment, Mp, calculated for this specimen is 1,010 ft-kips. When the test was terminated, the shear was 102.3 kips and a slight buckle had formed in one of the end panels. The compression flange had also deflected horizontally about $^{5}/_{8}$ in. over the length of an end panel. Yield lines began to appear rather early in the test probably due to welding residual stresses; the first of these was noted at a load of 60 kips.

Test S1-T2

Computations indicated an ultimate shear force of 109.9 kips would cause failure in this specimen. This shear force was exceeded by about 20 kips; however, a slight buckling of the web started developing when the calculated shear force was reached.

TABLE 1

SUMMARY OF EXPERIMENTAL YIELD POINT STRESSES

SPECIMEN	TYPE STEEL	STATIC Y. P. ksi	DYNAMIC Y.P. ksi	ELONGATION %	ELONGATION G.L.
C1	SSS-100	109.6	113.3	32.0	2-In.
C2	"	-	113.1	29.0	"
C3	"	-	115.8	29.0	"
C4	"	-	114.7	31.0	"
C6	"	-	111.5	31.0	"
C7	"	-	114.7	30.5	"
C9	"	109.7	115.0	28.0	"
C10 1/2 In.	A36-60T	43.3	46.5	38.0	"
C11 3/16	"	36.9	41.0	36.0	"
Mill	SSS-100	110.9	-	23.5	8-In.
Mill	A36-60T	n.a.	n.a.	n.a.	-

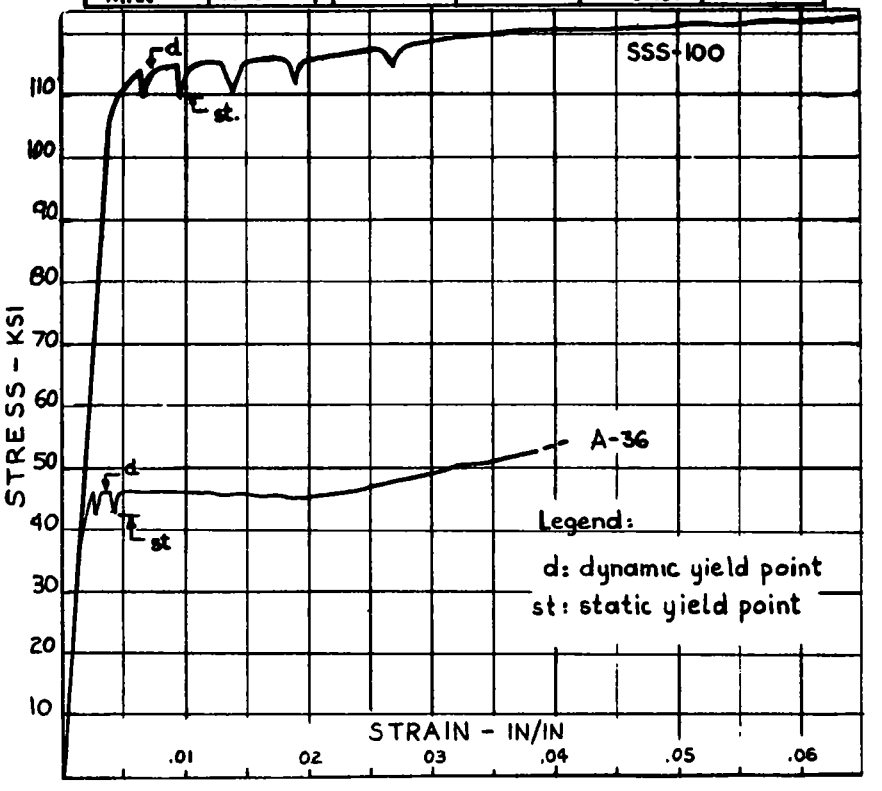

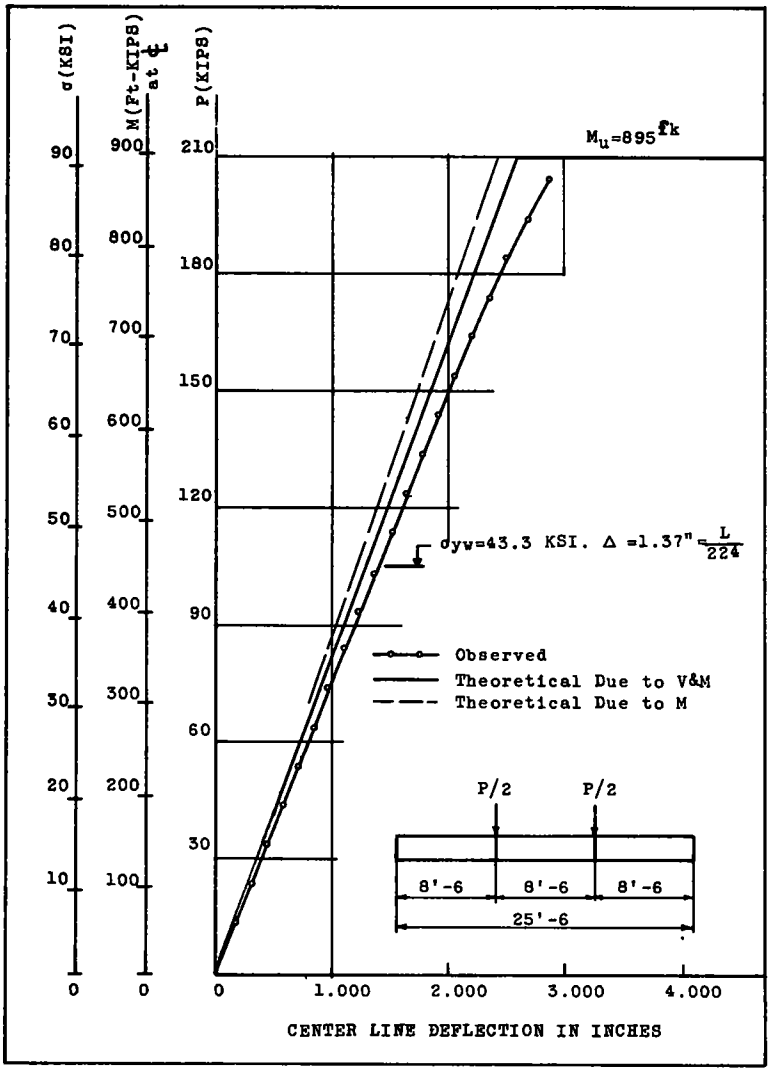

Figure 3. Load deflection curve S1 - T1.

TABLE 2

REFERENCE MOMENTS AND LOADS

Test	M_p (ft-kips)	M_u (ft-kips)	V_p (kips)	V_u (kips)
S1-T1	1,010.2	895	148	105.1
S1-T2	1,010.2	715	148	109.9
S2-T1	963	793	95.1	93.3
S2-T2	963	885	95.1	83.5
S2-T3	963	885	95.1	83.5

This buckle continued to develop and can be seen in Figures 4a and 4b. The end of the girder shown is not the one in which a buckle occurred previously in S1-T1.

The load deflection curve (Fig. 5) for this test is similar to the curve for the first test on this specimen.

Test S2-T1

The ultimate shear force predicted for this test was 89.3 kips, resulting in a moment of 759 ft-kips. These values had been exceeded when the test was terminated with a shear of 97.3 kips.

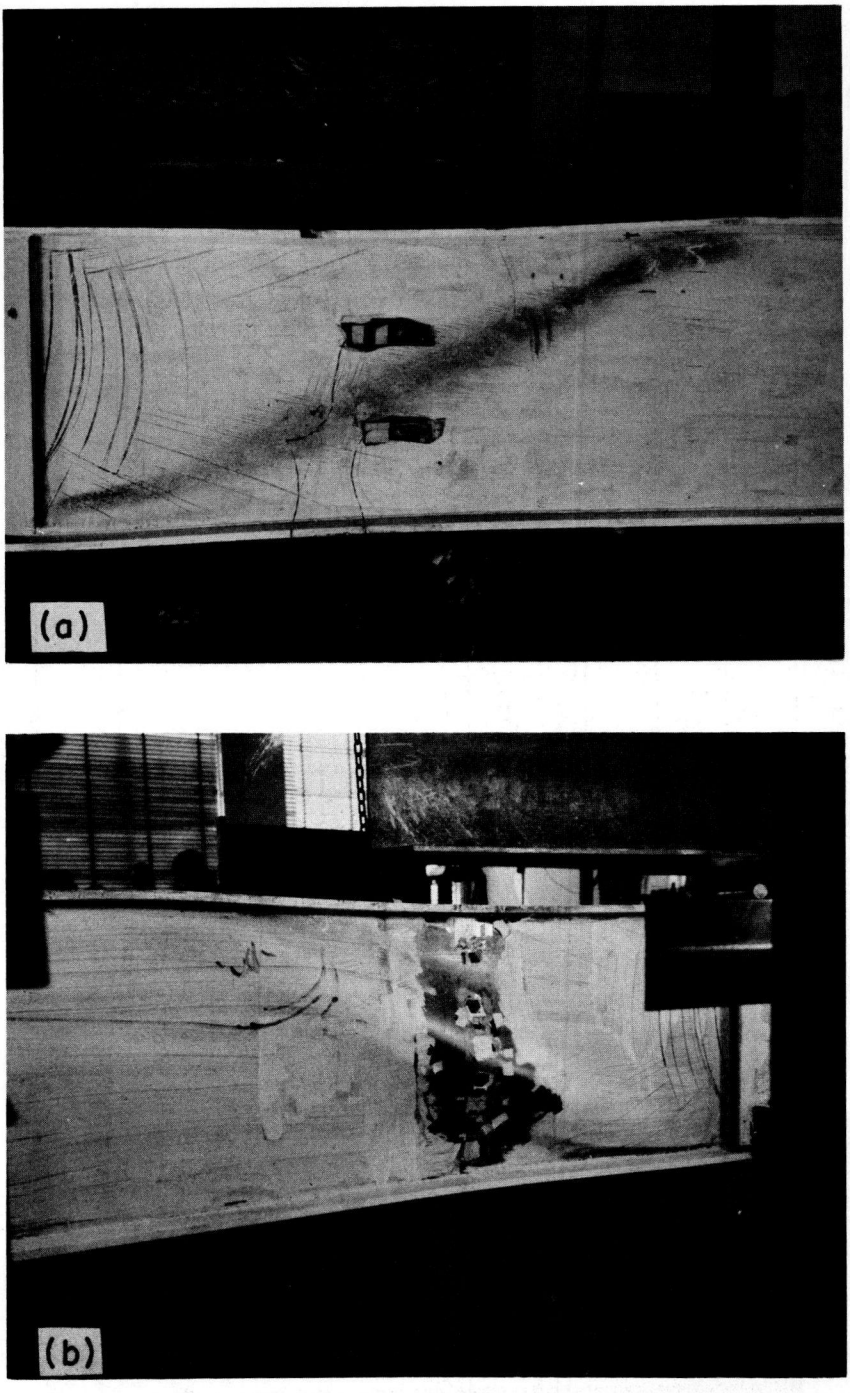

Figure 4. End panel of S1 after completion of test S1 - T2. (a) Looking from south. (b) Looking from northeast.

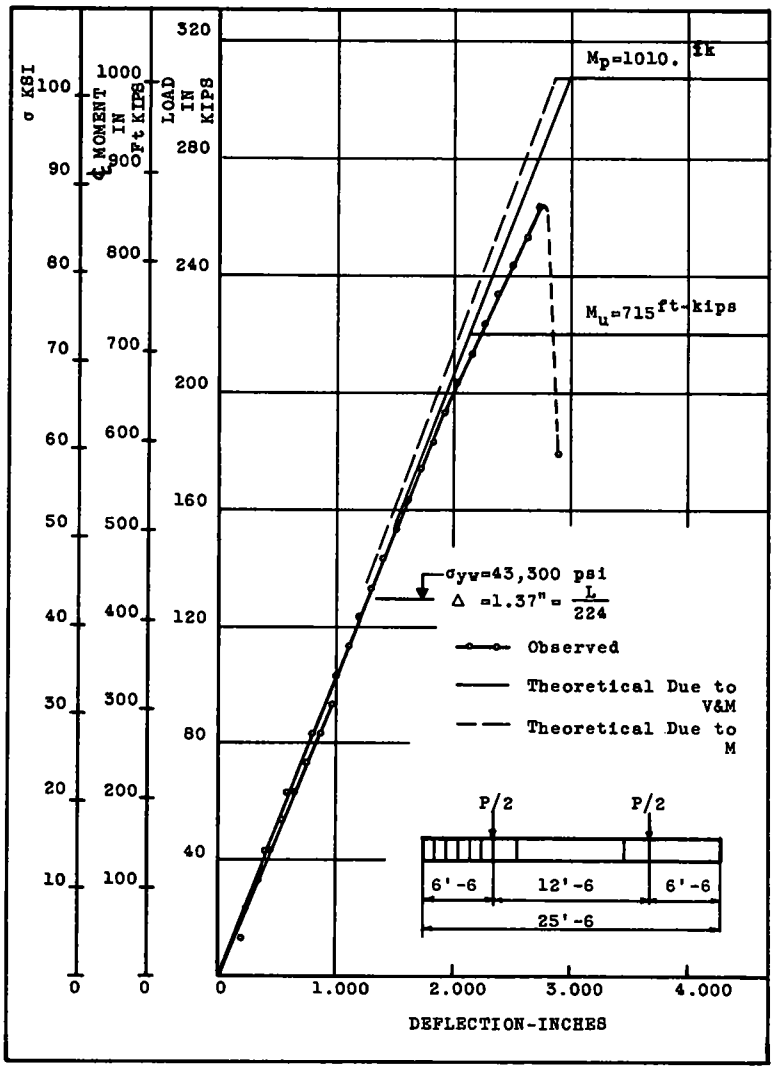

Figure 5. Load deflection curve for test S1 - T2.

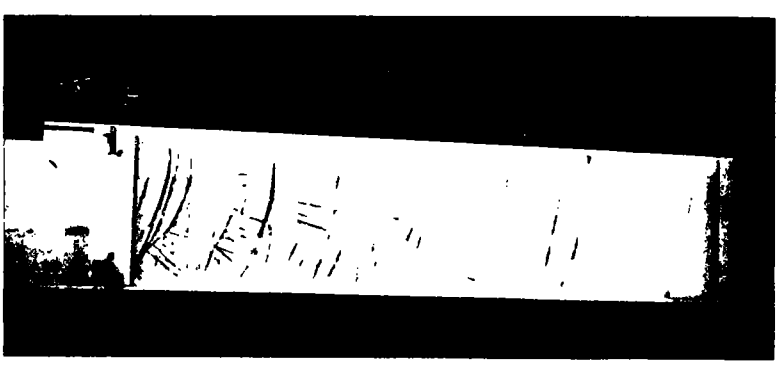

Figure 6. End panel of specimen after completion of test S2 - T1 (west end of girder, 8 panels from reaction, north side of web).

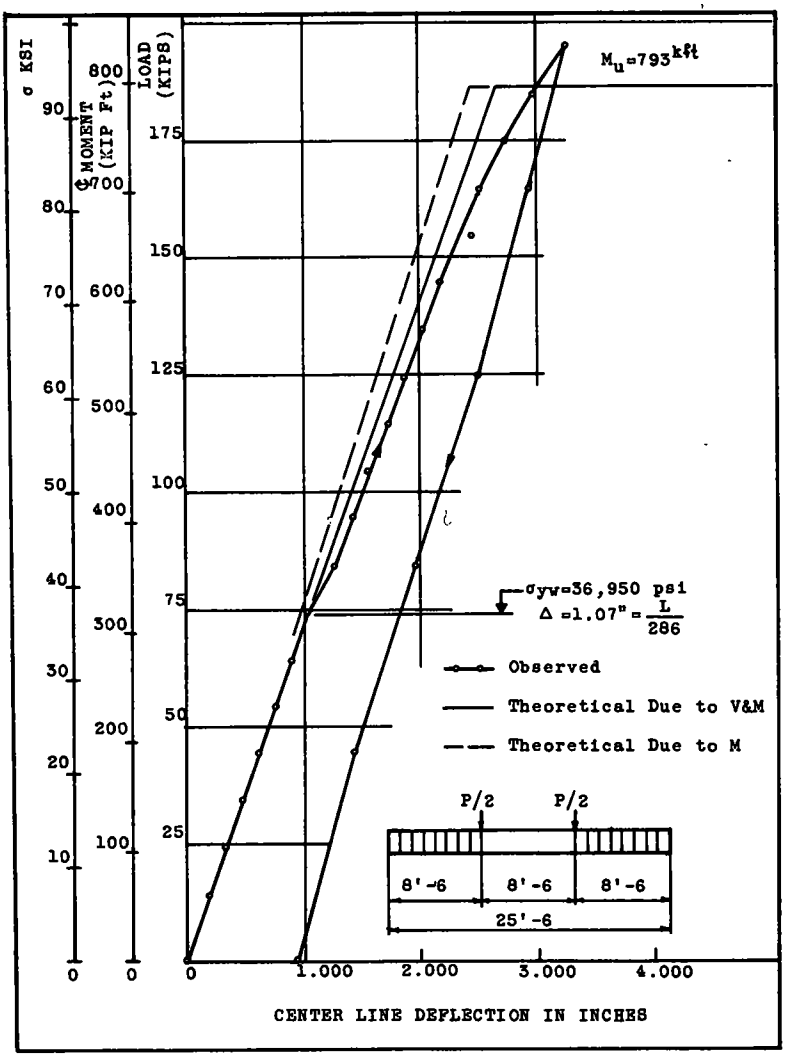

Figure 7. Load deflection curve for test S2 - T1.

The end web panels of this specimen were almost completely yielded when the test was stopped. The extent of this yielding can be seen in Figure 6. Yield lines were first evident when the load reached the 20-kip level and they were apparently due to residual stresses.

The deflection curve for this specimen (Fig. 7) shows a sudden increase in deflection as the yield point of the web material is reached. After this sudden increase a straight line relationship between load and deflection is again apparent until the load reaches the 145-kip level.

Test S2-T2

The ultimate shear force for this test was calculated to be 81.8 kips. This would correspond to an ultimate moment of 868 ft-kips. The test was completed before this value was attained. Failure occurred when the shear force was 76.5 kips and was due to the failure of a lateral brace.

The first yield lines appeared when the load was a mere 10 kips. These lines

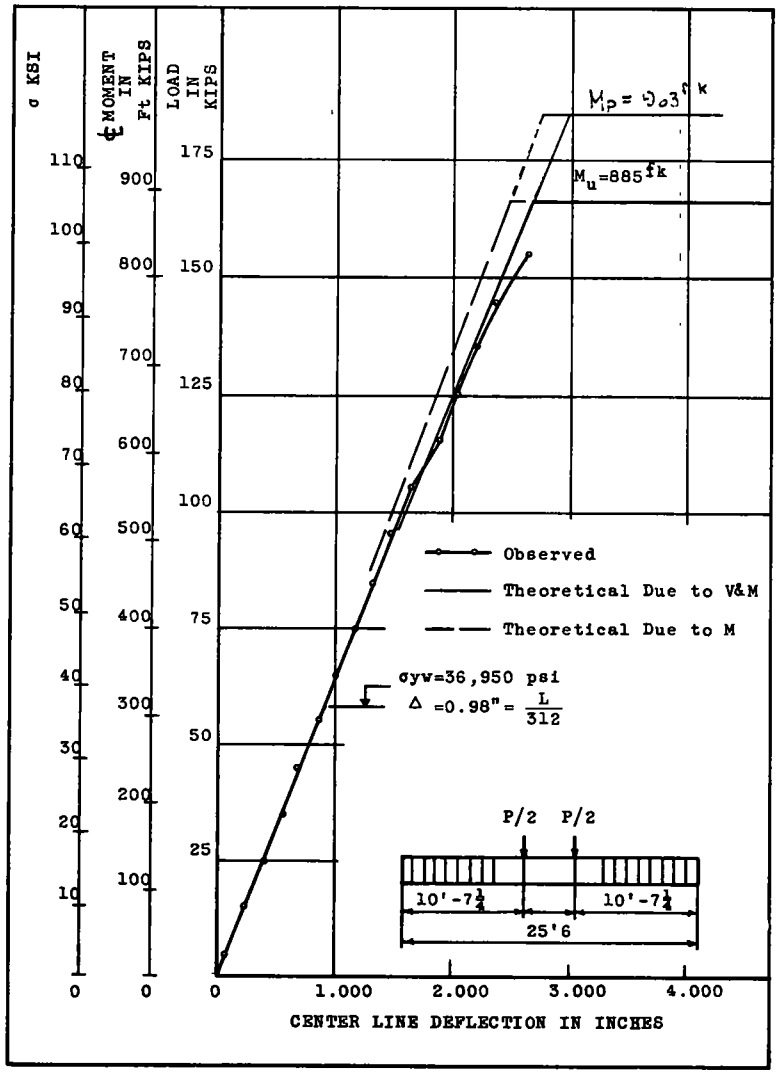

Figure 8. Load deflection curve for test S2 - T2.

appeared at the bottom of the new bearing stiffeners and were due to residual stresses from welding. A general pattern of yield lines had developed by the time the load reached 30 kips.

The load deflection curve for this test (Fig. 8) indicates elastic behavior far above the yield point stress in the web. This was due to strain hardening of the web in test S2-T1.

Test S2-T3

Test S2-T3 was a repetition of test S2-T2. However, behavior of the specimen could be expected to be somewhat different from that in S2-T2, inasmuch as part of the center portion of the web had not been stressed before, and the end portion had been yielded in test S2-T1 and S2-T2. Another factor that influenced the results of this test was that the web had some initial curvature in the panels where the splices were made. This initial curvature caused some concern when the early development of yield lines adjacent to the splice indicated that buckling might occur; however, buckling failed to

Figure 9. Buckle in panel adjacent to load in test S2 - T3.

develop at this location. Figure 9 shows these yield lines and the buckling condition in the panel adjacent to the load point. Concurrently with the buckling of this panel the compression flange of the girder buckled horizontally into an S-curve under the load of 150 kips. The permanent lateral deflection due to the lateral buckling of the flange can be seen in Figure 10.

The deflection curve for this test (Fig. 11) did not agree as closely with the theoretical curve as that of test S2-T2. A slight change in slope is again evident at the point where the extreme fiber stress of the web reached the yield point of 36,950 psi. When the load was removed and then reapplied, this point moved up the curve to approximately the level at which a change in slope occurred in test S2-T2.

Strain Gage Measurements

SR-4 electrical strain gages were used to measure strains at various load levels and compared to theoretical strains derived using the ordinary flexure formula $\sigma = My/I$ and a modulus of elasticity of $E = 30,000,000$ psi. Uniaxial gages were applied at the midspan of each girder to measure strains for pure moment condition and at one moment-shear panel, 3 ft 9 ½ in. from the end reaction for both specimens.

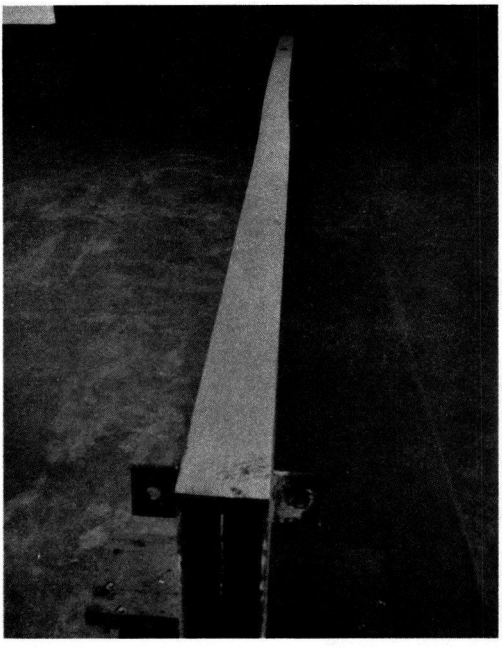

Figure 10. Girder at completion of test showing permanent set in flange due to lateral buckling.

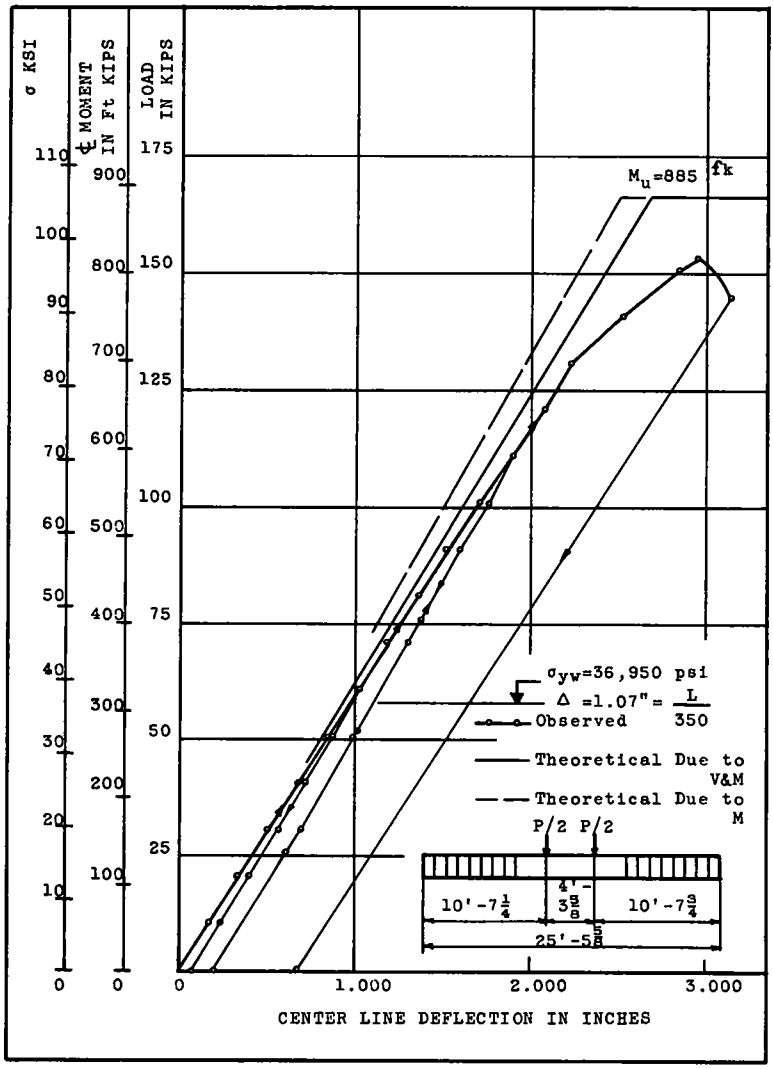

Figure 11. Load deflection curve for test S2 - T3.

Figures 12a and 12b show the measured strains for specimen S1-T1. Figures 13a and 13b show the same for S1-T2. Measured and theoretical strains for specimens S2-T1, and S2-T2 are shown in Figures 14a and 14b and 15a and 15b, respectively.

These results indicate that strains are proportional to stresses, under pure moment condition, even though the web has yielded throughout. Therefore, the assumption of plane sections before bending remaining plane after bending holds true for hybrid girders. The strain gage data indicates that the flanges of the specimens never reached their yield point strain $\Sigma_y = 109.6/30,000 = 0.00365$ in. per in. This was also verified by visual inspection for yield lines in the flanges, as it has been discussed elsewhere.

SUMMARY OF TEST RESULTS

Yield lines were evident in the web at an early load level in all tests. However, no yield lines caused by bending stress were observed in the flanges during any of the tests. The first yield lines always appeared adjacent to the load points, where residual stresses from welding of the bearing stiffeners may be expected to be concentrated.

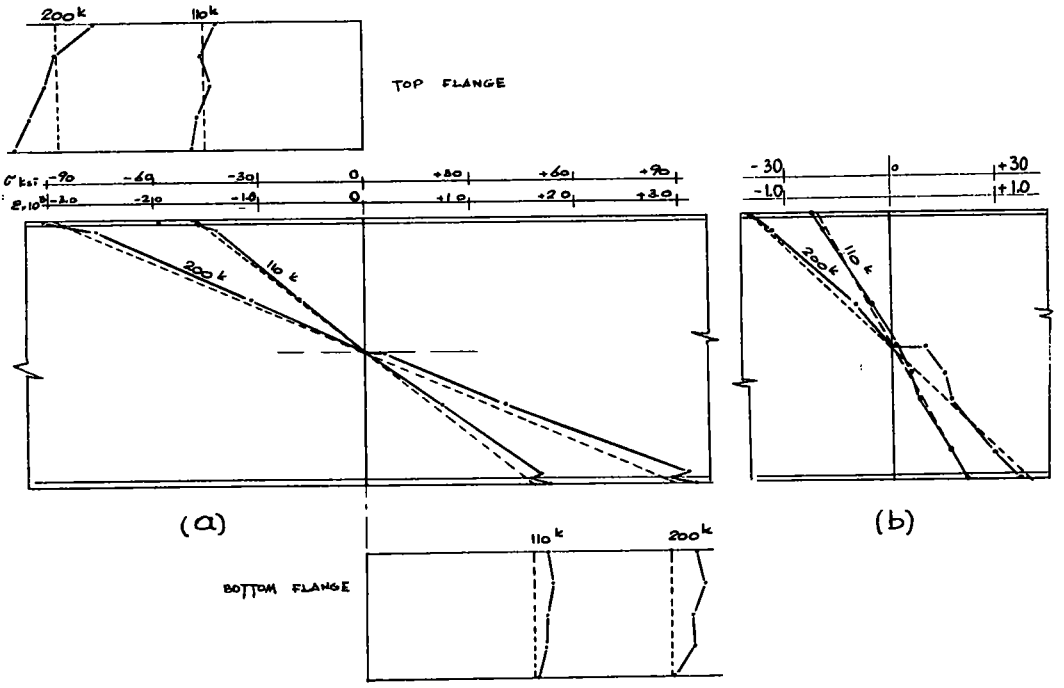

Figure 12. Comparison of measured and calculated strains (specimen S1 - T1). (a) Pure moment section. (b) Moment - shear section.

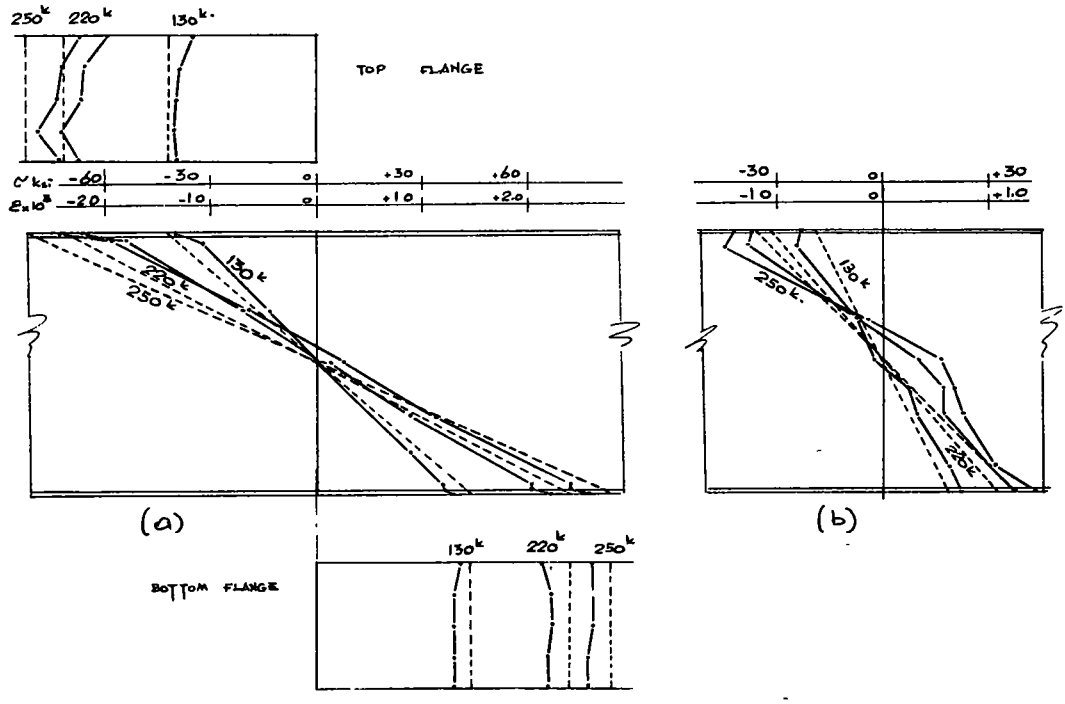

Figure 13. Comparison of measured and calculated strains (specimen S1 - T2). (a) Pure moment section. (b) Moment - shear section.

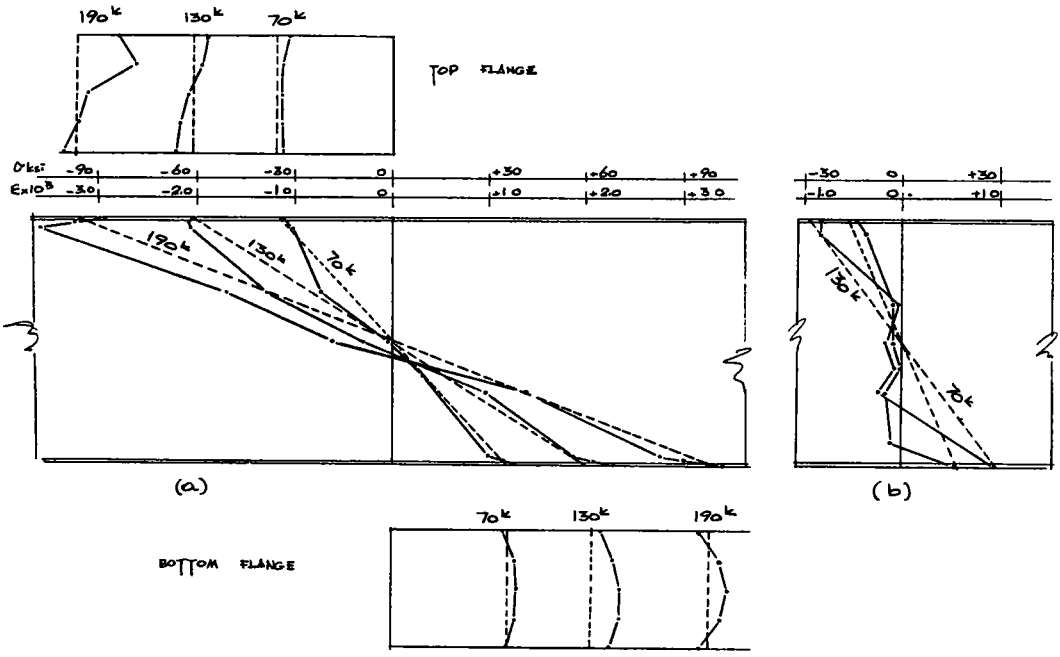

Figure 14. Comparison of measured and calculated strains (specimen S2 - T1). (a) Pure moment section. (b) Moment - shear section.

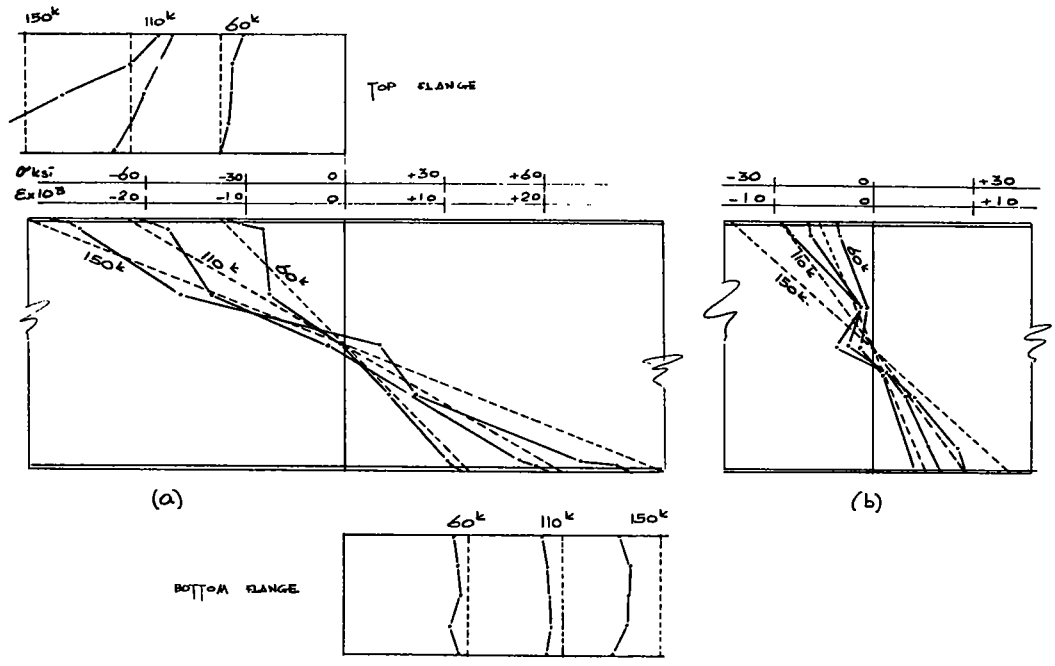

Figure 15. Comparison of measured and calculated strains (specimen S2 - T2). (a) Pure moment section. (b) Moment - shear section.

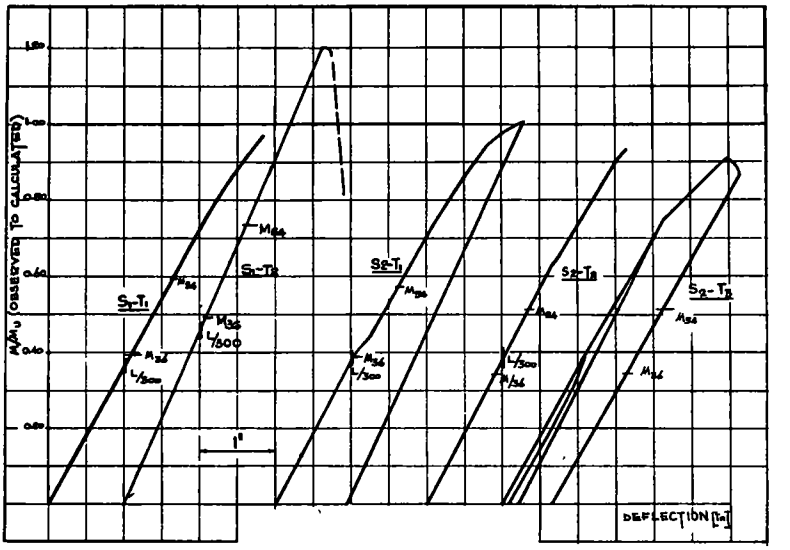

Figure 16. M - Δ curves.

This yielding did not seem to influence the behavior of the specimens because no changes in deflection are evident in any load-deflection curves until after the yield point of the web material is exceeded.

Figure 16 summarizes all the moment-deflection curves and Table 3 gives load factors based on the M_u observed M_{max} and the moments at 36 ksi and 54 ksi extreme fiber stress. The load factors indicate that 36 ksi is a more feasible allowable stress at the present. Examination of the load-deflection curve for test S2-T1 shows an abrupt change as the yield point of the web is reached (see also Fig. 7). This test was also marked by extensive yielding in the end panels.

The load deflection curves for all tests show that behavior of the specimens was very nearly elastic throughout the entire load range. Perhaps the best demonstration of the behavior of a girder of this type can be seen in the curves for tests S2-T1S2 T2S2-T3. These curves show that as yielding takes place in the web a redistribution of stress occurs that permits the member to continue to deform elastically. When the load is removed, residual stresses are induced in the web as the flanges attempt to return to their original shape. When load is reapplied to the member, adjustment of the deflection curve occurs until the residual stresses are overcome and the yield stress of the web is again reached. Such readjustment of the stresses in a member is not detrimental to its behavior; in fact, it is necessary in numerous structural members.

The important fact that was brought out by these tests was that the member continued to act elastically even after a considerable portion of the web had been yielded. A sudden readjustment in deflection may take place as the yield point of the web is reached. This occurred during the testing of specimen S2-T1 and S2-T2, but after that the beam continued upward in a straight line. This would seem to indicate continued elastic behavior in spite of the extensive yielding in the web and shows the dominating effect of the flanges on over-all structural behavior.

TABLE 3

LOAD FACTORS

Test	$\frac{M_u}{M_{36}}$	$\frac{M_u}{M_{54}}$	$\frac{M_{max}}{M_{36}}$	$\frac{M_{max}}{M_{54}}$
S1-T1	2.52	1.65	2.45	1.65
S1-T2	2.04	1.35	2.34	1.56
S2-T1	2.61	1.74	2.70	1.80
S2-T2	2.91	1.94	2.70	1.80
S2-T3	2.91	1.94	2.65	1.76

Deflection of a flexural member varies inversely with the moment of inertia. In an I-shaped member the flanges account for most of the moment of inertia because they are farthest from the neutral axis. When high-strength steel is used for the flanges, the designer can reduce their area to such an extent that the moment of inertia of the section is reduced to a value that is inadequate for deflection purposes. Where the dead load comprises a major portion of the total load, this reduction in cross-section can be overcome by cambering the member an amount equal to the dead load deflection; however, this cambering is not a solution in overcoming excessive live load deflection. The designer must either increase the depth or resort to composite construction.

When stresses as high as 54,000 psi are considered, all specimens in these tests had deflections much larger than the allowable live load deflection of L/800 as specified for bridges by the American Association of State Highway Officials and L/360 as specified for buildings by the American Institute of Steel Construction. This fact cannot necessarily be used as a measure of the usefulness of this type of member because almost all of the load in these tests could be considered as live load. This fact would indicate that the proper place to use this type of member is on long heavy spans where the dead-to-total-load ratio is high. Moreover, when the specimens were designed, deflection considerations were not taken into account. The level of moment at which the extreme fiber stress is 36 ksi and the deflection 1/300 of the span is indicated on all the curves in Figure 16. For the specimens tested, these two points almost coincide for all tests. However, this discussion does not imply that in actual practice this would be the case. In an actual structure designed with 36 ksi, the live load stresses will be only a fraction of this allowable stress and the deflections will be proportionately smaller.

In some of these tests the specimens tended to buckle laterally. Any saving in weight by reducing the size of the flanges can be erased by the need for additional support; however, this would be true only in the negative moment region of continuous spans if the top flange is supported by a slab.

Both the lateral buckling problem and the deflection problem encountered through the use of high-strength steel flanges can be resolved by using composite construction. The use of this method of construction not only furnishes lateral support for the compression flange but also increases the moment of inertia of the section so that it will not deflect as much. Because the stress in the compression flange of a composite section is usually quite low, this flange would not need to be composed of high-strength steel. The use of composite construction seems to offer the most possibilities for the efficient use of high-strength steel and carbon steel combinations.

CONCLUSIONS AND RECOMMENDATIONS

The results of these tests indicate the following:

1. When a girder with high strength steel flanges and carbon steel web is loaded so that the yield point of the web is exceeded, a redistribution of stress will occur and allow the girder to continue to deform elastically. When, after having the load removed, the girder is reloaded, complete elastic behavior extends over a load range almost twice the first range.
2. Girders of this type are particularly adaptable to long heavy spans where the ratio of dead-to-total-load is high and live load deflection is not critical. Also, this type of girder would be adaptable to composite construction in which the slab can be used in positive moment regions to reduce deflections.
3. Deflection and lateral buckling become more important when this type of girder is used because of the reduction in flange cross-section.
4. The fact that the web is stressed beyond its yield strength has little adverse effect on the ultimate carrying capacity of the member.
5. Stresses can be calculated to a high degree of accuracy using ordinary beam theory.
6. Deflections can be calculated by virtual work or any other similar method. When shear deflections are included theoretical deflections check the experimental results to a very good accuracy especially at low loads.

Research to determine the fatigue properties of girders of this type needs to be undertaken. Composite girders with a carbon steel compression flange and web and high-yield strength steel tension flange should be tested. These should be tested with shear connectors over the full length and with shear connectors over that portion of the length where composite action is required for bending stresses.

Hybrid girders are adaptable to construction where static loads are involved and live load deflection is of minor importance. An allowable stress of 36 ksi should insure adequate safety and satisfactory performance. To insure elastic behavior throughout the working stress range, the member could be preloaded during fabrication to redistribute the stresses.

ACKNOWLEDGMENTS

The author wishes to express his thanks to the American Institute of Steel Construction, Texas Structural Steel Institute, the Bureau of Engineering Research, and the Civil Engineering Department, University of Texas, for sponsoring jointly this project.

The author would like to thank Roy Engler of SIRAD Corporation, Austin, Texas, for carrying out the test program reported.

REFERENCES

1. Hollister, L. C., and Sunbury, R. D., "High-Strength Steels Show Economy for Bridges." Civil Eng., 30:60-63 (June 1960).
2. Basler, K., "Strength of Plate Girders." Ph.D. thesis, Lehigh Univ. (Oct. 1959).

Appendix

COMPARATIVE STUDY OF A CARBON STEEL AND HYBRID PLATE GIRDER FOR STATIC LOADS

A design of a hybrid plate girder is presented using constructional alloy steel flanges and low carbon steel (ASTM A 36) web. The design is based on the results of the investigation presented in this report. For comparative purposes, an example of a building plate girder has been worked out using standard AISC specifications for buildings, and ASTM A 7 steel throughout. Figure 17 shows the loads and the dimensions of the simple span plate girder chosen to be designed by both methods.

Design A—Carbon Steel Girder

$V_{max} = 272^{k}$ and $M_{max} = 5,590$ ft K. Calculations for this girder are not presented because design procedures for this are well known and standardized. Figure 18 gives the results of this design.

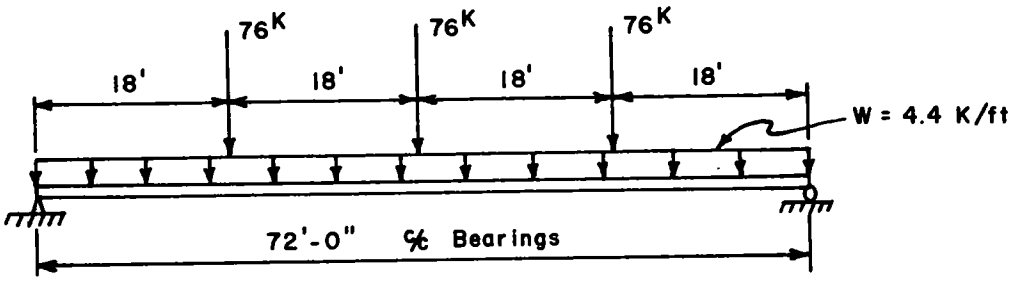

Figure 17. Girder dimensions and working loads.

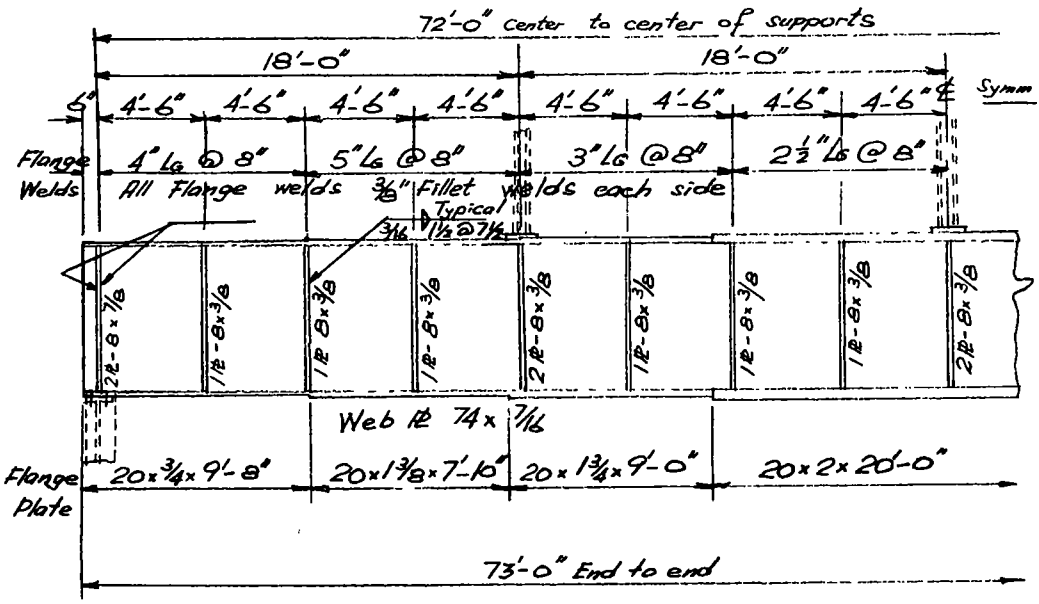

LIST OF MATERIALS		
Item	Plate Size	Weight
Flange	2 - 20" x 2" x 20'-0	5,450
	4 - 20 x 1¾" x 9-0	4,290
	4 - 20" - 1⅜" x 7'-10	2,930
	4 - 20" x ¾ x 9'-8	1,970
Web	1 - 74" x 7/16 x 73-0	8,020
Stiff.	18 - 8 x ⅜ x 6'-2	1,132
	4 - 8 x 7/8 x 6'-2	586
	Total =	24,378 #

Figure 18. Dimensions, and weights for carbon steel girder. (Design A)

TABLE 4

RELATIVE COST ANALYSIS

Design	Weight (lb)			Cost in Place Index		Relative Cost (unit)		
	Flange	Web	Stiff.	Flange	Web and Stiff.	Flange	Web and Stiff.	Total
A	14,640	8,020	1,718	1.0	1.0			24,378
B	7,450	6,900	2,185	1.6	1.0	11,900	9,085	20,985

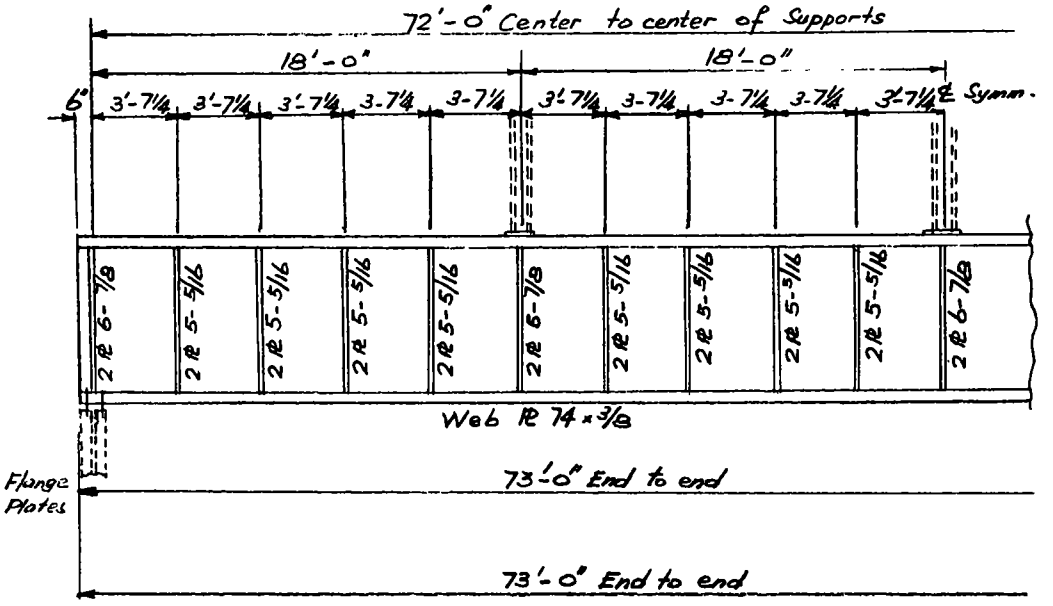

LIST OF MATERIALS		
Item	Plate Size	Weight
Flange	2- 15" x 1" x 73'-0	11,900
Web	1- 74" x 3/8" x 73-0	6,900
Stiff.	32- 5x5/16x6'-2 10- 6x7/8x6'-2	1,065 1,120
	Total =	20,985#

Figure 19. Dimensions, and weights for hybrid girder. (Design B)

Design B—Carbon Steel Web and Constructional Alloy Steel Flanges (Limit Design Method)

Using the same dead loads and live loads just mentioned and a load factor of 1.85 according to AISC plastic design specifications,

$$\text{max. } M = 5,590 \times 1.85 = 10,350 \text{ ft k} \qquad \sigma_\gamma \begin{cases} \text{flange} = 100 \text{ ksi} \\ \text{web} = 36 \text{ ksi} \end{cases}$$
$$\text{max. } V = 272 \times 1.85 = 503 \text{ k}$$

Web Design (2)

Try 74 by 3/8 web (A = 27.8 sq in.)

$$\tau_\gamma = \frac{\sigma_\gamma}{\sqrt{3}} = 20.8 \text{ ksi}; \quad V_p = 27.8 \times 20.8 = 579 \text{ k}$$

$$Z_w = 515 \text{ in.}^3 \text{ and } M_w = (36 \times 515)/12 = 1,545 \text{ ft k}$$

Intermediate Stiffeners

Try 74-in. spacing: $a = 74/74 = 1$; $K = 5.34 + 4 \times 1^2 = 9.34$

$$\tau_{cr} = \frac{k\pi^2 Et^2}{12(1-\gamma^2)b^2} = \frac{9.34 \times 9.87 \times 30 \times 10^3 \times 0.375 \times 0.375}{10.92 \times 74 \times 74} = 6.55 \text{ ksi} < \frac{272}{27.8} = 9.8 \text{ NG}$$

Try 54-in. spacing: $a = 0.73$; $k = 7.47$; $\tau_{cr} = 9.86$ NG

Try 43¼-in. spacing: $a = 0.585$; $k = 6.71$; $\tau_{cr} = 13.8$ ksi > 9.8 OK

Size of stiffeners: $A = 0.0005d^2 = 0.0005 \times 74^2 = 2.74$ sq in. Use two 5- by $\frac{5}{16}$-in. stiffeners.

Check ultimate available shear capacity:

$$\frac{V_u}{V_p} = \frac{\tau_{cr}}{\tau_y} + \frac{\sqrt{3}}{2} \frac{1 - \tau_{cr}/\tau_y}{\sqrt{1 + a^2}}$$

$\tau_{cr}/\tau_y = 13.8/20.8 = 0.664$ and $V_u/V_p = 0.915$. Ultimate shear force $V_u = 0.915 \times 579 = 535$ k.

Design of Flange

Try 1-in. thick flange throughout

$$M_f = \text{max. } M - M_w = 10,350 - 1,545 = 8,805 \text{ ft k}$$

$$A_f = \frac{8,805 \times 12}{100 \times 75} = 14.1 \text{ sq in.}$$

Use 15- by 1-in. plate of constructional alloy steel.

Summary

$V_p = 579$ k, $V_u = 535$ k; $v_{cr} = 27.8 \times 13.8 = 386$ k; and $V_{des.} = 272$ k. Figure 19 gives the dimensions and materials list for design B.

Factors of Safety

Against elastic buckling = 386/272 = 1.42
Against ultimate shear = 535/272 = 1.96
Against ultimate bending = 1.85+

Cost Comparison

Table 4 gives an index of cost for the two plate girders. A relative cost is thus found by assigning carbon steel fabricated and in place the index of 1.00, whereas for constructional alloy steel the index is 1.60. Table 4 shows that use of hybrid girders results in savings. In Design B, girder costs are 86 percent of those in A. The cost reduction could have been larger than 14 percent if thinner plates were used at low moments instead of using 1-in. thick flange throughout.

Flexure, Shear and Torsion Tests on Prestressed Concrete I-Beam

B. C. GERSCH and WILLARD H. MOORE, Texas Highway Department

This paper presents the results of a series of full-scale tests performed to evaluate design procedures, determine ultimate strengths, and answer other design questions concerning prestressed concrete I-beams. To provide this information several beams both with and without compositely acting roadway slabs were tested in moment, shear, and torsion.

Data from these tests are recorded and discussed and some conclusions are drawn. These tests will provide useful information for bridge designers and also serve as a basis for planning further investigations and tests of prestressed concrete I-beams.

•EARLY IN 1959 the Texas Highway Department recognized the need to investigate and evaluate design methods and criteria currently in use by the department in designing prestressed concrete I-shaped beams. Some of the design methods and criteria used in designing these prestressed concrete beams were theoretical in nature and not completely substantiated by experimental evidence. Also, some of the methods used by the Texas Highway Department were not in general use by other State highway departments. This series of tests was performed to verify design methods and criteria and to provide new information on prestressed concrete I-beams.

Current design practice of the Texas Highway Department was to design prestressed concrete beams with composite slabs using the same modulus of elasticity for both slab concrete and beam concrete. The beams were considered to act compositely with the slabs without the presence of shear keys in the top of the beams. The evaluation of the soundness of these design assumptions was one of the objectives of this investigation.

At the time these tests were undertaken there was no well-established method for calculating ultimate moment and shear capacities of prestressed concrete I-beams with compositely acting slabs. Also unknown was the effect of occasional overloads on such members and whether these overloads would produce permanent and excessive deflections in the member. Identification of these ultimate moment and shear capacities and new knowledge concerning overloading were further objectives of the investigation.

The final concern of this investigation was the reaction of a prestressed concrete I-shaped beam to a torsional load. Because little information was available on this subject, tests were conducted to provide new data that might indicate the allowable value of resisting moment and angular rotation that these beams were capable of withstanding.

EXPERIMENTAL CRITERIA

Beams

The beams tested were of I-shaped cross-section and of the type designated as C-beams by the Texas Highway Department. Roadway slabs were cast on two test beams to provide a composite section for investigation under shear and flexure loadings. One of these beams was a standard pretensioned beam, and the other was a nonbonded post-tensioned beam. The pretensioned beam was not loaded to complete flexural failure so that shear tests could be made on the ends of the beam. To determine the effect of end blocks on the beam, one end of the beam was cast with an end block and the other without. Percentage of stirrup reinforcing steel was the same for both ends of the beam.

Two beams were tested as noncomposite sections; one beam in bending and the other beam in torsion. The beam tested in torsion was a beam that had been rejected from a bridge project due to excessive honeycombing at one location in the beam.

Design

The elastic theory was used for prestressed concrete members under design loads at working stresses. Assumptions were made that (a) strains will vary linearly over the depth of the member throughout the entire load range; (b) before cracking of the concrete, stress is linearly proportional to strain; (c) after cracking of the concrete, tension in the concrete will be neglected; and (d) for the composite section, the modulus of elasticity used was that calculated for the beam concrete.

Temporary allowable stresses in the concrete before losses are 0.60 f'ci in compression and $6\sqrt{f'ci}$ in tension where f'ci is the compressive strength of the concrete at initial prestressing. Minimum allowable f'ci = 4,000 psi. Allowable stresses at design load, and after losses have occurred, are 0.40 f'c in compression and zero in tension where f'c is the compressive strength of the concrete at 28 days.

Prestressed members were designed for a computed ultimate load capacity of not less than 1.5 dead loads plus 2.5 live loads including impact. Beams were designed to act compositely with the roadway slab so that failure of the steel rather than of the concrete would occur at ultimate loading.

Section Properties

Pretensioned members conformed to the beam properties shown in Figure 1, which also shows a composite slab cast integrally with the beams. Prestressing forces are applied with 45⅜-in. diameter stress relieved strands at 14,000 lb per strand. Figure 2 shows the configuration of the post-tensioned beam with a composite slab. This beam was designed with the same assumptions and allowables as the pretensioned beams and differs only by the change in type of stressing. The post-tension tendons A, B, and C are 13¼-in. diameter stress relieved wires, and tendons D, E, and F are 10¼-in.

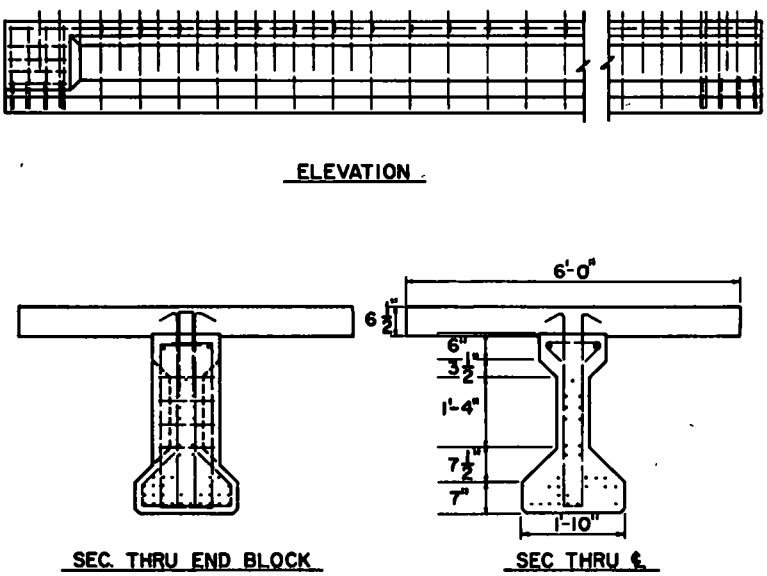

Figure 1. Pretensioned test beam details.

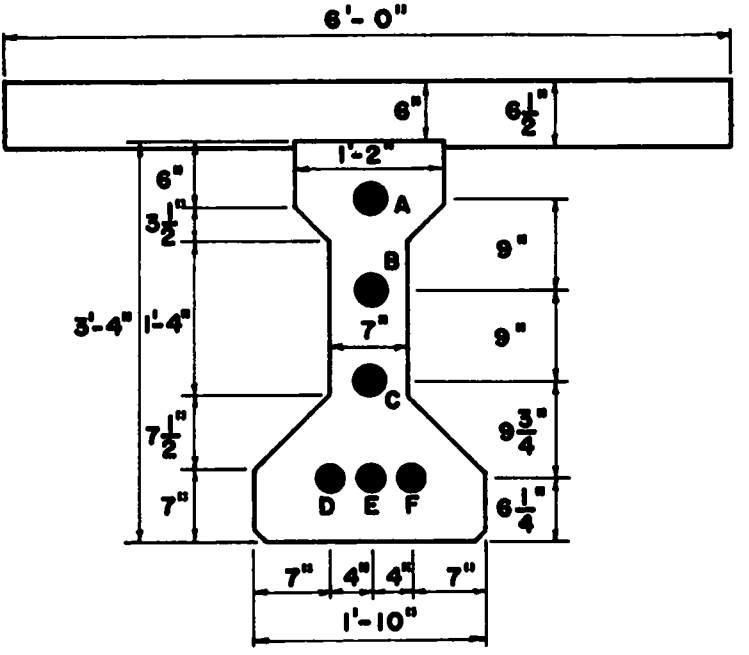

Figure 2. Post-tensioned test beam details.

diameter stress relieved wires. These wires were not grouted in their conduits. This beam was designed to produce the same initial and final design stresses as those produced by the pretensioned beams.

Concrete

Specifications for beams require Texas Highway Department Class F concrete having a compressive strength of 5,000 psi in 28 days. Maximum size of the coarse aggregate used was 1 in. A cement factor of 6.50, a water factor of 5.25, and a workability factor of 0.82 was used. Measured average slump per batch was 3 in. Specifications for slab concrete require Texas Highway Department Class A concrete having a compressive strength of 3,000 psi in 28 days.

Steel

Prestressing steel was $\frac{3}{8}$-in. diameter stress-relieved seven-wire strands with a minimum specified ultimate strength of 250,000 psi. Post-tensioning tendons were made of $\frac{1}{4}$-in. diameter stress-relieved steel wire with a minimum specified ultimate strength of 240,000 psi. Plain reinforcing steel for stirrups, etc., was intermediate grade billet steel.

TESTING EQUIPMENT

Permanent testing facilities were constructed at Texas Highway Department District 14 Headquarters in Austin to accommodate the testing of these beams and for use in any future testing programs that might be undertaken. A concrete slab 8 ft wide, 12 in. thick, and 102 ft long was cast to form a smooth-working surface. Two movable concrete abutments served to support the beams while testing. A steel frame built of 12BP53 steel members straddled the testing bed to provide a loading yoke for the jacking systems. The legs of the loading yoke were sunk 10 ft deep into 24-in. diameter shafts drilled 20 ft through layers of shale and Austin chalk. Ten $1\frac{1}{8}$-in. diameter reinforcing bars were welded to the loading frame legs and extended into the 3-ft diameter

bells on the bottom of the concrete-filled drilled shafts. At appropriate distances from the loading yoke, 18-in. diameter drilled shafts were located under the test bed to provide support for the abutments under the high reaction loads required in the shear tests.

Load was applied to the beam by one of two jacking systems. The first jacking system consisted of two 100-ton capacity hydraulic jacks connected in series to provide a total capacity of 200 tons. High pressure lines connected the jacks to a manual pumping unit on which a pressure gage and a relief valve were mounted. This system was calibrated in a verified hydraulic testing press before use in the tests. The second jacking system used a single 150-ton capacity jack with the same pumping system.

INSTRUMENTATION

Stresses in the composite pretensioned beam were estimated by measuring strains, determining Young's Modulus of representative specimens of the material under strain, and calculating the stresses from the relation between these data. Strains were measured (a) electrically by means of bonded wire strain gages, and (b) mechanically by means of a 20-in. Berry strain gage.

For the electric strain gages the SR-4, Type A-9 gage was selected. Concrete is recognized as a heterogeneous mixture of discrete particles. The largest particles, in this particular case, were about 1 in. in maximum dimension, which is as large as or larger than the usual electric strain gage. The A-9 type with its 6-in. gage length extends over a sufficient distance to be affected by a statistically representative portion of the material under test, yet is small when compared to the size of the beam.

For the moment test on the composite section, the gages were arranged in longitudinal lines on both sides of the beam and in transverse belts around the beam called stations. Two lines of gages extend along the top of the floor slab immediately above the upper flange of the beam, 5 in. to each side of the longitudinal centerline, and two lines were similarly placed along the underside of the lower flange. All of the previously mentioned gages were oriented with their major axes parallel to the longitudinal centerline of the beam. At the quarter points and at midspan, gages were placed on the top and bottom of the roadway slab at the center of the overhang on both sides. These gages had their major axes perpendicular to the longitudinal centerline. The arrangement of the gages is shown in Figure 3.

In the case of the shear test on the end of the beam having a conventional end block, the gages were arranged as shown in Figure 4. In the delta strain rosettes on either side of the beam, 7 ft 9 in. from the end, one gage was vertical and the other two placed so as to complete an equilateral triangle. This orientation was chosen in anticipation

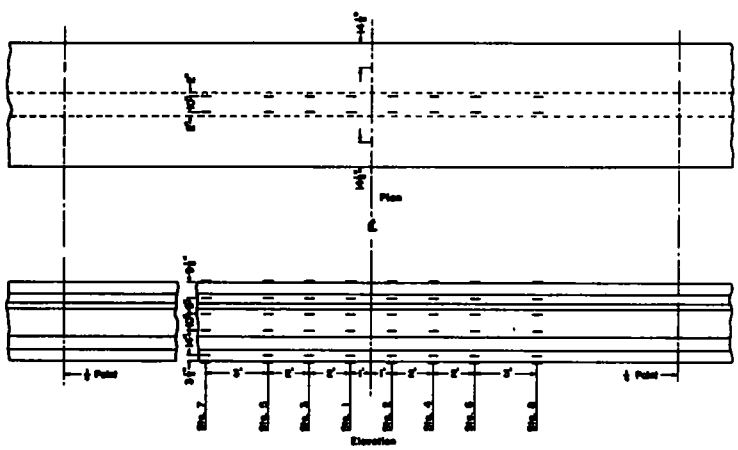

Figure 3. Strain gage locations, composite moment test, pretensioned beam.

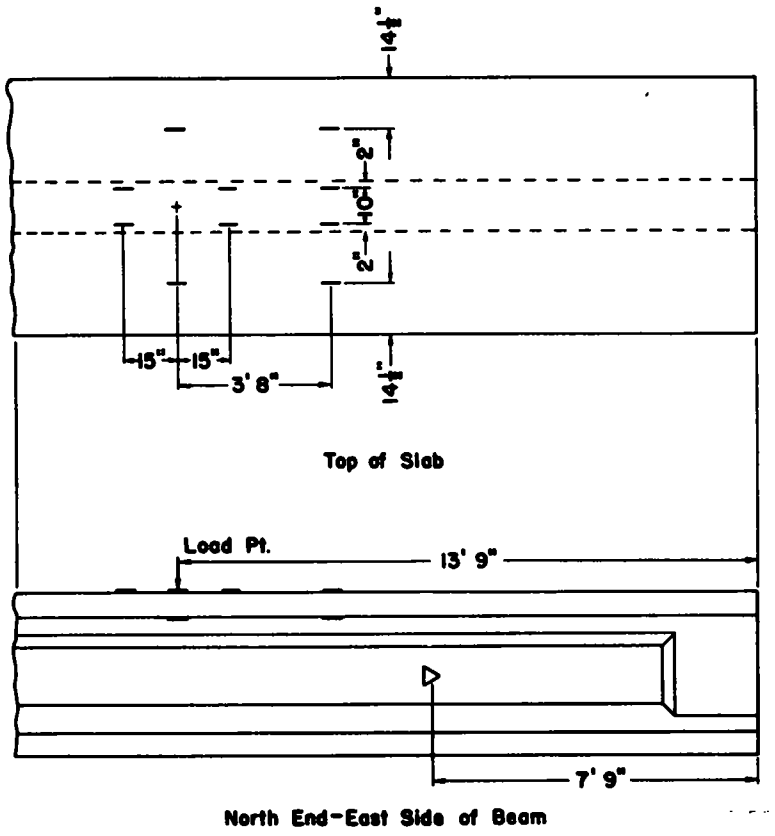

Figure 4. Strain gage locations, composite shear test, pretensioned beam.

that the direction of the major principal stress would be very nearly parallel to one of them. The strain gages on the top and underside of the floor slab had their major axes parallel to the longitudinal centerline of the beam. No strain gages were placed on the opposite end of the beam for the shear test at that point.

In the noncomposite moment test (i.e., on the beam without a roadway slab), the gages were placed in the pattern used for the composite beam test except that only four belts of gages were used, those in Stations 1, 2, 3, and 4 as shown in Figure 3. Also, those longitudinal gages previously located on the slab were now mounted directly on top of the beam.

The compensating or dummy gages were attached to concrete cylinders made from the same concrete batch used in casting the beams. These cylinders were cured with the beams and kept with them during each move.

To apply the gages to the beam, the locations were marked and the necessary area ground smooth with an offset grinder. A dark smear left by the adhesive in the abrasive disc interfered with the adhesion of epoxy cement to the concrete and final surface preparation was by sand blast. After sand blasting each position, a smooth thin layer of Armstrong A-1 epoxy cement was applied to a 1- by 10-in. area. When this layer had hardened, a pressure sensitive cement was used to fasten the gages to the epoxy layer. Gage leads were cemented to the epoxy layer with small additional quantities of epoxy cement. After the lead wires had been soldered to the gage leads, several coats of Di-Jell waterproofing wax were applied to each installation, extending well up on the insulation of the lead wires. The layer of epoxy, purposely kept very thin, served to insulate the gages from the beam, and the wax layer provided protection from the weather. All lead wires were cut to a 23 ft length. The cables contained eight

No. 22 AWG stranded, insulated copper wires. Color coding was helpful in following connections. The opposite end of each wire was soldered to a banana jack in a plexiglass switching panel. Eight wires with banana plugs soldered to both ends were used to connect the switching panel to the measuring bridge.

The bridge circuit used to measure the strain indicated by the gages was built especially for this application. It was patterned after a circuit published by Matlock and Ripperger (1) and is shown schematically in Figure 5. Essentially, it is a Kelvin double bridge with dual leads to the active and dummy gages, which serve to reduce or eliminate temperature effects in the lead wires, and with voltage splitters of selected resistance at the battery corners to reduce the error caused by small differences in contact resistance at the switching panel. The equations describing the reduction of error are discussed by Matlock and Thompson (2). In this adaptation resistances R_1 and R_2, R_3 and R_4, R_5 and R_6, R_B and R_D are selected pairs of nominal 300-ohm strain gages whose actual measured resistances are equal to the nearest 0.01 ohm. These pairs of gages were cemented to 1½- by ⅛-in. mild steel straps supported in a vertical position. R_7, R_8, and R_9 are short connectors of extremely low resistance. The helical slide wire consisted of 112 ft of No. 12 B & S Manganin wire having a resistance of 0.043 ohms per ft wound in 73 turns about a grooved Lucite cylinder 6 in. in diameter and 19 in. in length. The sliding contact was mounted so that it could be placed on any desired turn of wire. Consequently, no more than one complete revolution of the cylinder was required for balancing and it was possible to make fixed connections to the ends of the coil, rather than brush contacts. A sensitive Brown Electronik null indicator connected as shown in the diagram completed the bridge. Everything inside of the dashed line in the drawing was mounted in a box with a hinged lid.

Calibration of the slide wire was accomplished by the following procedure. A-9 strain gages from the lot to be used in the project were connected into the active and dummy positions of the bridge. The dummy was shunted with a 20,000-ohm fixed resistor; the slide wire contact was placed near one end of the coil and the bridge was

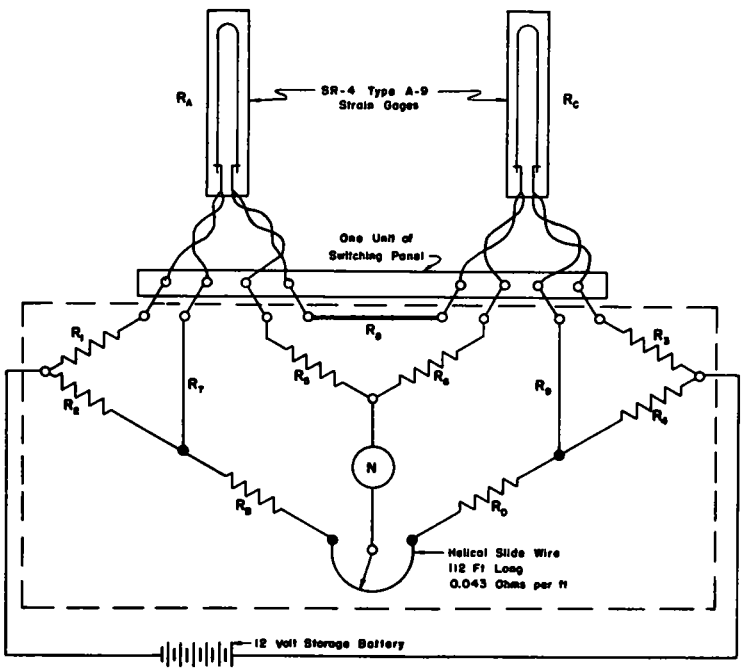

Figure 5. Bridge circuit used for measuring strains.

balanced by means of a variable decade resistance (Dekabox) shunted across the active arm. A mark was made on the slide wire cylinder. Then the variable resistance was changed by a calculated amount that resulted in a change of unit resistance of the active bridge arm equivalent to 25 μ in. per in. of strain. The bridge was balanced by moving the slide wire contact and a new point on the cylinder was marked 25. Many repetitions of this procedure served to calibrate and mark the entire slide wire coil. A distance of approximately 2½ in. on the wire was equivalent to 25 μ in. per in. of strain. A vernier scale fastened to the contact arm close to the coil made it possible to read strain to the nearest 1 μ in. per in.

In use, the bridge was balanced for each gage with no load applied to the beam and the balance point recorded. When the gages were strained a new balance point was determined for each one and the difference between initial and subsequent readings indicated the strain produced by the loading. If strain gages having a gage factor different from that factor used in this calibration are employed, the readings must be corrected by the ratio of the two gage factors.

In the moment test of the composite beam full advantage was not taken of the dual lead feature because single leads connected the gages to the switching panel. Dual leads connected the panel to the bridge. Because there was a dummy gage and all leads were of the same material, length, and exposure, the temperature compensation was adequate. Matlock and Ripperger (1) point out additional precision could have been realized by reversing the battery connections and gage leads on every reading and taking an average of the four values of strain thus obtained.

In the mechanical measurement of strains, reference points for the 20-in. Berry gage were on steel discs (⅛-in. slices from a No. 5 reinforcing bar) that were bonded to the beam at 10-in. intervals with Armstrong A-1 epoxy cement. Thus, it was possible to set overlapping 20-in. gage lengths with the standard punching template. The punch marks were then deepened with a No. 54 drill. There were gage lines containing twelve such points on both sides of the beam at midheight of the web and along the lower flanges 6 in. above the bottom. These lines extended 55 in. left and right of the center of the beam. Strains were measured after every increment of load was applied. This system of measurement was intended to insure that test data should be available even though damage might cause the electric strain gage circuits to become inoperative or unreliable.

Wood scales made from 2-ft lengths of folding rules were fastened in vertical and horizontal positions at the bearing points, center, and quarter points of each beam. These scales were nailed to blocks and braces that had been set in epoxy cement and could be read accurately to $\frac{1}{100}$ ft. A precise level stationed about 50 ft from the beam was used to read vertical movements, and a theodolite stationed about 50 ft beyond one end of the beam was used to read horizontal movements.

To measure deformations in the first torsion test, a large protractor type scale having a radius of 19 in. was fastened to the top of each end of the beam. The smallest division of this scale was 15 min. A heavy pointer was fastened to the center of the scale on a loose-fitting pin. As the beam was twisted, the scale moved; but gravity kept the pointer vertical so that the difference in initial and final readings indicated the angle of deformation. It was apparent in the course of the first test that greater precision in measuring the angle of deformation was desirable, so another device was constructed for the second test. A horizontal arm extending equally to each side of center was fastened to the bottom of the beam at each end. Two-ft sections of these mentioned wooden scales were hung on loose pins at the outer ends of the cross pieces, exactly 3.438 ft left and right of center of the beam. Metal weights fastened to the bottom of these free-swinging scales kept them in a vertical position. Initial rod readings were taken on each of these scales with a precise level at no load and at each increment of load. The length of these gage arms (3.438 ft) was selected so that when one-half of the algebraic sum of the rod deflections is 0.060 ft, the angle of rotation of the beam is 1°.

Bourdon gages (Carver) of appropriate capacity were connected into the oil pressure lines to the hydraulic jacks. Each jack and gage combination was calibrated in a press that had been verified by precision instruments. Large-scale calibration curves were used to convert hydraulic pressure to load in pounds.

Portable radio sets were used to coordinate the activities of the several people involved in the tests. They were particularly useful when possible danger from flying fragments made it advisable to work behind protective barricades.

EXPERIMENTAL INVESTIGATIONS

Composite Moment Test

A standard pretensioned beam was placed on the testing bed for investigation under moment loading. The beam was seated on a 6- by 18- by ¾-in. 70 durometer neoprene bearing pad as is usual in bridge construction. A compositely acting slab 6½ in. thick and 6 ft wide was cast on this beam with all formwork being supported by the beam. The over-all beam length was 59 ft 6½ in. with a center-to-center-of-bearing length of 58 ft 10½ in. The dead load of the slab caused a 5/16-in. deflection in the beam. Longitudinal strains and horizontal and vertical deflections were recorded at predetermined increments of load. Standard cylinder tests were made of beam and slab concrete samples taken at the time of pour. Beam cylinders had an average compressive strength of 8,923 psi and the slab cylinders had a compressive strength of 5,215 psi. Calculated modulus of elasticity of the prestressed concrete was 4.91×10^6 psi.

AASHO H20-S16 design load for this span length and beam spacing was found equivalent to a concentrated load of 41.7 kips including impact. Based on the composite section, initial cracking was calculated to occur at a load of 76 kips or dead load plus 1.82 live loads. Ultimate design according to the AASHO Specification used is 1.5 DL + 2.5 (LL+I) or 193.65^{K}. For comparison with final concentrated loads, only an ultimate load of .5 DL + 2.5 (LL+I) or 134.1^{K} is used as one dead load is already acting on the beam. Load in increments of 8 kips was applied at midspan of the beam until a total load of 65 kips was reached. No cracking of the beam or slab was noted. Load increments were then reduced to 4 kips and the total load was increased to 76 kips. In the loading increment from 76 kips to 80 kips initial tensile cracking in the bottom of the beam was observed. Vertical deflection at this load was 0.028 ft. Tensile strain on the bottom of the beam was 260μ in. per in. Compressive strain at the top of the slab reached 193μ in. per in. Eighty kips of load corresponds to 1.92 live loads.

The first loading cycle was continued in increments of 4 kips until a total of 130 kips, or dead load plus 3.12 live loads, was reached. Tensile strain measurements were no longer reliable due to the multitude of flexural cracks that had penetrated up into the top flange of the beam. Flexural cracking had been induced over a region approximately 8 ft on either side of the loading point. Compressive strain in the top of the slab had now reached 520μ in. per in. Vertical deflection at midspan had reached 0.180 ft. At this point the load was released and a check on initial deflection readings showed no residual deflection left in the beam.

Three loading cycles were employed to complete this test due to the excessive time required to record the readings of the 108 strain gages plus the deflection readings. In the first cycle of loading, compressive strains in the slab were very large, whereas on subsequent loadings the relaxation of strain differentials between the beam and slab and redistribution of strains within the slab, showed smaller strains. Figure 6 shows load vs strain, with the average of strains measured at Stations 3 and 4.

The second loading cycle began and the load was quickly brought up to the 130-kip load which marked the termination of the first loading cycle. To facilitate the plotting of a smooth curve a few measurements of strains and deflections were made in this range. Load increments of 4 kips was then applied until a total load of 160 kips or 3.84 live loads was on the beam. Vertical deflection at midspan had reached 0.457 ft. Compressive strain in the slab now reached 928μ in per in. Total load was increased to 164 kips at which point flexural cracking in the bottom of the slab was noted. Flexural cracking had progressed outward to each quarter point of the beam. Cracks had extended the complete depth of the beam in the area 3 ft to either side of the loading point. The load was released and a residual deflection of 0.046 ft was recorded.

Loading for the third cycle was begun and the total load brought up to 168 kips or 4.03 live loads or 1.25 times ultimate loading. Vertical deflection reached 0.552 ft with a measured compressive strain of 1,057 μ in. per in. Flexural cracking of the slab

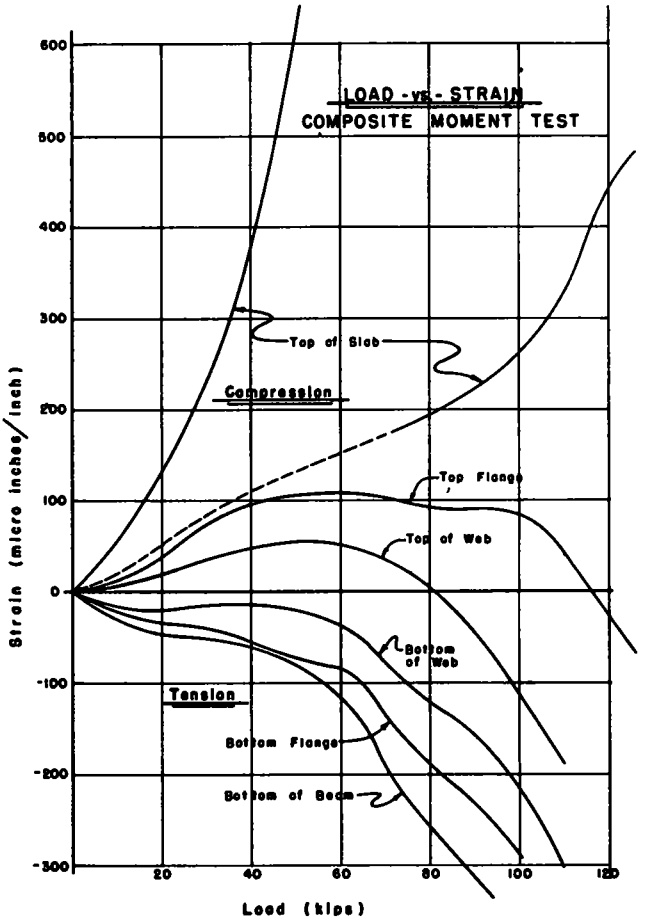

Figure 6. Load vs average strain, composite moment test, pretensioned beam.

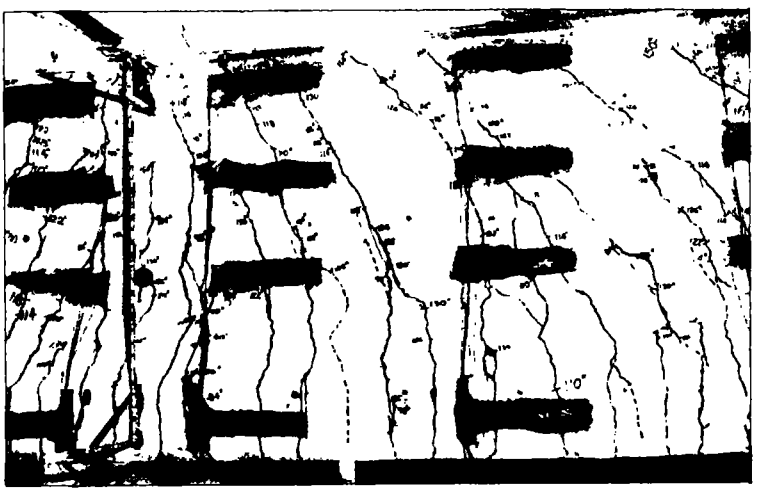

Figure 7. Load vs deflection, composite moment test, pretensioned beam.

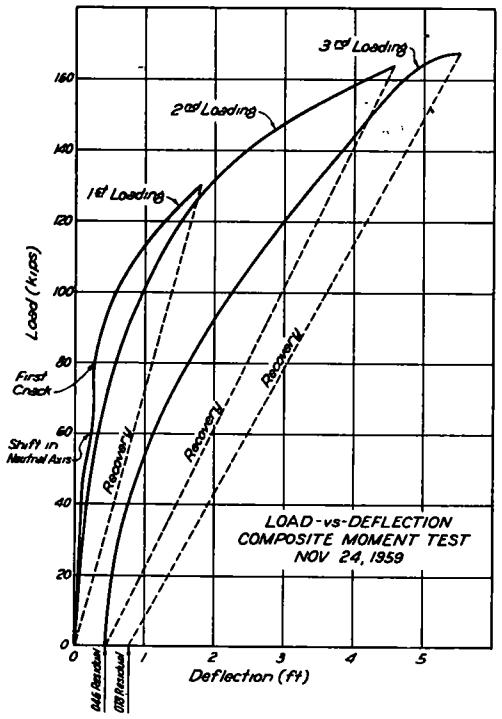

Figure 8. Cracking pattern, composite moment test, pretensioned beam.

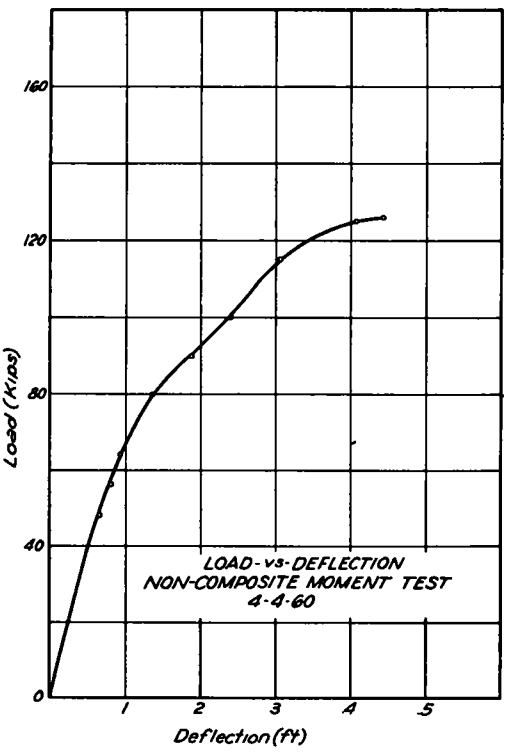

Figure 9. Load vs deflection, noncomposite moment test, pretensioned beam.

penetrated approximately 2½ in. Flexural cracking of the beam under the loading point was extensive, as shown in Figure 7. Figure 8 shows a load vs deflection.

At this point it was decided to discontinue loading to keep the beam intact for use in other tests. On release of the load, the beam showed a total residual deflection of 0.078 ft.

Noncomposite Moment Test

For the noncomposite moment test a standard pretensioned beam was used without a slab cast on the beam. The over-all beam length was 59 ft 6½ in. with a distance center to center of bearing of 58 ft 10½ in. Longitudinal strains along with vertical and horizontal deflections were measured. Standard cylinder tests were made of beam concrete samples taken at time of casting of the beam. Compressive strength of the concrete at the time of testing was 9,126 psi. Calculated cracking load was 67^{k}.

Load increments of 16 kips each were placed on the beam until a total load of 64 kips was on the beam. Deflection reached 0.095 ft under this load as shown in Figure 9, a plot of load vs deflection for this test. Tensile strains on the bottom of the beam showed 480μ in. per in. of strain induced with compressive strains on the top of the beam of 600μ in. per in. Figure 10 is a plot of load vs average strains measured at Stations 3 and 4. Loading continued to 80 kips where initial flexural cracking was observed in eleven places. Vertical deflection was 0.137 ft with a compressive strain of 925μ in. per in. and a tensile strain of 940μ in. per in. Later observation of the plotted strain indicated that minute cracking could have been present around a load of 64 kips, and a measured tensile strain of 495μ in. per in., without having been detected. At 100 kips, compressive strains reached 1,575μ in. per in. on the top of the beam. Recorded deflection at midspan was 0.239 ft. Flexural cracks had increased in number and length

until cracks were present approximately 7 ft to either side of the loading point and had extended high into the web. Continued loading to 125 kips produced the beginning compressive failure in the top of the beam. At 127 kips, complete collapse of the beam occurred. Deflection at 125 kips reached 0.409 ft, and measured compressive strain was 1,809 μ in. per in. Figures 11, 12, and 13 show the extent of failure in the beam.

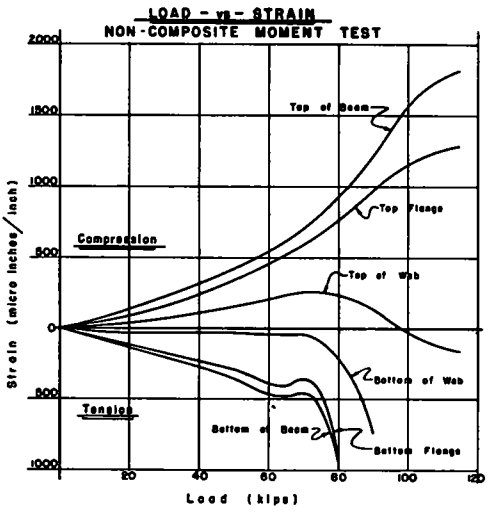

Figure 10. Load vs average strain, non-composite moment test, pretensioned beam.

Composite Shear Tests

Because of the limited number of beams available, the beam used for the composite moment test was also used for the shear tests. This beam was cast without an end block on one end. Flexural cracks were present in the center portion of the beam, but were not expected to be of major importance other than possibly resulting in larger deflections. However, these cracks did influence the choice for location of a loading point for the shear tests. If the load point was located from 1D to 4D, D being the depth of the beam, away from the reaction then a shear compression type of failure would be expected to occur. Loading in a range from 4D to 7D should result in unrestrained diagonal tension failure. Unfortunately, the presence of the flexural cracks forced the loading point into the shear compression failure range. Loading point for both shear tests was located 13 ft 5 in., or 3.5 D, from the reaction. Strain measurements were made only on the section that had the end block. For both tests the vertical and horizontal deflections were recorded. Hydraulic jacks supplied the load to the sections.

Figure 11. Beam failure, noncomposite moment test, pretensioned beam.

Figure 12. Beam failure, noncomposite moment test, pretensioned beam.

Figure 13. Beam failure, noncomposite moment test, pretensioned beam.

Test Without End Block.—Load increments of 20 kips each were placed on the beam until a total load of 140 kips was reached. Deflection reached 0.093 ft at the load point. In the loading increment from 140 to 160 kips, flexural cracking occurred under the loading point and extended high into the web. Increments of load were reduced to 10 kips and the total load brought up to 200 kips. In this loading range only flexural cracking was observed. Figure 14 shows the deflection under the load point had increased to 0.210 ft. This load of 200 kips was held on the beam for about 5 to 10 min while the crack pattern was being marked. Just before loading was resumed there was a sharp report and two diagonal tension cracks appeared between the loading point and the near reaction. These cracks were at an approximate angle of 25° to the bottom of the beam and extended through the web and into the upper and lower flanges. Only a slight increase of 0.002 ft in deflection was noted. Two short cracks, inclined at about the same angle, appeared and were contained in the web above the bearing point in the region the end block normally occupies. Loading continued to 210 kips where two additional diagonal cracks appeared nearer the loading point and extended through the bottom of the beam. Loading continued to 230 kips with a recorded deflection of 0.310 ft. Additional flexural cracks appeared and the initial diagonal tension cracks lengthened. Due to darkness, loading was discontinued and the load released with a residual deflection of 0.027 ft noted.

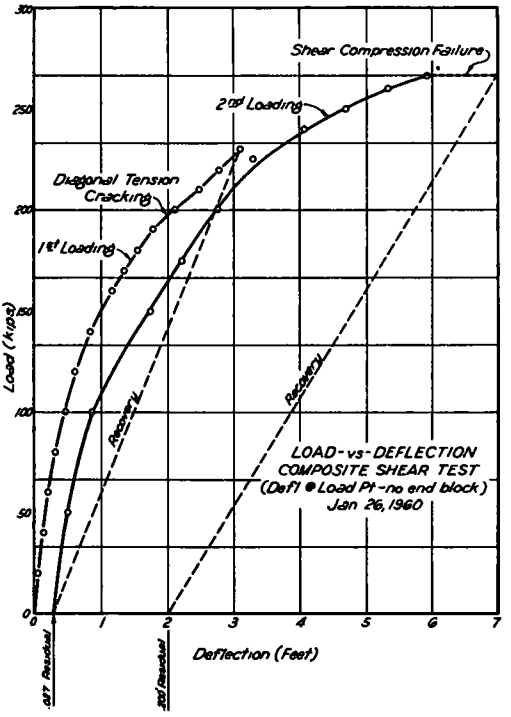

Figure 14. Load vs deflection, composite shear test.

Loading for the final cycle began with large increments of load being applied until a total load of 250 kips was placed on the section. Diagonal tension cracks turned in the lower flange and were parallel to the bottom of the beam. Slight cracking was noted in the lower surface of the slab. Deflection under the loading point had reached 0.590 ft. At 266.25 kips, continued deflection with no increase in load was noted. Loading was discontinued at this point. With this load maintained on the beam, a radiograph gamma ray exposure was made of the stirrups intersecting the most critical diagonal tension cracks. No evidence of fracture of the stirrups was noted. A final deflection of 0.700 ft was recorded.

Initial diagonal tension failure occurred at an equivalent design load of 1 dead load plus 6.54 live loads including impact.

Final inspection of the beam showed a longitudinal split in the bottom of the beam approximately 2 ft long and located 4½ ft from the loading point toward the near reaction: Figures 15 and 16 show the final cracking pattern of the beam, and Figure 17 shows the longitudinal and transverse cracking of the slab.

Test With End Block.—For the second test it was decided to measure strains in the slab and in the web region where diagonal tension failure was expected to occur. Figure 4 shows the location of the electrical strain gages used. Vertical and horizontal deflections were recorded at the center of bearings and at the loading point.

Load in 20 kip increments was applied until initial flexural cracking under the load point occurred at 160 kips. Compressive strains in the slab reached 275 μin. per in. with a vertical deflection of 0.129 ft. Figure 18 shows a plot of load vs deflection. Principle strain components of the web in the horizontal direction measured 276 μ in.

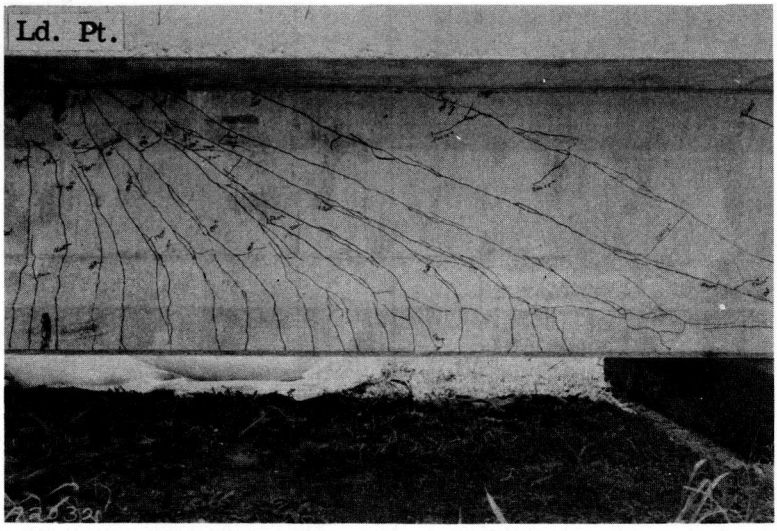

Figure 15. Cracking pattern, composite shear test, pretensioned beam.

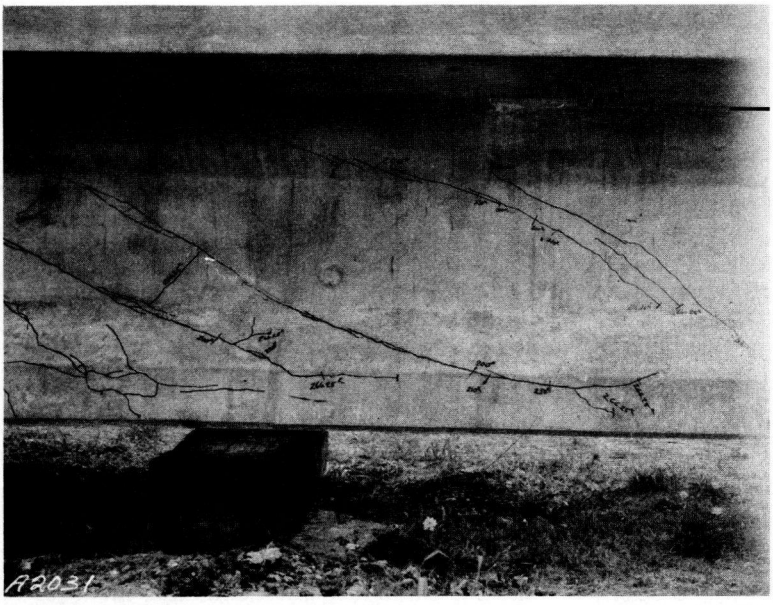

Figure 16. Cracking pattern, composite shear test, pretensioned beam.

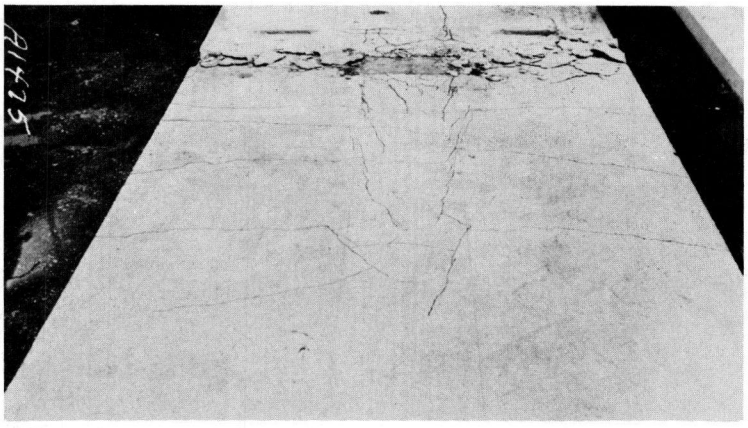

Figure 17. Slab-cracking pattern, composite shear test, pretensioned beam.

per in. with 66 μ in. per in. measured in the vertical direction. At 190 kips, compressive strains in the slab reached 491 μ in. per in. with a vertical deflection of 0.205 ft. Diagonal tension failure occurred before rosette strains in the web could be read. Flexural cracking had extended high into the upper flange of the beam. Three diagonal tension cracks occurred and were inclined at an angle of approximately 25° from the bottom of the beam. No cracks appeared above the bearing point as occurred in the test without the end block. Loading continued up to 240 kips where initial flexural cracking in the bottom of the slab was noted. Flexural cracking continued near the loading point with a small increase in length of the diagonal tension cracks. Loading continued to 260.45 kips where compression failure of the slab occurred. Deflection at this point reached 0.607 ft. Compressive strains in the slab had reached 1,801 μin. per in.

Initial diagonal tension cracks occurred at an equivalent design load of 1 dead load plus 4.56 live loads including impact. Shear compression failure occurred at 1 dead load plus 6.25 live loads, including impact. As in the previous test, longitudinal cracking in the bottom of the beam was noted. Figures 19 and 20 show the final cracking pattern of the beam, and Figure 21 shows longitudinal cracking of the slab.

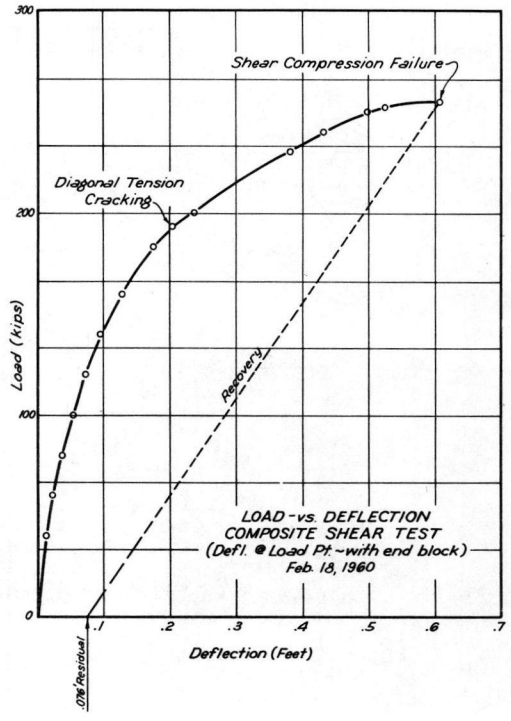

Figure 18. Load vs deflection, composite shear test, pretensioned beam.

Composite Moment Test (Post-Tensioned Beam)

This post-tensioned beam with nonbonded tendons was not in the original testing schedule. However, as the beam was made available at the time the other beams were being tested it was felt that worthwhile knowledge could be gained from testing it also. A 6½-in. thick, 6-ft wide, compositely acting slab was cast

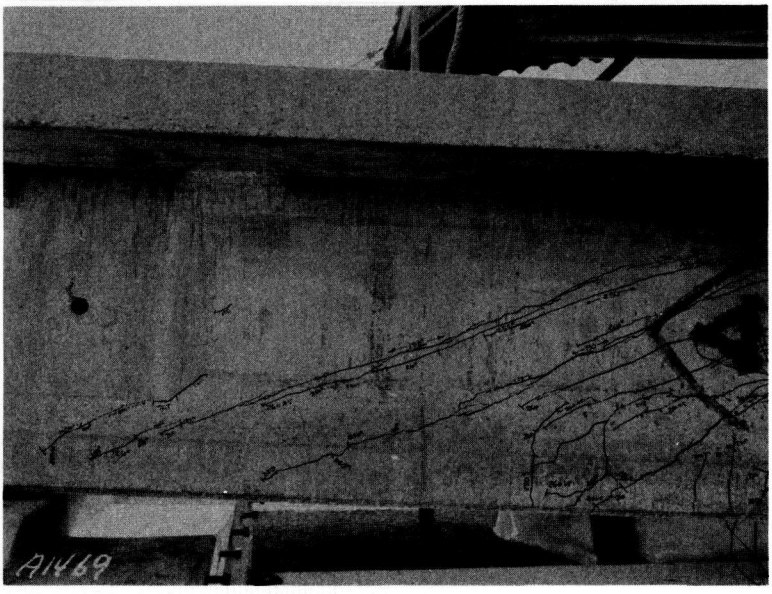

Figure 19. Cracking pattern, composite shear test, pretensioned beam.

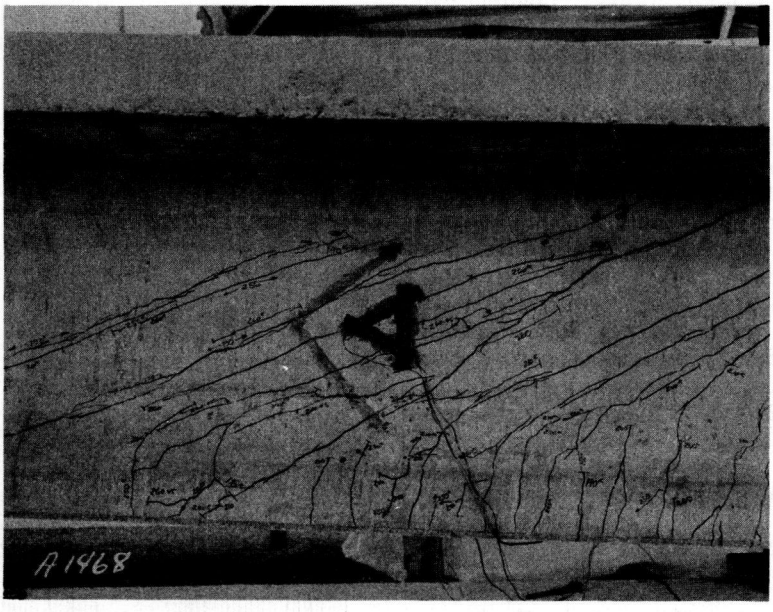

Figure 20. Cracking pattern, composite shear test, pretensioned beam.

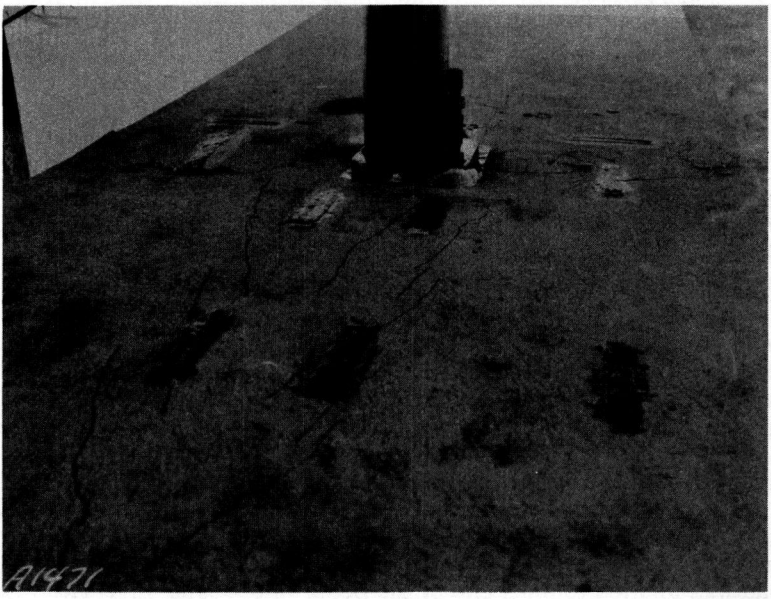

Figure 21. Slab-cracking pattern, composite shear test, pretensioned beam.

on the beam shown in Figure 2. Tendons for post-tensioning the beam were not grouted as is normally required. No strain measurements were made on this test. Over-all length of the beam was 59 ft 6½ in., with a center-to-center-of-bearing length equal to 58 ft 10½ in. Vertical and horizontal deflections were measured at bearing points, quarter points, and midspan. Load was applied at midspan and the load was brought up to 46 kips where initial flexural cracking ocurred. Figure 22 shows a plot of load vs deflection with a deflection of 0.025 ft at 46 kips. A single flexural crack extended up through the bottom flange into the web where it split into a Y-shape. Loading was continued in 10-kip increments up to 70 kips where first cracking on the underside of the slab was noted. Deflection had reached 0.417 ft. The single flexural crack through the bottom flange had opened to a width of approximately ⅜ in. No other flexural cracks through the bottom flange were initiated during the test.

Loading continued to 80 kips where a network of cracks appeared on the underside of the slab with some cracks penetrating approximately 2½ to 3 in. into the slab. The initial flexural crack in the beam continued to widen. In the loading from 80 to 100 kips, no increase in length of cracks was noted. The flexural crack through the beam had opened to about 2½ in. at the bottom flange. Deflection increased rapidly with a small additional amount of load. At 100 kips, the deflection had reached 0.527 ft.

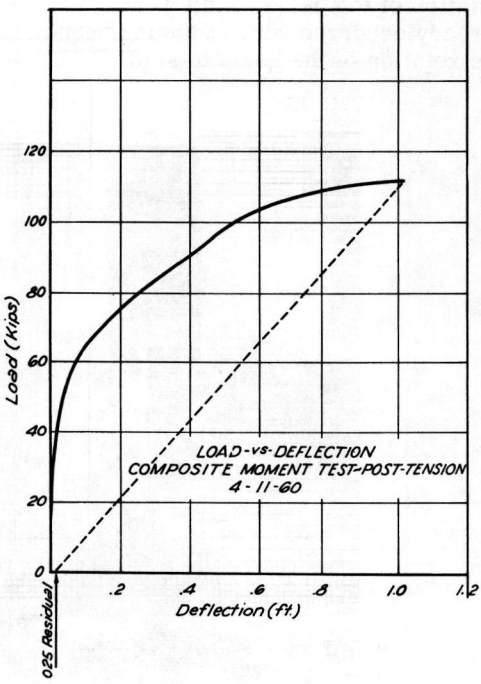

Figure 22. Load vs deflection, composite moment test, post-tensioned beam.

Between 100 and 112 kips, the deflection increased 0.608 ft to a total of 1.135 ft. In the loading from 100 to 110 kips, compressive failure in the top of the slab occurred with spalling of the slab approximately one-third the depth of the slab. Due to lack of jack travel and clearance between the beam bottom and the testing bed it was decided to discontinue loading of the beam. A quick estimate of the stresses in the tendons showed that with the maximum attainable deflection of 2 ft, only about 236,000 psi could be induced in the bottom tendons of the beam. Therefore, the load was released and the beam allowed to recover. After a short wait original deflection readings were checked and a residual deflection in the beam of 0.025 ft was noted. Figures 23 and 24 show the beam under the maximum loading.

Torsion Test

A standard pretensioned beam was scheduled to be tested in torsion as an aid in helping to establish maximum criteria for handling and hauling as well as supporting overhanging formwork and fluid concrete during superstructure construction. The beam used was 64 ft long with end blocks cast on each end. This beam had been cast for a bridge project, but was rejected due to excessive honeycombing at one end of the beam. Near one end of the beam five strands were visible in the bottom flange due to this condition, but in an effort to make use of every available test specimen, it was decided to use the beam as it was, realizing that failure probably would occur in this area.

No strain measurements were made. Only the angular rotation and load were recorded. Load was applied to each end of the beam in opposing directions through eccentrically loaded collars which encircled the beam and were bolted to tilting jigs mounted on concrete abutments. Length between centers of collars was 62 ft $2\frac{5}{8}$ in. Figure 25 shows the beam in position for the test. Rotation was applied at both ends simultaneously in increments of $\frac{1}{2}^{0}$. Relatively soon after the test began, difficulties in obtaining accurate load readings in one pumping unit became apparent. Rotation of the beam was stopped and efforts were made to correct this difficulty. In this interim the constant torque applied to the beam caused initial cracking of the section. Angular rotation of the beam at this time was just under 2^{0}. As the point of initial failure had already occurred without having been accurately recorded, it was decided to continue the rotation of the beam to study its behavior visually. The failure of the beam had been

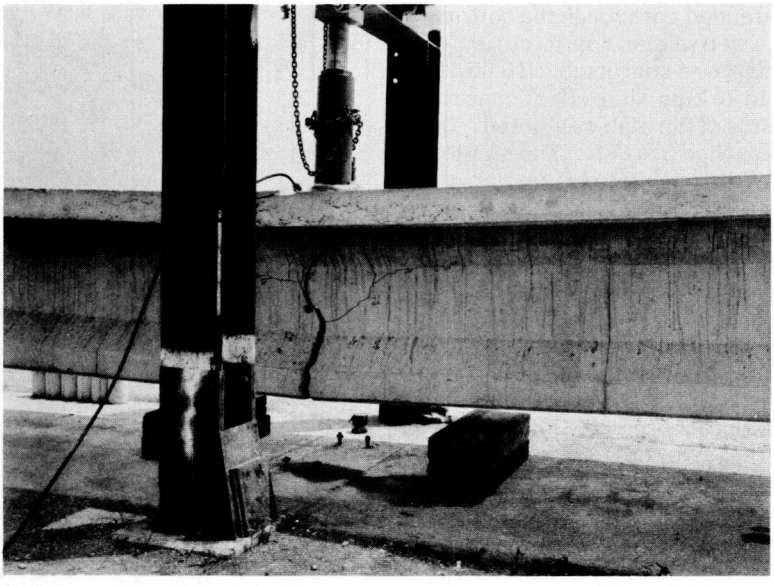

Figure 23. Post-tensioned beam under maximum load.

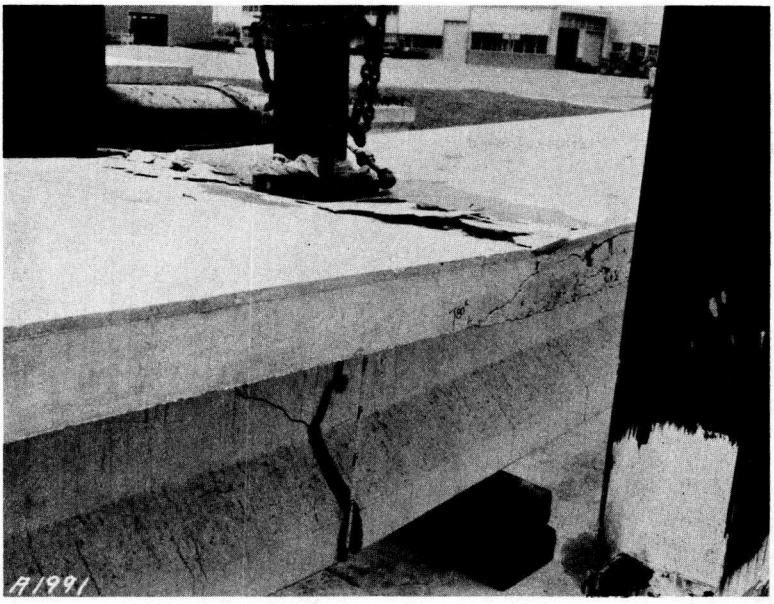

Figure 24. Post-tensioned beam under maximum load.

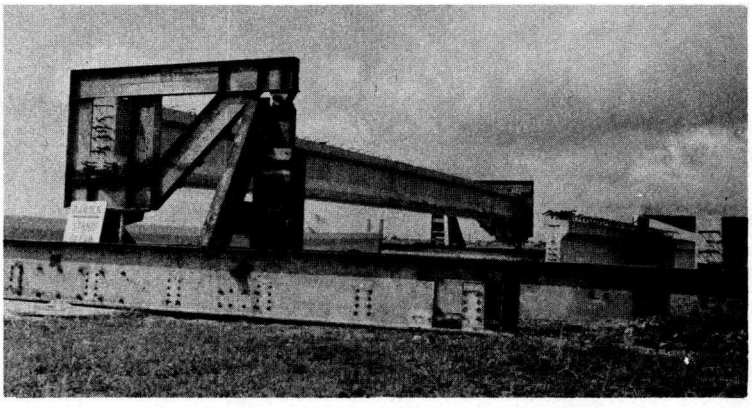

Figure 25. Pretensioned beam in position for torsion test.

confined to one end of the span and a thorough inspection of the remainder showed no outward signs of damage. It was then decided to cut off the damaged section and perform a new test on the intact section of the beam. The undamaged portion of the beam was about 50 ft long. For the second test the distance between centers of collars was 48 ft 5 in. The jacking systems were checked out and pressure gages permitting more accurate load readings were installed.

For the second test it was decided to rotate one end of the beam at a time and then only in increments of $\frac{1}{4}^{0}$. Again, only loads and angle of rotation were recorded. To coordinate the jacking operations, portable walkie-talkies were used to inform the men working the pumping units of the rate of rotation required for each increment of loading.

Torsion was applied to the beam and when the total angle of rotation reached 2^{0} the first cracks were initiated. A total of 229.60 ft-kips of resisting moment was produced in the beam. Initial cracking of the beam occurred near the south end of the beam and

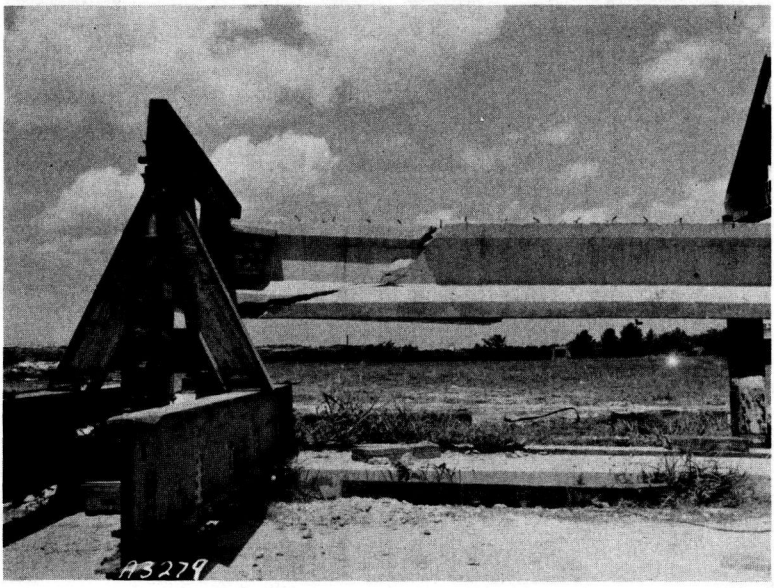

Figure 26. Beam failure, torsion test, pretensioned beam.

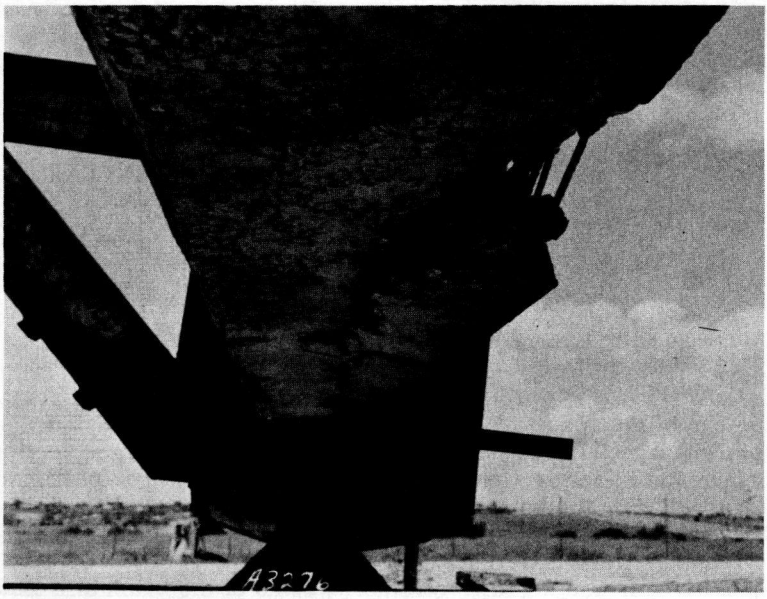

Figure 27. Beam failure, torsion test, pretensioned beam.

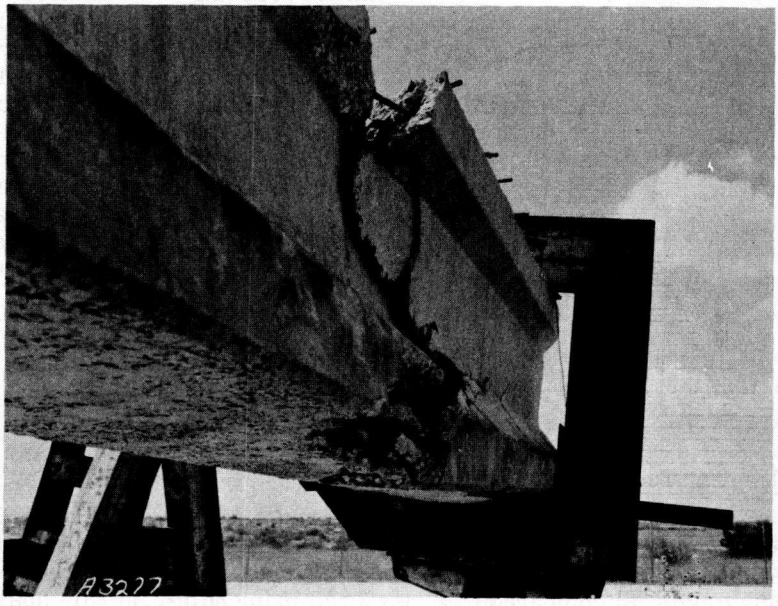

Figure 28. Beam failure, torsion test, pretensioned beam.

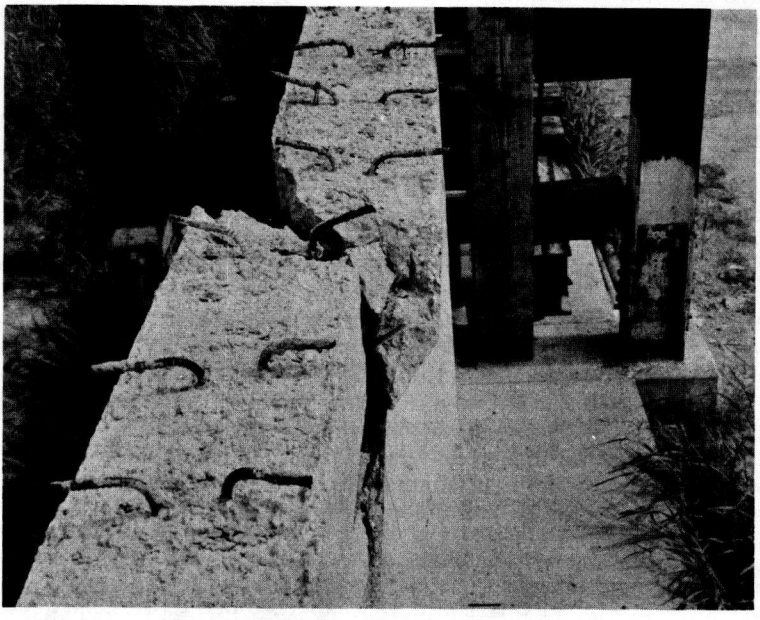

Figure 29. Beam failure, torsion test, pretensioned beam.

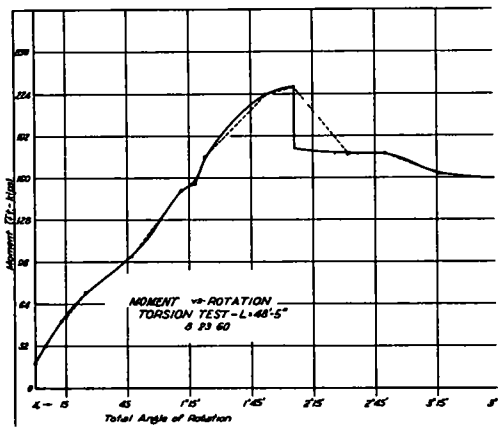

Figure 30. Resisting moment vs angle of rotation, torsion test, pretensioned beam.

appeared suddenly in the top and bottom flanges and inclined through the web of the beam. Resisting moment was reduced at initial cracking and continued to drop off as the angle of rotation was increased. Diagonal tension cracks appeared following the direction of principal tensile strains on either side of the beam. As rotation increased the main plane of failure widened with some spalling in the general area. No failure of stirrups was in evidence as cracking seemed to follow a plane along the side of the area enclosed by the stirrups. When a total of 12° of rotation was reached the test was stopped. Figures 26 through 29 show final cracking of the beam. Figure 30 is a partial plot of total applied moment vs angle of rotation.

ANALYSIS

Composite Moment Test (Pretensioned Beams)

Working as a composite section this beam showed a capacity equal to 1.25 times the required minimum ultimate moment produced by 1.5 DL + 2.5 (LL+I) as set forth by tentative AASHO specifications (3). Calculated ultimate moment based on a flanged section was 2,669 ft-kips as compared to a measured moment of 2,907 ft-kips or 1.09 times greater than the calculated value. Considering distribution to adjacent sections of a bridge it appears that the beam in actual service would be capable of an even higher ultimate capacity than that shown by the tests. Complete failure of the section could be safely assumed to occur as anticipated in that yielding of the prestressing steel would lead to collapse of the section. This region of strand yielding was barely reached in the test as was shown by the small residual deflection of 0.078 ft left in the beam after removal of the load. However, after the load had been released, a load equal to the design load was reapplied to the beam and the resulting additional deflection, above and beyond the residual deflection, was still within the allowable deflection of $\frac{1}{800}$ of the span length. Therefore, the beam, even in its state of having been damaged almost up to ultimate failure could have passed traffic over the bridge safely without collapsing.

Initial cracking of the beam, if deemed to be a point of control, may be estimated although never definitely fixed due to constant changing of the modulus of elasticity through time and loading. Stresses in the bottom of the beam due only to prestressing and dead loads are added to unit stresses calculated by taking the modulus of rupture in bending as $7.5\sqrt{f'c}$ to provide a stress at which first cracking should appear. In this case the estimated stress was about 687 psi or 275 μ in. per in. of strain as compared to 235 μ in. per in. of strain measured.

From the test results it can be seen that the design criteria used for this beam is more than adequate for the design situation produced by the beam span and spacing used. Possibly more accurate solutions of the calculated results could be obtained by determining equivalent areas for the slab concrete in respect to beam concrete, and then calculating stresses using the transformed section method.

Noncomposite Moment Test (Pretensioned Beam)

The compressive failure of this beam was expected due to the absence of an additional compressive area furnished by a compositely acting slab. Calculations of percentage of steel for this beam show the beam overreinforced, based on balanced beam steel percentage as set forth by the Bureau of Public Roads criteria. As noted in the test results, the cracking pattern near ultimate loads had not progressed as high in the beam as was noted in the underreinforced condition when the beam had a composite

slab acting integrally with the beam. Near the ultimate capacity of the beam the cracks ceased to extend themselves and finally a load was reached at which the strength of the concrete in the compressive zone was no longer strong enough to counterbalance the tensile forces acting in the steel. At this point the flexural capacity of the beam was reached and further loading resulted in compressive failure of the concrete.

Measured moment at failure was found to be 2,305 ft-kips as compared to a calculated moment of 2,126 ft-kips.

Because this beam was designed as a component part of a bridge acting integrally with the slab, this type of loading and failure would not be probable.

Composite Shear Tests (Pretensioned Beam)

Initial cracking in the lower load ranges was due to flexural stresses under the loading point. As very little shear is present directly under the loading point these initial cracks progressed vertically up into the beam. As flexural cracks appeared on either side of the loading point, the influence of shear stresses may be seen as the cracks start vertically in the flange and then begin to bend over, toward the loading point, in the web where shear stresses become larger. Within reasonable limits of loading these cracks in the beam will close if the load is released. In contrast to flexural cracks, the diagonal tension cracks appeared in the web suddenly and traversed the web quickly due to the presence of high shearing stresses. As these diagonal cracks reached the bottom flange they turned to run almost parallel to the bottom of the beam where the largest mass of prestressing steel was located. Removal of the load did not allow these cracks to close again as happened with the flexural cracks.

In both shear tests more than one initial diagonal crack appeared at the same time. The crack nearest to the load point should have been subjected to somewhat greater stresses than the others, but hardly enough to state that one crack was initiated slightly before the other. With continued loading flexural cracks occurred near the point where the diagonal cracks entered the bottom flange of the beam. As these new cracks progressed into the web where large shear stresses were present they quickly traversed the web and extended up into the top flange following a slope close to that made by diagonal cracks

All of the flexural and diagonal cracks progressed toward the loading point on top of the slab. In the latter stages of loading, flexural cracking had appeared on the underside of the slab. All of this cracking tended to reduce the available working compressive area of the section and, as in the noncomposite moment test, finally reached a point where the compressive forces could no longer balance the tensile forces, thus causing compressive failure in the slab.

Apparently the lack of an end block did not affect the structural capacities of the beam. Initial flexural, diagonal tension, and compression failure loads were nearly equal in both tests. From this it could be surmised that the exclusion of the end block would be permissible with the exception of those cases where higher stresses encountered at the ends of the beam might tend to cause splitting.

Composite Moment Test (Post-Tensioned Beam)

By not bonding the stressing tendons, these tendons were allowed to distribute the induced elongation throughout the entire length of the stressing steel. This elongation of the tendon essentially let the beam act as a nonreinforced member once the prestressing forces have been overcome. Only the reinforcing steel in the top of the beam flange and in the slab was available for any work and that was contained in the compressive zone of the section. Therefore, initial cracking of this "nonreinforced member" occurred under the loading point where the highest stresses in the concrete occurred. After the initial cracking of the beam no other flexural cracks were found in the bottom of the beam. This initial crack could only progress higher up into the beam and become wider as the load was increased because no transfer of stresses from the steel to the concrete was possible. Again compression failure in the slab occurred when the flexural capacity of the beam was exceeded.

Total deflection of this beam under load far surpassed that recorded for the preten-

sioned beam, with the residual deflection in the beam, after unloading, being approximately one-third as great.

Visual cracking of the beam occurred at 45 kips or 1DL + 1.1 (LL + I) as compared to 78 kips or 1DL + 1.87 (LL + I) for the composite moment test of the bonded pretensioned beam.

Torsional Tests

When subjected to torsional forces, prestressed concrete, like plain concrete, will fail when the ultimate tensile strength of the material is reached. The torsional strength of concrete is low, but failure may be delayed by the addition of web reinforcement that is placed to intercept the potential failure cracks and by imposing a compressive force on the beam. Although the web reinforcement may only add strength to a small degree, the addition of the prestressing force will greatly increase the torsional strength of a concrete member.

Due to the presence and spacing of vertical reinforcement the beam did not fail with the explosive type of failure with flying debris that is characteristic of nonreinforced prestressed concrete. Initial cracking was not extensive enough to cause the beam to be unable to support itself. Only after extensive damage had occurred did the beam sag down to rest on timber staging placed to arrest complete collapse of the beam.

Although the resisting moment of the beam was as adequate as expected, the angle of rotation before initial cracking occurred was smaller than anticipated. Initial cracking for both tests occurred at approximately the same total rotation and torsional moment, which does not follow the theory that torsional stiffness is a function of length. This result could have been caused by the original tested length being weak due to the excessive honeycombing in one end of the beam, and further, gage readings for the first test were not very reliable. Clearly this test shows the need for additional experimentation in the torsional behavior of I-section prestressed beams.

ACKNOWLEDGMENTS

The authors wish to acknowledge the excellent assistance provided by both the office and shop personnel of the Equipment and Procurement Division, the Materials and Tests Division, and District 14 Headquarters.

Acknowledgment is also made to the Engineering Department instructors of the University of Texas for their many helpful suggestions, and to Span Prestressed Concrete Products for the use of the hydraulic jacks that were used in the tests, and for the prestressed beam contributed to the testing program. Valuable assistance was also provided by the Prescon Corporation along with the post-tensioned beam donated to the testing program.

REFERENCES

1. Matlock, H., and Ripperger, E. A., "Measurement of Soil Pressure on a Laterally Loaded Pile." Proc., ASTM, 58:1245-1259 (1958).
2. Matlock, H., and Thompson, S. A., "Creep in Bonded Electric Strain Gages." Proc., Soc. Exper. Stress Analysis, 12:No. 2, pp. 181-188 (1955).
3. American Association of State Highway Officials, "Standard Specifications for Highway Bridges." Tentative Revision 1.13.7 (1958).

Lateral Distribution of Load in Multibeam Bridges

C. L. HULSBOS, Research Professor of Civil Engineering, Fritz Engineering Laboratory, Lehigh University

•THIS PAPER presents a summary of the research conducted since 1954 at Fritz Engineering Laboratory, Lehigh University, on the lateral distribution of load in multibeam bridges. This type of bridge is constructed from precast rectangular beams made of either reinforced or prestressed concrete. These beams are placed side by side on the abutments and the interaction between the beams is developed by continuous longitudinal shear keys and lateral bolts that may or may not be prestressed.

The investigation has included a field test (1), a theoretical study (2), and a series of tests on a large-scale model bridge (3). The results of this work are summarized and an example application of the proposed design procedure is included.

THEORETICAL INVESTIGATION

The multibeam bridge can be analyzed as an orthotropic plate that considers the bending stiffness in the longitudinal direction, $(EI)_x$, as different from the bending stiffness in the lateral direction, $(EI)_y$. The stiffness in the lateral direction is dependent on the efficiency of the shear keys and lateral bolts. If slip occurs between adjacent beams, the problem of determining the lateral bending stiffness becomes more complex. Due to this discontinuity (slip), deflection and stress distribution do not follow the rules of the plate theory. It was therefore necessary to evaluate the change of the internal forces by empirical approximations.

The basic assumptions in the theory of orthotropic plates are the following:

1. The thickness of the plate is small compared with its other dimensions.
2. The deflections are small compared with the thickness of the plate.
3. The transverse stresses σ_z are small and their influence on the deformation can be neglected.

For a right-hand coordinate system (x, y, z) where x and y are the plane of the plate and parallel to the two distinct directions of the orthotropic plate, the differential equation for the deflection w parallel to the z direction can be written as

$$\frac{\partial^4 w}{\partial x^4} + 2\beta \frac{\partial^4 w}{\partial x^2 \partial y^2} + \alpha \frac{\partial^4 w}{\partial y^4} = \frac{P(x, y)}{(EI)_x}$$

in which $\alpha = \dfrac{(EI)_y}{(EI)_x}$; and

β = coefficient of torsional rigidity.

It is possible to determine the deflections w and the internal forces under a given loading P(x, y) by the use of three parameters (2):

$$\frac{B}{L} = \frac{\text{half the bridge width}}{\text{total bridge length}}$$

$$\frac{a}{h} = \frac{\text{width of one beam}}{\text{depth of one beam}}$$

$$\alpha = \frac{(EI)_y}{(EI)_x} = \frac{\text{lateral bending stiffness}}{\text{longitudinal bending stiffness}}$$

The first and second parameters are dependent on the geometry of the bridge and individual beams respectively. The third parameter is difficult to evaluate theoretically because the lateral stiffness is not a constant. In fact, it varies from point to point in the bridge and it is also dependent on the magnitude and location of the applied load as well as the amount of lateral prestressing. The procedure used to evaluate α is described later.

The coefficient of torsional rigidity, β, can be expressed as a function of α and K (2)

$$\beta = 3K(1 - \alpha^{3/2}) + \alpha$$

in which K is a numerical factor for torsion of rectangular beams depending on a/h (4).

The differential equation for an orthotropic plate for two free edges and supported by knife edges at two opposite sides was solved (2). The solutions were obtained with a UNIVAC Digital computor for various combinations of B/L, a/h and α.

The design of multibeam bridges is governed principally by the longitudinal bending moments. Hence, the most important characteristic of such a structure is the lateral distribution of these moments over the cross-section of the bridge. However, in a plate the load is transmitted not only by the longitudinal bending but also by the lateral bending moment, the twisting moments, and the shear forces. Figure 1 shows the qualitative distribution of various quantities over the cross-section.

Because internal forces cannot be measured directly, it is more convenient to compare the measured deflection from the tests with the theoretical calculations. However, the moments are not proportional to the deflections; therefore, the distribution curves for the moment coefficients and the deflection coefficients are not identical. (It is convenient to present distribution coefficients, rather than the actual moments, shear forces, or deflections. The coefficient for a particular point is defined as the ratio of the moment — shear force or deflection — at this point to the average moment — shear force or deflection — of the entire cross-section. These coefficients are dimensionless and, in the range of elastic deformation, independent of the amount of load). This can be visualized by considering the following— with a concentrated load at the center point of the bridge, the deflected shape of an edge beam is somewhat similar to the shape of a uniformly loaded beam, whereas, the middle beam acts more or less like a simple beam under a single concentrated load. The moment-deflection ratio for these two cases differs by 25 percent. In the practical case of a multibeam bridge these effects lead to a deviation between the coefficients of the longitudinal bending moments and the deflection coefficients which may be as high as 50 percent.

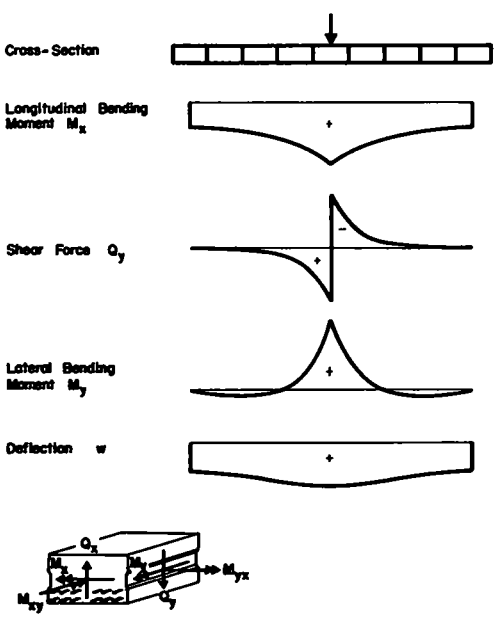

Figure 1. Distribution of moments, shear forces, and deflections at the midspan cross-section (center loading).

COMPARISON BETWEEN THEORY AND TESTS

A series of tests (3) was conducted on the laboratory model bridge shown in Figure 2. A direct comparison was made between the theoretical and measured deflection distribution. It was assumed that if the theoretical and experimental deflections were in good agreement, then the moments in the beams could be calculated by the theory of orthotropic plates.

Because it was not possible to obtain a

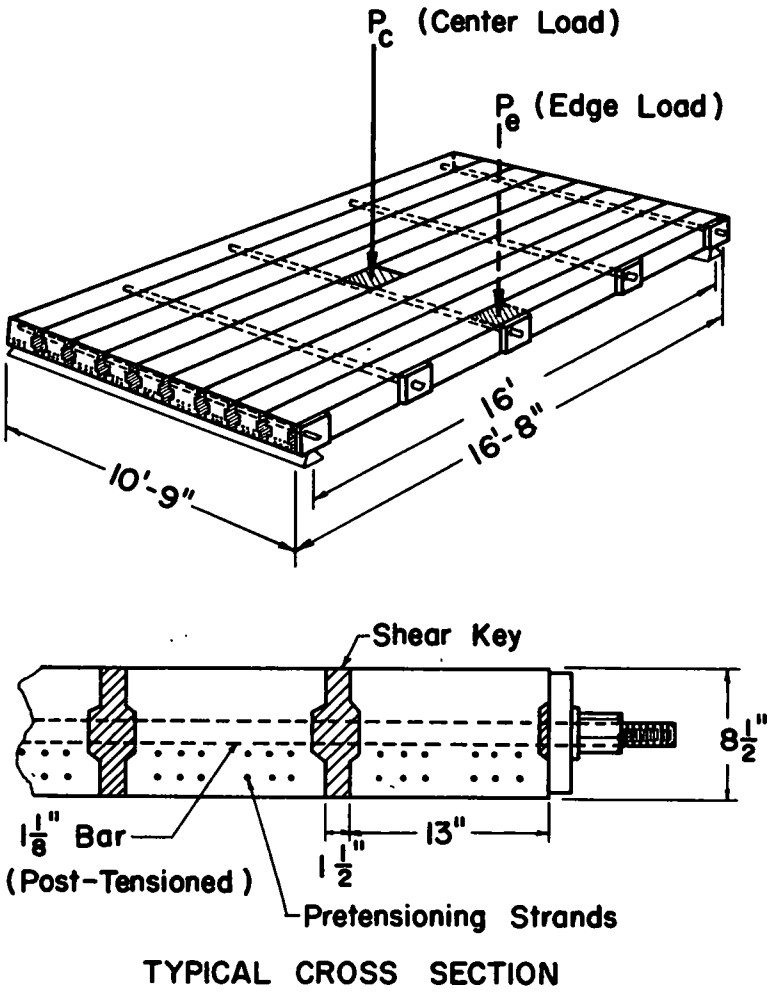

Figure 2. Test bridge.

theoretical value of α, and the α values have to be derived from the same tests that serve to check the adaptability of the theory. This means that only the deflected shape, and not the magnitude of the deflections, can be compared for this particular purpose. For this comparison the distribution of the deflection coefficients was calculated as a function of α; the other two parameters, B/L and a/h, are constant for a given bridge. By varying α, the theoretical curve with the same maximum deflection coefficient as the experimental one could be found and the correlation between the distribution of the measured and theoretical coefficients could be checked. A comparison of the theoretical and experimental deflection coefficients for four tests (3, 5) is shown in Figure 3. The theoretical moment coefficient distribution is also shown in Figure 3. The deflection coefficient S_w is defined as

$$S_{wi} = \frac{\Delta^i}{\Sigma\Delta^i/m}$$

S_{wi} = deflection coefficient for i^{th} individual beam in bridge.

in which Δ_i = deflection of an individual beam at a given cross-section of bridge;

$\Sigma\Delta_i$ = sum of all deflections of individual beams at same cross-section of bridge; and

m = number of individual beams in bridge.

The moment coefficient S_m is defined as

$$S_m = \frac{M_x}{(M_x)_{av.}}$$

in which S_m = moment coefficient for a point in a cross-section of bridge;

M_x = longitudinal bending moment per unit of width for a point in same cross-section of bridge;

$(M_x)_{av.}$ = total bending moment of same lateral cross-section of bridge divided by width of bridge.

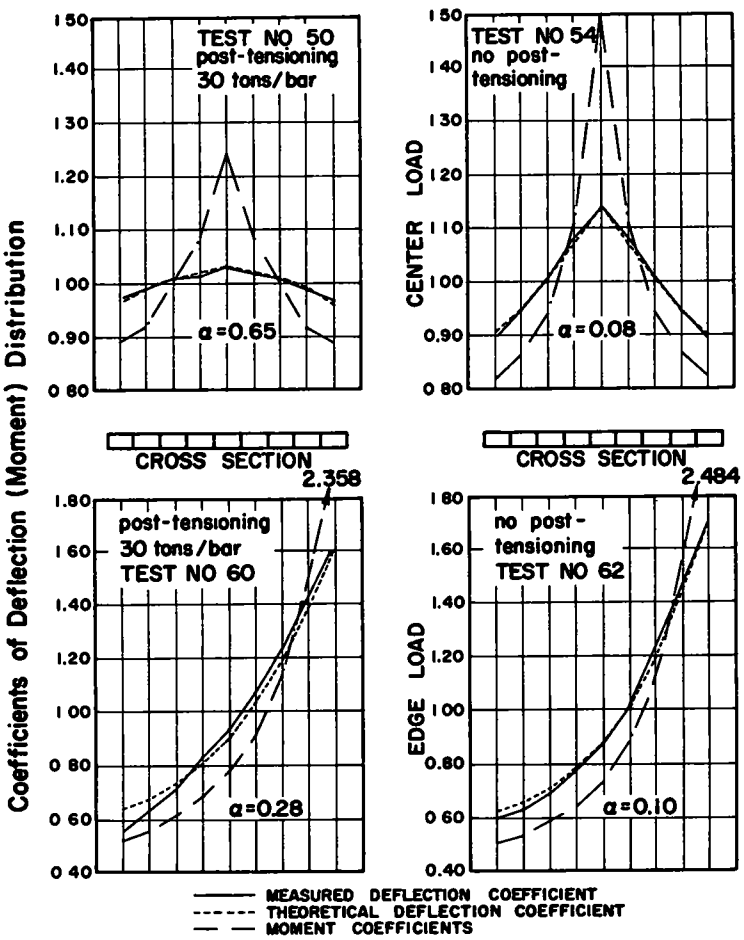

Figure 3. Theoretical and measured deflection distribution.

Figure 3 shows that if the proper value of α is used in the calculation, the theory yields a solution for the deflection distribution which agrees very closely with the experimental results.

To analyze a given multibeam bridge, the value of α as well as the geometric properties must be known. For an isotropic and homogeneous plate, $(EI)_x = (EI)_y$, $\alpha = 1$. For an articulated plate that is, one formed of strips with adjacent sides connected by continuous hinges $(EI)_y = 0$, $\alpha = 0$. For other intermediate conditions α will vary between the limits of 0 and 1. It was found that α could be expressed as a function of F and P:

$$\text{For a center load:} \quad \alpha = 0.23 \sqrt{F/P_c}$$

$$\text{For an edge load:} \quad \alpha = 0.1 \sqrt[3]{F/P_e}$$

in which F = lateral post-tensioning force; and

P = load applied at the center or edge of the bridge.

The equations are intentionally conservative and represent the lower boundaries of the values of α determined experimentally (see Figs. 4 and 5). If a bridge is subjected to a load resulting from several trucks, P (center or edge) is not the total load at the cross-section. For highway loading, P_c is equal to two wheel loads and P_e is equal to one wheel load.

In comparing the theoretical solutions for distribution of moment it was found that the distribution can be considered as dependent on $(S_m)_{max}$ only, no matter from what combination of B/L, a/h, and α this $(S_m)_{max}$ may result. Hence, the distribution curve is known if $(S_m)_{max}$ is known. The values of $(S_m)_{max}$, dependent on B/L, a/h, and α, are given in Figures 6 to 9. Linear interpolation or extrapolation will be necessary if a/h is not equal to either 1.0 or 1.7.

The values of $(S_m)_{max}$ were computed on the assumption that no slip occurred. Data from the model (3) and field (1) tests indicated that slip may occur and will increase the maximum moment coefficient. The amount of increase can be approximated with the curve shown in Figure 10. The data for the curve drawn for no shear keys were obtained from the model tests and the data for the curve drawn for shear keys were obtained from both the model and field tests.

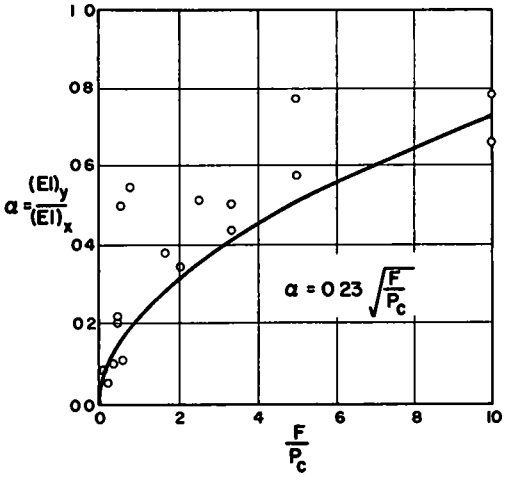

Figure 4. Relation between α and $\frac{F}{P_c}$ (center load).

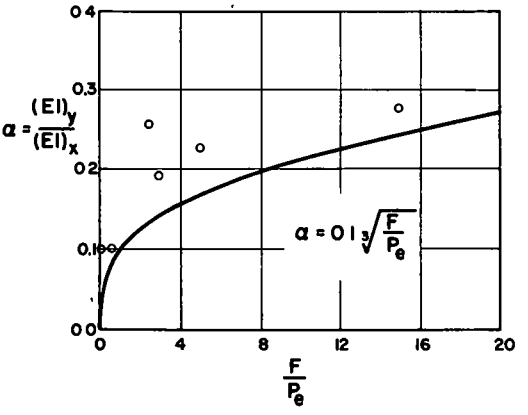

Figure 5. Relation between α and $\frac{F}{P_e}$ (edge load).

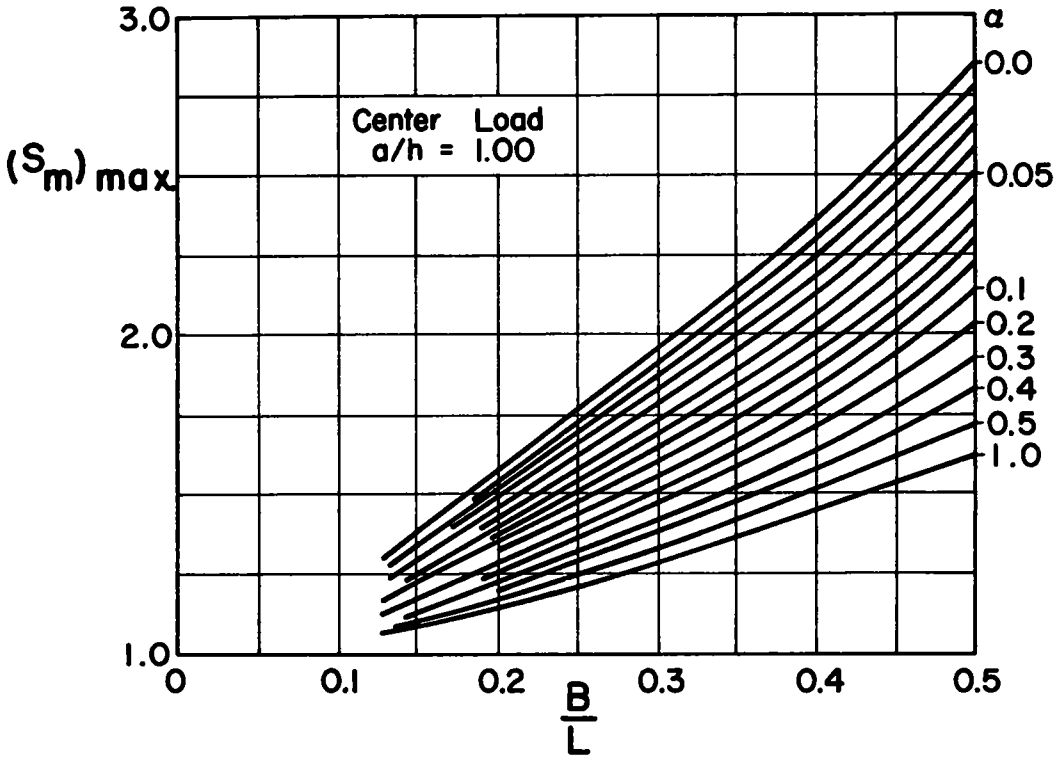

Figure 6. Maximum values of coefficient of lateral distribution of moment.

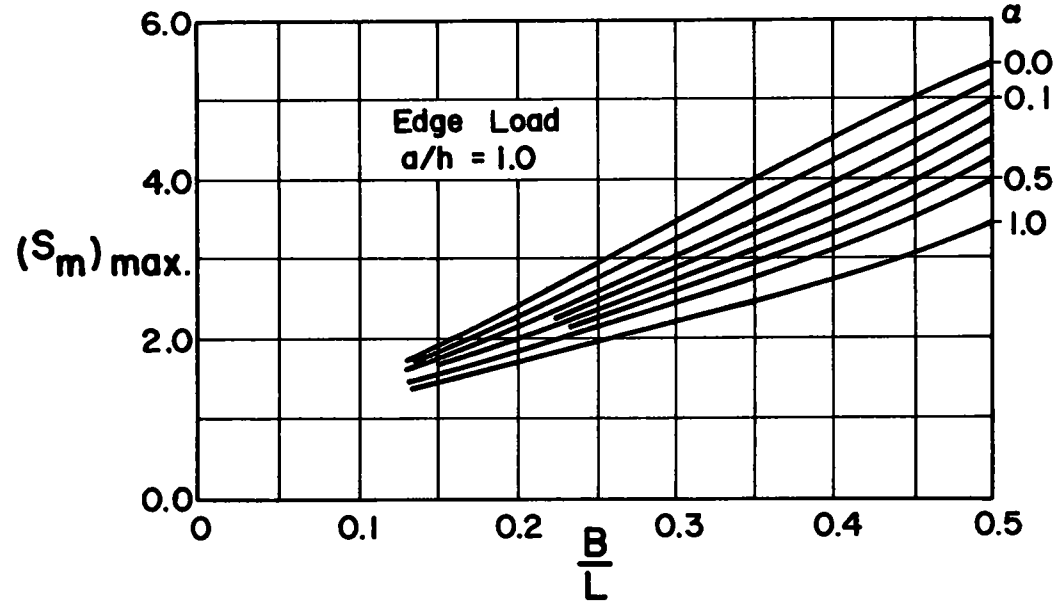

Figure 7. Maximum values of coefficient of lateral distribution of moment.

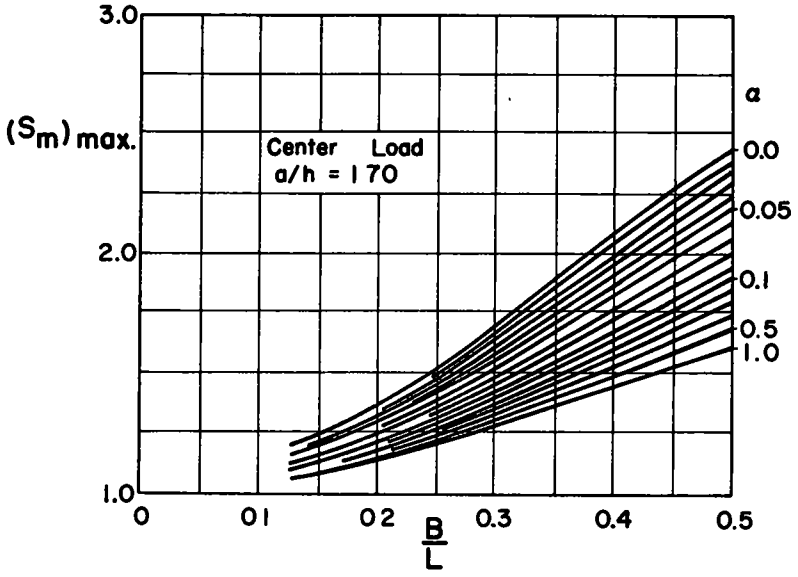

Figure 8. Maximum values of coefficient of lateral distribution of moment.

Once the maximum value for S_m is calculated, the distribution curve can be taken from Figures 11 and 12 for center and edge load, respectively. These distribution curves can also be considered as influence lines for the longitudinal bending moments.

The equivalent load used for design of either the center or edge individual beam can be obtained as

$$W_{eq} = W \frac{S_m}{m}$$

or for a series of loads at one cross-section of the bridge

$$W_{eq} = \sum_{o}^{n} W \frac{S_m}{m}$$

when the individual loads at one cross-section are equal, as the case for standard highway loading,

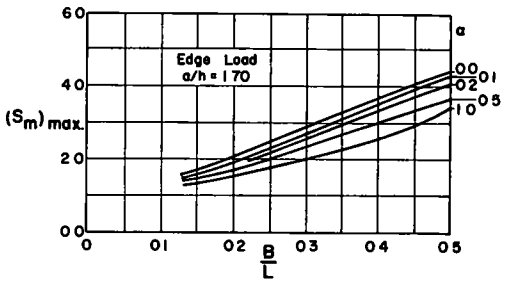

Figure 9. Maximum values of coefficient of lateral distribution of moment.

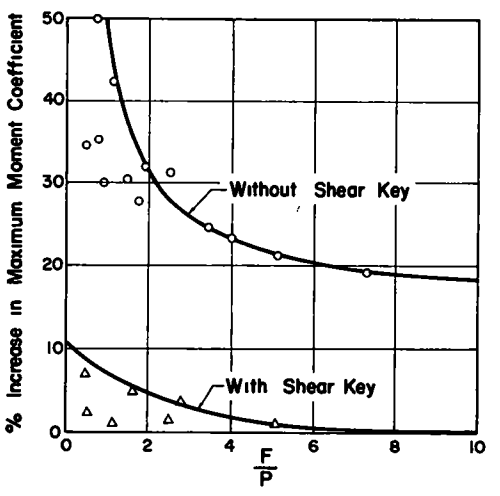

Figure 10. Increase in moment coefficient due to slip and incomplete interaction of shear key (center or edge load).

$$W_{eq} = W \sum_{o}^{n} \frac{S_m}{m}$$

in which W_{eq} = equivalent load applied to one individual beam;

W = one wheel load (all other wheel loads across a lateral section are equal);

S_m = moment coefficient (defined previously);

m = number of beams; and

n = number of wheel loads at one cross-section of the bridge.

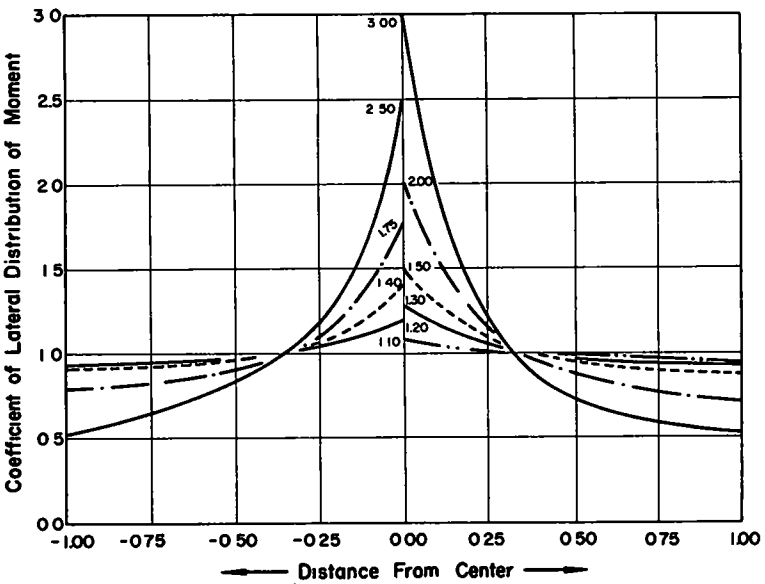

Figure 11. Distribution of moment coefficients for center load as a function of $(S_m)_{max}$.

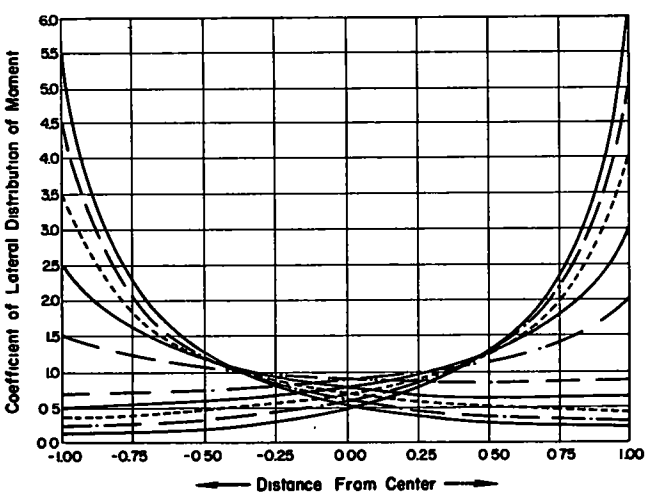

Figure 12. Distribution of moment coefficients for edge load as a function of $(S_m)_{max}$.

The quantity $\sum_{0}^{n} \frac{S_m}{m}$ is, in other words, the fraction of a wheel load to be applied to an individual beam making up the complete bridge.

The lateral distribution of moment is least uniform at midspan; therefore, W_{eq} becomes greatest at the midspan section. If the factor $\sum_{0}^{n} \frac{S_m}{m}$ is used for all loads along one beam, the resulting design will be conservative. Although this factor was derived for bending, it may also be used to calculate the shear for an individual beam.

EXAMPLE

Given:

Length of bridge = 60 ft
Width of roadway = 48 ft
AASHO specifications
Loading = H20-S16

Chosen:

Assumed cross-section = 36 by 36 in.
Lateral post-tensioning = 3 ⅝-in. diameter bars; working force per bar = 26,000 lb
Shear keys are used
Use 17 box beams at 3.0 ft plus 16 joints at ½ in. = 51 ft 8 in.

Calculations:

1. Determination of α
   (a) Center loading
   $$\frac{F}{P_c} = \frac{26,000\ (3)}{(2)\ (16,000)} = 2.44$$
   from Figure 4, $\alpha = 0.36$
   (b) Edge loading
   $$\frac{F}{P_e} = \frac{26,000\ (3)}{16,000} = 4.88$$
   from Figure 5, $\alpha = 0.17$
2. Determination of the maximum coefficient of lateral distribution of moment
   $$\frac{a}{h} = \frac{\text{width of beam}}{\text{depth of beam}} = \frac{36}{36} = 1$$
   $$\frac{B}{L} = \frac{\text{half of the bridge width}}{\text{length of the bridge}} = \frac{51.67/2}{60} = 0.43$$
   (a) Center loading
   from Figure 6, $S_m = 1.67$
   Effect of slip and incomplete interaction of the shear keys from Figure 10, 3.5 percent increase
   $S_m = 1.67\ (1.035) = \underline{\underline{1.73}}$
   (b) Edge loading
   from Figure 7, $S_m = 4.10$
   Effect of slip and incomplete interaction of the shear keys from Figure 10, 1.3 percent increase
   $S_m = 4.10\ (1.013) = \underline{\underline{4.15}}$
3. Final lateral distribution of moment curves.

The desired distribution moment curves are obtained from Figures 11 and 12. These curves are also the influence lines for the longitudinal bending moments for the centerline and edge beam.

In using an influence line to determine the maximum effect on a member, a concentrated load should be placed to coincide with the maximum ordinate. However, the AASHO specifications require that the lane loadings or standard trucks be assumed to

occupy any position within their individual design traffic lane which will produce the maximum effect. A solution will be made two ways to show the effect of these requirements. Also, the AASHO specifications permit a 25 percent reduction in load intensity when four or more lanes are loaded and a 10 percent reduction when three lanes are loaded to produce the maximum stress.

(a) Center loading

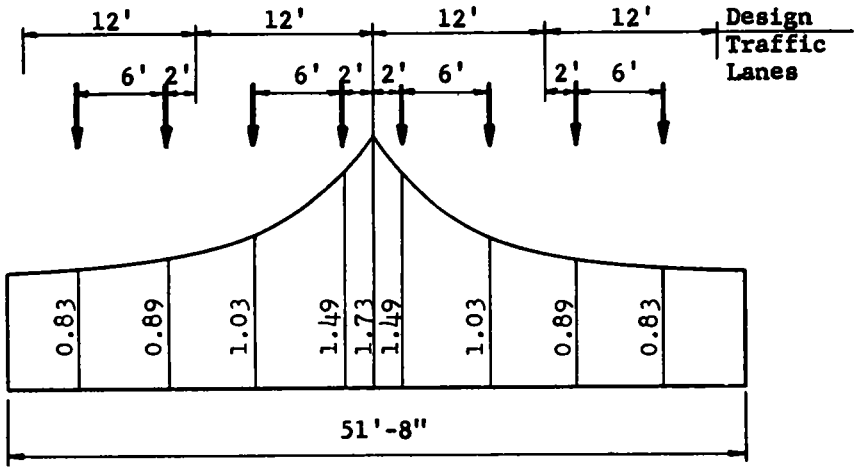

The percentage of a wheel load to be carried by the center beam is

$$\frac{\Sigma s_m}{m} = \frac{8.48}{17} (0.75) = 0.374 \text{ for four loaded lanes}$$

$$\frac{\Sigma S_m}{m} = \frac{6.76}{17} (0.90) = 0.358 \text{ for three loaded lanes}$$

$$\frac{\Sigma S_m}{m} = \frac{5.04}{17} = 0.296 \text{ for two loaded lanes}$$

or

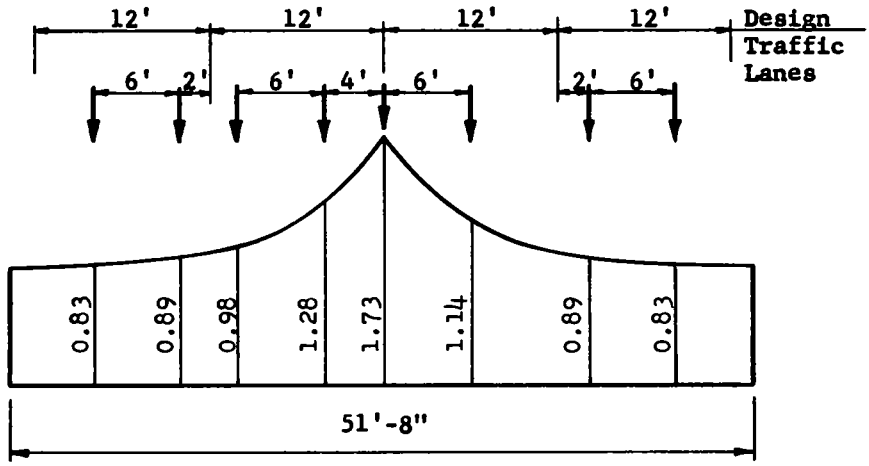

$$\frac{\Sigma S_m}{m} = \frac{8.57}{17} \quad (0.75) = 0.379 \text{ for four loaded lanes}$$

$$\frac{\Sigma S_m}{m} = \frac{6.85}{17} \quad (0.90) = 0.363 \text{ for three loaded lanes}$$

$$\frac{\Sigma S_m}{m} = \frac{5.13}{17} \quad = 0.302 \text{ for two loaded lanes}$$

(b) Edge loading

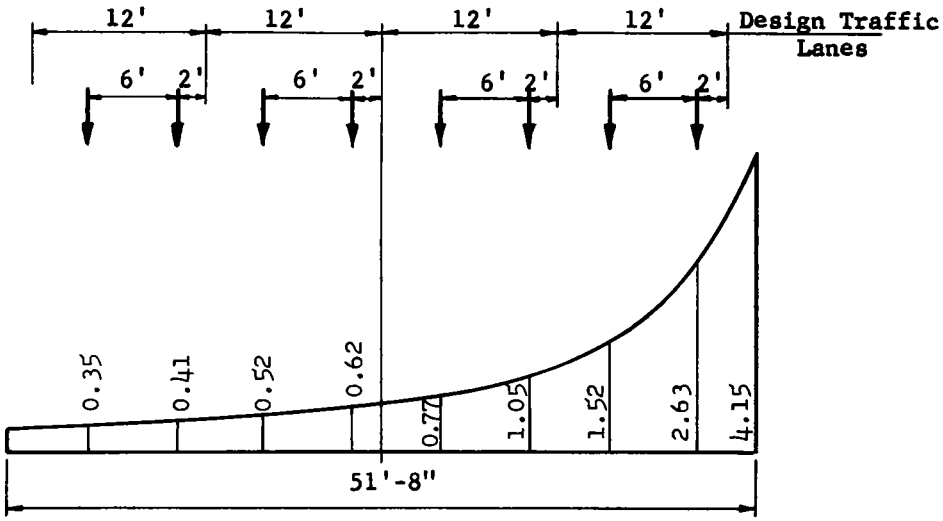

$$\frac{\Sigma S_m}{m} = \frac{7.87}{17} \quad (0.75) = 0.347 \text{ for four loaded lanes}$$

$$\frac{\Sigma S_m}{m} = \frac{7.11}{17} \quad (0.90) = 0.376 \text{ for three loaded lanes}$$

$$\frac{\Sigma S_m}{m} = \frac{5.97}{17} \quad = 0.351 \text{ for two loaded lanes}$$

or

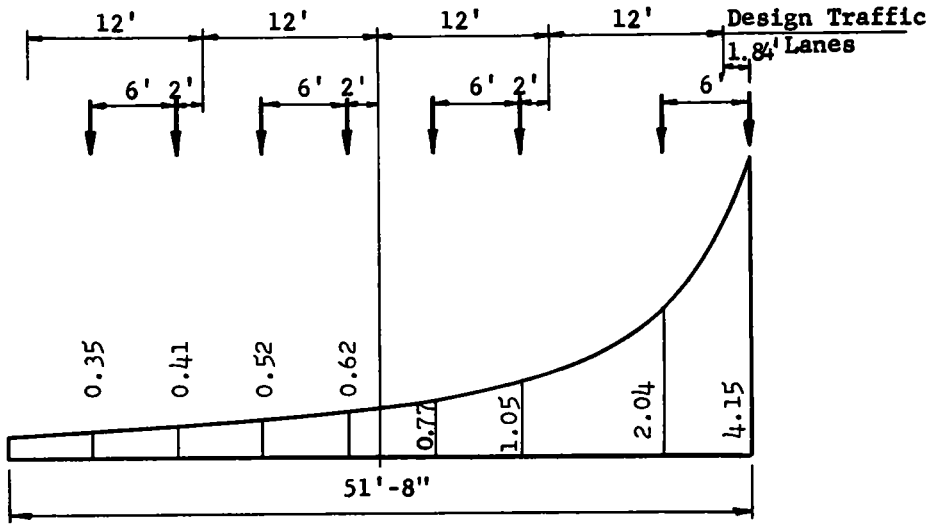

$$\frac{\Sigma S_m}{m} = \frac{9.91}{17} \quad (0.75) = 0.436 \text{ for four loaded lanes}$$

$$\frac{\Sigma S_m}{m} = \frac{9.15}{17} \quad (0.90) = 0.485 \text{ for three loaded lanes}$$

$$\frac{\Sigma S_m}{m} = \frac{8.01}{17} \quad = 0.471 \text{ for two loaded lanes}$$

4. If the loads are confined to the design traffic lanes, the live load distribution factor to be multiplied times the vehicle wheel loads is 0.376. However, if one vehicle is placed out of its design lane at the maximum ordinate of the influence line, the distribution factor is 0.485. The latter value is recommended for this particular example.

NOTATION

a = width of one beam
B = one-half width of bridge
$(EI)_x$ = longitudinal bending stiffness
$(EI)_y$ = lateral bending stiffness
F = total lateral post-tensioning force
h = depth of one beam
L = length of bridge
m = number of individual beams
M_x = longitudinal bending moment
M_y = lateral bending moment
M_{xy} = twisting moment
n = number of wheel loads at one cross-section
P = applied concentrated load (P_c, center; P_e, edge)
Q_x = longitudinal shear force
Q_y = lateral shear force
S_m = moment coefficient
S_w = deflection coefficient
w = deflection
α = $(EI)_y/(EI)_x$
β = coefficient of torsional rigidity

ACKNOWLEDGMENTS

This paper is based on the theoretical and experimental investigations presented in Fritz Engineering Laboratory Reports 223.9, 223.10, and 223.14 by C. E. Ekberg, Jr., W. J. Eney, A. Roesli, A. Smislova, and R. E. Walther. The research was sponsored by the Pennsylvania Department of Highways; U. S. Bureau of Public Roads; Concrete Products Division, American-Marietta Company; American Steel and Wire Division, United States Steel Corporation; John A. Roebling's Sons Corporation; Reinforced Concrete Research Council; and Lehigh University.

REFERENCES

1. Roesli, A., Smislova, A., Ekberg, C. E., Jr., and Eney, W. J., "Field Tests on a Prestressed Concrete Multibeam Bridge." Fritz Engineering Laboratory Report 223.9, Lehigh Univ. (Jan. 1956).
2. Roesli, A., "Lateral Load Distribution on Multibeam Bridges." Fritz Engineering Laboratory Report 223.10, Lehigh Univ. (July 1955).
3. Walther, R. E., "Investigation of Multibeam Bridges." Fritz Engineering Laboratory Report 223.14, Lehigh Univ. (Aug. 1956).
4. Timoshenko, S., "Theory of Elasticity." 2nd ed., McGraw-Hill (1951).
5. Walther, R. E., "Investigation of Multibeam Bridges." ACI Jour. (Dec. 1957).

On the Continuous Composite Girder

K. IWAMOTO, Bridge Engineer, Highway Section, Public Works Bureau, Hyogo Prefectural Office, Kobe, Japan

A marked increase in motor traffic in postwar Japan has made construction and improvement of roads an urgent necessity. In the cost of constructing a road the structures, such as bridges and tunnels, constitute a large segment and ways of constructing them more economically are an important consideration imposed on the engineers.

Composite bridge construction, developed rapidly in the postwar era, has made a remarkable contribution to the problem of economical design. Aboshi Bridge, the first example of the continuous composite girder bridge in Japan, is of three-span (3 at 32m) design, by which, compared with a noncomposite continuous girder, the weight of steel used and the construction cost were reduced by 14 and 10 percent respectively.

Following this pioneer work, a number of continuous composite girder bridges have been constructed in Japan.

This paper describes the design, erection, and various field tests of the Aboshi Bridge.

•IMPROVEMENT in transportation facilities, especially in construction of highways, is one of the urgent necessities for present-day Japan, where motor car traffic has remarkably increased owing to rapid development in industry after World War II. In the construction of highways, the structures (bridges and tunnels) constitute a major part of the cost, hence economical construction of these items is an important problem imposed on structural engineers.

Owing to the high price of steel in Japan, the question of how to cut down the cost of steel materials becomes the first problem to be solved whenever bridge construction expenses are considered.

The following methods are to be considered for economizing the amount of steel used for steel bridges:

1. Improvement of floor and floor construction.
2. Improvement of main girder construction.
3. Improvement of joint construction and materials.
4. Improvement of materials.
5. Prestressing method.

Among these methods, a composite girder, which combined methods 1 and 2, has contributed most efficiently in saving steel.

To apply the composite construction for a continuous girder, combination with the prestressing method is indispensable. The prestressing method implies the following:

1. Reduction of tensile stress of the slab concrete caused by negative moments at a support to an allowable value (in a narrow sense).
2. Positive improvement of stress distribution in the interior of structure (in a broad sense).

The methods of attaining the first purpose are (a) introducing opposite moment by moving the support of the girder (Bernhard Fritz method), and (b) increasing tensile force by applying prestress to the floor slab (Homberg method). For the latter purpose, the prestress is applied directly to the steel girder by means of high-strength steel bars, steel wires, etc. (Sattler and Dischinger methods).

PRESENT STATUS

In Japan, the continuous composite girder bridge has been used since 1958. Bridges of this type now existing or now under construction are summarized in Table 1. Aboshi Bridge, designed by the author, and Kema Bridge, constructed by Osaka City, adopted the true continuous composite girder for the first time in Japan.

It was the success of these two pioneer projects that induced application of the continuous composite girder to the three big bridges over the Kiso, Nagara, and Ibi Rivers on the Meishin (Nagoya-Kobe) Expressway, which is the focus of highway construction in present-day Japan. Although conditions in the United States may be different from those in Japan, the design and erection of Aboshi Bridge might have some significance for American bridge engineers.

TABLE 1

ASSUMED CONTINUOUS COMPOSITE GIRDER BRIDGES IN JAPAN

Bridge	Constructor	Dimensions (m)			Steel Weight		Prestressing Method	Date of Construction		Remarks[a]
		Total Length	Width	Span Length	Total (tons)	Unit (Kg/m^2)		Start	Finish	
Aboshi	Hyogo Pref Office	183 09	8.0	3 at 32.0	113.7	147	Raising and settlement	Aug. 1958	Mar. 1960	Including HT50
Inagawa	Japan Highway Publ. Corp	119 0	20.6	35 4 +47.2 +35.4	382.0	162	Raising and settlement	Aug 1959	Oct. 1960	Including HT50
Kawabe	Kagawa Pref. Office	208 4	6.0	3 × 3 at 22 95	136 0	109	Raising and settlement	Aug 1960	Mar. 1961	
Kurose	Namazu City	176 0	6.0	2 at 52 5 + 70	230.0	218	Raising and settlement, prestressing slab with steel rods	Dec. 1959	Under construc.	Including HT50
Kamishima	Chito Town (Shizuoka Pref.)	202.45	4 0	2 at 53 +66	144.0	178	Raising and settlement, prestressing slab with steel rods	Nov. 1960	Under construc.	Including HT50
Choshi	Japan Highway Publ Corp.	1,203 2	7 0	1 × 2 at 46 + 4 × 3 at 46 + 3 × 13 6 + 3 × 19 6	981.0	218	Raising and settlement	Dec. 1960	Under construc.	Including HT50
Kisogawa	Japan Highway Publ. Corp.	1,014 0	25.1	5 × 3 at 67.3	5,784	227	Raising and settlement, prestressing slab with steel wire	Mar. 1961	Under construc	Including HT50 and HT60
Nagaragawa	Japan Highway Publ. Corp.	630.0	25 1	3 × 3 at 69.69	3,515	222	Raising and settlement, prestressing slab with steel wire	Mar. 1961	Under construc	Including HT 50 and HT60
Ibigawa	Japan Highway Publ. Corp.	349.0	25.1	5 at 69.60	1,983.3	226	Raising and settlement, prestressing slab with steel rods	Mar. 1961	Under construc.	Including HT50 and HT60
Nishiki	Ministry of Construction	150.97	8 0 and 9.5	51.02 +49 10 +50 85	256.4	194	Prestressing girder with locked coil and slab with steel rods	Apr 1961	Under construc.	Including HT60
Kema	Osaka City	150.0	9.0	39 5 +55.0 +54 5	357.6	265	Raising and settlement, prestressing slab with steel rods	Dec. 1958	Feb. 1960	Including HT50

[a] HT = high-strength steel

The conversion units applicable throughout this paper are as follows:

Metric System	English System
1 kg	= 2.20 lb
1 ton (metric)	= 2,204.6 lb
1 m	= 3.28 ft (39.37 in.)
1 kg/cm^2	= 14.2 psi
1 kg/cm^2	= 1.42 × 10^{-2} ksi
1 t-m	= 7,233 lb-ft
1 t/m	= 672 lb/ft

ABOSHI BRIDGE

The Aboshi Bridge spanning the Ibo River in Aboshiku, Himje City, on the second-class highway between Kobe, Ako, and Okayama, is a first-class bridge with a total length of 183.33 m and a width of 8 m (Figs. 1 and 2). The bridge consists of three main parts — a three-span continuous composite girder section (L = 3 at 32.0 m = 96.0 m, three main girders); a Langer girder span (L = 57.0 m, rise of arch = 9.6 m); and a simple composite girder span (L = 28.0 m, three main girders), and is a skew bridge of 69° 27' (20° 33' in American practice) to the right.

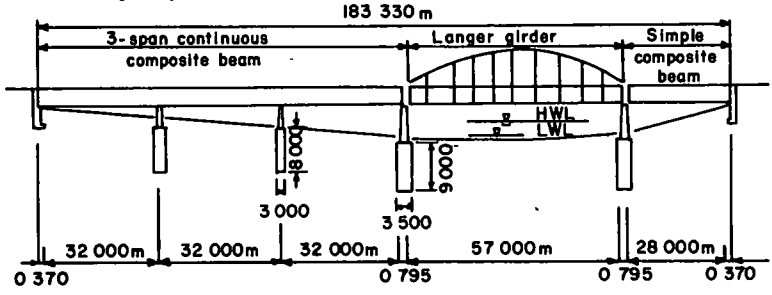

Figure 1. General elevation of Aboshi Bridge.

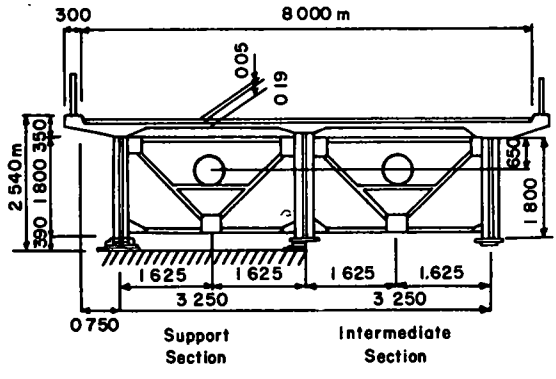

Figure 2. Standard cross-section of Aboshi Bridge.

The beam height of the bridge was kept at 1.8 m for the entire length. The surface of the bridge has a parabolic form; its slope is 1/250 in the longitudinal direction and 1/50 in the transverse direction. For the three-span continuous composite girder span which is the special feature of the bridge, the Bernhard Fritz method was adopted; namely, compressive prestress was given by settling the steel girder after composition to compensate the axial tensile force of the slab concrete expected on intermediate supports. The bridge was completed in March 1960 by Mitsubishi Heavy Industries.

Design

Design basis

1. Live load
   1st class load in accordance with steel highway bridge specifications in Japan.

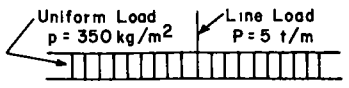

2. Young's modulus of steel, $E_S = 2.1 \times 10^6$ kg/cm^2.
3. Young's modulus of concrete:
   (a) When creep is not considered (live load stress, immediately after settlement of the composite girder, stress by the difference in temperature, etc.) $E_{co} = 3.0 \times 10^5$ kg/cm^2.
   (b) For the long-term load, in which the effect of creep must be considered (dead load, stress by settlement of the composite girder, etc.), $E_{ct} = E_{co}/(1 + 1.1\varphi)$ in which φ is a creep coefficient. The value of φ should be taken as about 1.5, by allowing sufficient time after the hardening of concrete before applying the long-term load so as to reduce the effect of creep. However, $\varphi = 2.0$ was chosen for this bridge, taking the period of erection into account. Hence, $E_{ct} = E_{co}/(1 + 1.1\varphi) = 0.9375 \times 10^5$ kg/cm^2.
   (c) For hardening, drying and shrinkage while considering the effect of creep, $E_{sh} = E_{co}/(1 + 0.52\varphi) = 1.4706 \times 10^5$ kg/cm^2.
4. Final shrinkage factor, $\epsilon_{sh} = 18 \times 10^{-5}$.
5. Temperature difference, $\Delta T = \pm 10$ C. The temperature was assumed to vary linearly between the top and the bottom of the composite girder section.
6. Allowable stress:
   (a) Steel

SS41 or SM41*	Tension	1,300 kg/cm^2
	Compression	1,200 kg/cm^2
SM50	Tension	1,860 kg/cm^2
	Compression	1,720 kg/cm^2

   *SS: Rolled steel for structure.
   SM: Rolled steel for welded structure.

   (b) Concrete $\sigma_{28} = 330$ kg/cm^2
   Compression $\sigma_a = 80$ kg/cm^2
   Tension $\sigma_a = 12$ kg/cm^2
   (c) Increase of allowable unit stress:
   Main load + creep drying, shrinkage + temperature:
   Compression edge 30 percent
   Tension edge 20 percent
   Main load + creep drying, shrinkage:
   Compression edge 15 percent
   Tension edge 5 percent
   Dead load + erection load 30 percent

Design Calculation

The design was based on Bernhard Fritz's book, "Vorschlüge für die Berechnung Durchlaufender Träger in Verbund-Bauweise." The outline of the design will be explained briefly.

1. Nomenclature

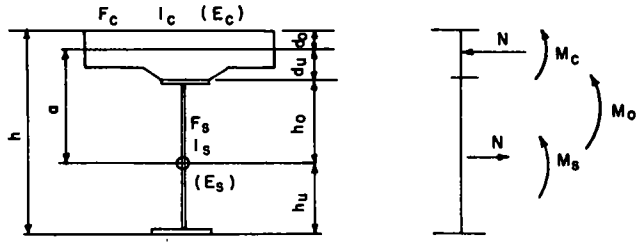

Figure 3.

F_C = Cross-sectional area of concrete section;
F_S = Cross-sectional area of steel section;
I_C = Moment of inertia of concrete section;
I_S = Moment of inertia of steel section;
E_C = Young's modulus of concrete;
E_S = Young's modulus of steel;

$$K_C = E_C F_C \quad K_S = E_S F_S \tag{1}$$

$$S_C = E_C I_C \quad S_S = E_S I_S \tag{2}$$

Setting

$$\frac{K_S K_C}{K_S + K_C} = K \tag{3}$$

gives

$$S_C + S_S + a^2 K = S = \epsilon_C I_C = E_S I_S \tag{4}$$

in which S is the flexural rigidity of the composite section.

2. Calculation of Moment at Support

(a) Moment at support by sustained load and live load. In calculation of the moments at supports M_1, M_2 ... M_r, it is sufficiently accurate to use auxiliary rigidities S_1, S_2, ... S_r, which are constant for each span of the continuous composite girder. For example, S_1, S_2, ... S_r at the stations of maximum span moment may be taken as the approximately representative values. Taking their standard value as S_C, and introducing reduced spans which are defined as $l_1' = l_1 S_C S_1$, $l_2' = l_2 S_C / S_2$ ... $l_r' = l_r S_C / S_r$, the fundamental equation of three moments is

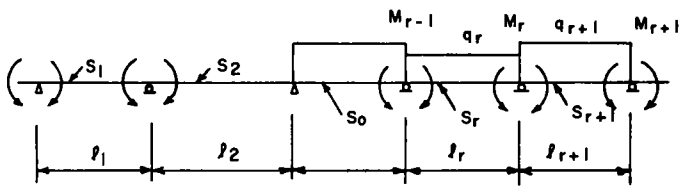

Figure 4.

$$l_r' M_{r-1} + 2(l_r' + l_{r'+1}) M_r + l_{r'+1} M_{r+1} = L_r \tag{5}$$

in which L_r is a load term.

(b) Shrinkage while considering the effect of creep. The load term for shrinkage is

$$L_r = -3\epsilon_{sh}\left(a_r l_r K_r \frac{S_c}{S_r} + a_{r+1} l_{r+1} K_{r+1} \frac{S_c}{S_{r+1}}\right) \tag{6}$$

in which, for the calculation of K and S, $E_c = E_{co}/(1 + 0.52\varphi)$ is to be used, ϵ_{sh} is the final shrinkage, and φ is the creep coefficient.

(c) Temperature difference.

The load term for the case where the temperature varies linearly between top and bottom of composite section is

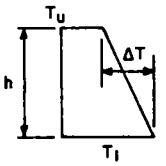

Figure 5. Difference of temperature.

$$L_r = -3\alpha_T \Delta_T S_c \left(\frac{l_r}{H_r} + \frac{l_{r+1}}{H_{r+1}}\right) \tag{7}$$

in which α_T is the expansion coefficient. In this case, the effect of creep is not considered.

(d) Settlement of support.

The load term for arbitrary settlement of a support is given by

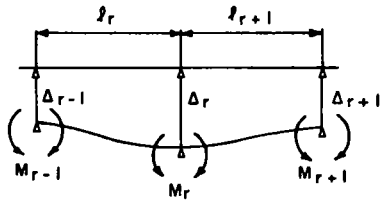

Figure 6.

$$L_r = 6S_c\left(\frac{\Delta_r - \Delta_{r-1}}{l_r} + \frac{\Delta_r - \Delta_{r+1}}{l_{r+1}}\right) \tag{8}$$

because of the nature of a sustained load, settlement of the support is influenced by creep. In this case, $E_c = E_{co}/(1 + 1.1\varphi)$ is used for the calculation.

3. Sectional Force.

After obtaining the moment at the support by the preceding method, the bending moment, M_O, in an arbitrary section can be calculated.

The sectional force caused by M_0 will be obtained from $N = a(K/S)M_0$, $M_C = (S_0/S)M_0$, $M_S = (S_S/S)M_0$.

4. Bending Moments Under Various Load Conditions.

(a) Bending moments due to dead and live loads. These moments are calculated by the three-moments equation. Moment due to the dead load, except pavement and accessories such as water pipes, acts solely on the steel girder; that due to live load and the rest of the dead load acts on the composite section.

(b) Moment due to raising of steel girder. Negative moment is caused by previously raising the steel girder 45 cm at the intermediate supporting points. This is the bending moment which acts on the steel girder alone. In Figure 7, at the outside girder, $M_1 = M_2 = -190.83$ t-m; at the inside girder, $M_1 = M_2 = -215.97$ t-m.

(c) Moment at support due to settlement of composite girder. The bending moments of the inside and outside girders at $t = 0$ (immediately after settlement) and $t = \infty$ are shown in Figures 8 and 9. These are the bending moments acting on the composite section.

(d) Indeterminate moment due to drying, shrinkage and creep of concrete occurs simultaneously with the shrinkage of the concrete. The resulting bending moment acts on the composite section, as follows (Fig. 10): outside girder, $M_{sh} = -102.86$ t-m; inside girder, $M_{sh} = -118.42$ t-m.

(e) Indeterminate moment due to temperature difference. The bending moment caused by a temperature difference ($\pm$10C) acts on the composite section, as follows: outside girder, $M_{tem} = \pm 83.68$ t-m; inside girder, $M_{tem} = \pm 92.76$ t-m.

5. Sectional Stress

Sectional stresses at various points caused by the previously mentioned sectional forces are summarized in Table 2.

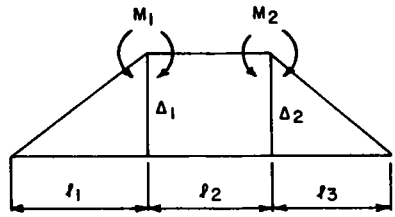

Figure 7. Moment diagram due to raising.

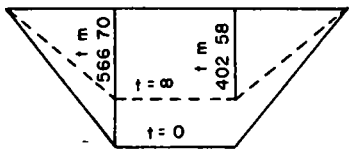

Figure 8. Moment diagram due to settlement, outside girder.

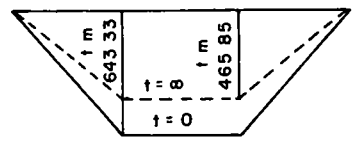

Figure 9. Moment diagram due to settlement, inside girder.

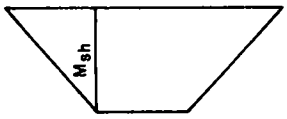

Figure 10. Moment diagram due to drying shrinkage and creep of concrete.

Measurement During Erection

After erection of the steel girder the end supports were lowered 5 cm and the intermediate supports were raised 40 cm. The end supports were prevented from springing up by the weight placed on them. The concrete work was scheduled so that the slabs around the intermediate supports were done last. Three weeks after finishing the concrete slab, the compressive strength of the concrete had reached 350 kg/cm^2. The support of the composite girder was then lowered, using interlocking oil jacks. Adjustment was made at each 2 cm so as to avoid unequal settlement and stressing. The last operations were pavement surfacing and setting of the handrailings.

Measurements of stress variation were made during erection to confirm the amount of prestress introduced and determine the amount of prestress decrease due to concrete shrinkage and creep. Measurements were taken at 13 locations (Fig. 12), each of which has three measurement points (that is, the middle of the concrete slab, and the top and bottom flange surfaces of the steel girder), making a total of 39 measuring points. Carlson-type strain meters were used for the measurements.

Measurements of the steel girder stress during lowering of supports A and D and raising of supports B and C show the measured values to be generally about 100 to 120 percent of the calculated ones. This results from the addition of stress due to the fairly large temperature difference (about 10 C) between the top and bottom flanges of the steel girder.

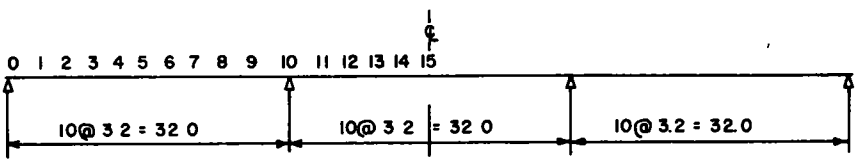

Figure 11. Stress measurement points.

TABLE 2

SECTIONAL STRESSES[1]

Stress Due to	Point 10				Point 15			
	σ_{cu}	σ_{cl}	σ_{su}	σ_{sl}	σ_{cu}	σ_{cl}	σ_{su}	σ_{sl}
1. Raising	-	-	1,032.4	-766.9	-	-	1,523.4	-779.7
2. Dead weights	-	-	1,160.1	861.8	-	-	-575.5	294.6
3. Settlement t = 0	-68.3	-39.1	-295.2	1,447.7	-74.5	-41.2	-287.1	1,613.9
4. Settlement t = ∞	-35.6	-26.8	-577.6	1,109.0	-40.9	-30.7	-681.3	1,234.5
5. Shrinkage of concrete	15.5	15.3	-159.4	-226.5	14.4	13.9	-180.7	-250.9
6. Temperature difference	±10.3	±6.0	±41.6	∓215.8	±11.0	±6.1	±42.4	∓238.3
7. Live loads	19.4	11.3	78.8	409.7	-15.0	-8.3	-57.9	325.5
8. 1 + 2	-	-	2,192.5	1,628.7	-	-	947.9	485.1
9. 1 + 2 + 3	-68.3	-39.1	1,897.3	-181.0	-74.5	-41.2	660.8	1,128.8
10. 1 + 2 + 4 + 7	-16.2	-15.5	1,693.7	-929.4	-55.9	-39.0	208.7	1,074.9
11. 1 + 2 + 4 + 5 + 6 + 7	9.6	5.8	1,575.9	-1,371.7	-52.5	-31.2	-14.4	1,062.3

[1] σ_{cu} = upper fiber stress of concrete
σ_{cl} = lower fiber stress of concrete
σ_{su} = upper fiber stress of steel
σ_{sl} = lower fiber stress of steel

TABLE 3

COMPARATIVE STRESSES AFTER SETTLING THE COMPOSITE GIRDER

Location	Gage Point	Stress (kg/cm^2) Meas.	Calc.	Ratio (%)
4	1	-16	-22.9	70
	2	-84	-96	88
	3	515	543	95
5	1	-18	-21.3	85
	2	-82	-70	117
	3	593	537	110
6	1	-16	-22.9	70
	2	-59	-96	62
	3	496	543	91
7	1	-	-56.7	-
	2	-191	-232	82
	3	563	1,396	40
8	1	-26	-51.7	50
	2	-206	-161	128
	3	-	1,222	-
9	1	-50	-56.7	88
	2	-240	-232	103
	3	1,280	1,396	92
10	1	-49	-60.3	81
	2	-183	-242	76
	3	1,382	1,546	90
11	1	-	-55.7	-
	2	-166	-151	110
	3	1,350	1,692	80
12	1	-	-60.3	-
	2	-158	-242	65
	3	1,370	1,546	89
13	1	-55	-56.7	97
	2	-189	-232	82
	3	1,370	1,396	98
14	1	-51	-51.7	99
	2	-254	-161	157
	3	540	1,222	44
15	1	-49	56.7	86
	2	-336	-232	145
	3	1,200	1,396	86

The floor slab was installed on several successive days between February 19 and March 5, 1960. Measurements were made when all slab work had been completed. The measured values were about 80 to 110 percent of the calculated values and seem to be reasonable, considering the increase in thermal stress, the longer period of operations, and the effect of the sequency in operations.

TABLE 4

COMPARISON OF STEEL USED, CONTINUOUS GIRDER BRIDGES

Item	Steel Weight (kg)					
	Composite					Noncomposite
	Steel SS41	Steel SM41	Steel SM50	Cast Steel	Total	Steel SS41
Main girder	58,848	26,751	12,061	-	97,660	115,389
Lateral and sway	12,020	-	-	-	12,020	12,020
Shoe	-	-	-	4,008	4,008	4,008
Total	70,868	26,751	12,061	4,008	113,688	131,419
Unit weight (kg/m^2)					146.8	169.8

TABLE 5

COMPARISON OF CONSTRUCTION COSTS[1] STEEL GIRDERS OF CONTINUOUS GIRDER BRIDGES

Item	Composite			Noncomposite		
	Quantity (kg)	Unit Cost (yen)	Cost (yen)	Quantity (kg)	Unit Cost (yen)	Cost (yen)
Material:						
SS41	70,868	56,500	4,004,042	127,409	56,500	7,198,608
SM41	26,751	58,500	1,564,933			
SM50	12,061	70,500	850,300			
Fabrication:						
SS41	70,868	46,400	3,288,275	127,409	46,400	5,911,777
SM41	26,751	46,400	1,241,246			
SM50	12,061	51,000	615,111			
Transport	113,688	4,500	511,596	131,417	4,500	591,376
Painting	113,688	3,500	397,908	131,417	3,500	459,959
Shoe	4,008	250,000	1,022,000	4,008	250,000	1,022,000
Erection	113,688	28,000	3,183,264	131,417	23,000	3,022,591
Total			16,678,675			18,206,311

[1] 1 yen = \$1/360, or \$1 = 360 yen.

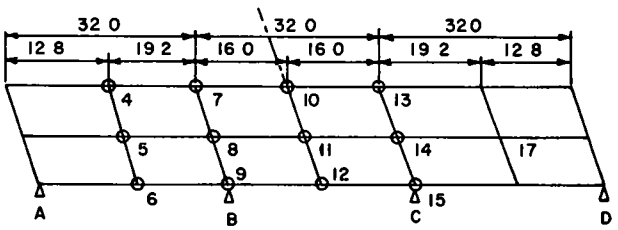

Figure 12. Measurement locations.

After installation of the floor slab the concrete was cured for about three weeks before the supports of the composite girder were finally adjusted. The measured stresses are given in Table 3, which indicates that 70 to 100 percent of the predetermined calculated stress was successfully introduced, considering the accuracy of the measuring instrument, the stress due to temperature difference, etc.

The stress variation caused by concrete shrinkage was measured between completion of the floor slab concreting and settlement of the composite girder. The measured values include the effect of the load due to the forms and the stress caused by temperature difference; hence, it cannot be concluded that the variation is solely caused by shrinkage. The temperature difference ($\Delta T = \pm 10$ C) caused a stress of ± 10.3 kg/cm^2 in the floor concrete, and ± 42 kg/cm^2 and ± 216 kg/cm^2, respectively, at the top and bottom flanges of the steel girder. Although the second purpose of the measurement could not be achieved, the foregoing results are a valuable guide for future measurement.

Steel and Cost Savings

Table 4 compares the amount of steel used in Aboshi Bridge with the amount used in a noncomposite girder bridge designed for the same class load and having the same girder height, number of girders, and span. Table 5 compares the construction costs for these same two bridges. The data show a 14 percent reduction in steel weight and an 8 percent reduction in cost, despite the higher cost of erection due to prestressing.

THE NATIONAL ACADEMY OF SCIENCES—NATIONAL RESEARCH COUNCIL is a private, nonprofit organization of scientists, dedicated to the furtherance of science and to its use for the general welfare. The ACADEMY itself was established in 1863 under a congressional charter signed by President Lincoln. Empowered to provide for all activities appropriate to academies of science, it was also required by its charter to act as an adviser to the federal government in scientific matters. This provision accounts for the close ties that have always existed between the ACADEMY and the government, although the ACADEMY is not a governmental agency.

The NATIONAL RESEARCH COUNCIL was established by the ACADEMY in 1916, at the request of President Wilson, to enable scientists generally to associate their efforts with those of the limited membership of the ACADEMY in service to the nation, to society, and to science at home and abroad. Members of the NATIONAL RESEARCH COUNCIL receive their appointments from the president of the ACADEMY. They include representatives nominated by the major scientific and technical societies, representatives of the federal government, and a number of members at large. In addition, several thousand scientists and engineers take part in the activities of the research council through membership on its various boards and committees.

Receiving funds from both public and private sources, by contribution, grant, or contract, the ACADEMY and its RESEARCH COUNCIL thus work to stimulate research and its applications, to survey the broad possibilities of science, to promote effective utilization of the scientific and technical resources of the country, to serve the government, and to further the general interests of science.

The HIGHWAY RESEARCH BOARD was organized November 11, 1920, as an agency of the Division of Engineering and Industrial Research, one of the eight functional divisions of the NATIONAL RESEARCH COUNCIL. The BOARD is a cooperative organization of the highway technologists of America operating under the auspices of the ACADEMY–COUNCIL and with the support of the several highway departments, the Bureau of Public Roads, and many other organizations interested in the development of highway transportation. The purposes of the BOARD are to encourage research and to provide a national clearinghouse and correlation service for research activities and information on highway administration and technology.